**Materials and Components
Technology Division
Materials and Components
Technology Division
Materials and Components
Technology Division**

Sodium Heat Engine Development Program: Phase I Final Report

by J. P. Singh, D. S. Kupperman,
S. Majumdar, S. Dorris, N. Gopalsami,
S. L. Dieckman, R. A. Jaross,
D. L. Johnson, J. S. Gregar,
R. B. Poeppel, A. C. Raptis,
and R. A. Valentin

Argonne National Laboratory, Argonne, Illinois 60439
operated by The University of Chicago
for the United States Department of Energy under Contract W-31-109-Eng-38

DISTRIBUTION OF THIS DOCUMENT IS UNLIMITED

Available to DOE and DOE contractors from the
Office of Scientific and Technical Information
P.O. Box 62
Oak Ridge, TN 37831
Prices available from (615) 576-8401, FTS 626-8401

Available to the public from the
National Technical Information Service
U.S. Department of Commerce
5285 Port Royal Road
Springfield, VA 22161

Distribution
Category:
Energy Research
(UC-317)

ARGONNE NATIONAL LABORATORY
9700 South Cass Avenue, Argonne, Illinois 60439

ANL--91/45

DE92 012398

ANL-91/45

SODIUM HEAT ENGINE DEVELOPMENT PROGRAM: PHASE I FINAL REPORT

by

J. P. Singh, D. S. Kupperman, S. Majumdar, S. Dorris, N. Gopalsami,
S. L. Dieckman, R. A. Jaross, D. L. Johnson, J. S. Gregar,*
R. B. Poeppel, A. C. Raptis, and R. A. Valentin

Materials and Components Technology Division

Work Completed: September 1991
Report Published: January 1992

Work sponsored by

U.S. DEPARTMENT OF ENERGY
Conservation and Renewable Energy Program
Office of Industrial Technology

---

*Chemistry Division

CONTENTS

FIGURES

TABLES

SODIUM HEAT ENGINE DEVELOPMENT PROGRAM: PHASE I FINAL REPORT

by

J. P. Singh, D. S. Kupperman, S. Majumdar, S. Dorris, N. Gopalsami,
S. L. Dieckman, R. A. Jaross, D. L. Johnson, J. S. Gregar, R. B. Poeppel,
A. C. Raptis, and R. A. Valentin

ABSTRACT

The Sodium Heat Engine (SHE) is an efficient thermoelectric conversion device which directly generates electricity from a thermally regenerative electrochemical cell that relies on the unique conduction properties of its β"-alumina solid electrolyte (BASE). While laboratory models of a variety of SHE devices have demonstrated the feasibility and efficiency of the system, engineering development of large prototype devices has been slowed by a series of materials and fabrication problems. Failure of the electrolyte tubes has been a recurring problem and a number of possible causes have been postulated. To address these failure issues, a two-phase engineering development program was undertaken. This report summarizes the final results of the first phase of the program, which included extensive materials characterization activities, a study of applicable nondestructive evaluation methods, an investigation of possible stress states that would contribute to fracture, and certain operational issues associated with the electromagnetic pumps used in the SHE prototype. This work was closely coordinated with activities at the Environmental Research Institute of Michigan (ERIM), where the major SHE development activity is centered.

Mechanical and microstructural evaluation of commercially obtained BASE tubes revealed that they should be adequate for SHE applications and that sodium exposure produced no appreciable deleterious strength effects. Processing activities to produce a more uniform and smaller grain size for the BASE tubes was completed using isostatic pressing, extrusion, and slip casting. Green tubes were sintered by both conventional and microwave plasma methods. This work was the initial phase of a task designed to improve uniformity, strength, and reliability of the tubes. Further study will be needed to optimize the fabrication process. Of particular interest is the residual stress state in the BASE tubes, and both analysis and nondestructive evaluation methods were employed to evaluate these stresses. Both X-ray and neutron diffraction experiments were performed to determine the bulk

residual stresses in commercially fabricated BASE tubes; however, tube-to-tube variations and variations among the various methods employed did not allow formulation of a definitive definition of the as-fabricated stress state in a typical tube. Failure-mechanics analysis of the potential cracking due to anisotropic expansion from the uptake of neutral sodium indicated that grain size should be reduced to less than 20 μm. In addition to materials-related work, a test of the electromagnetic pump system was completed to develop performance curves as a function of operating parameters. The resulting design relationship can be used to investigate effects of altered current and magnetic field strength for a pump of given duct geometry.

1 Introduction

The Sodium Heat Engine (SHE) is an efficient thermoelectrical conversion device based on a regenerative electrochemical cell using a solid electrolyte fabricated from β"-alumina. The fundamental physics of the SHE are well understood and laboratory demonstration devices have operated for extended periods. Unfortunately, it has not been possible to operate engineering prototypes under realistic conditions for extended periods. Failure of the β"-alumina solid electrolyte (BASE) tubes, usually through fracture, has made it impossible to achieve consistent, long-term reliability. To achieve a better understanding of this reliability problem and to develop possible solutions, DOE's Office of Industrial Technology sponsored the current study of materials issues associated with observed failures. In addition, the work included certain operational questions related to the electromagnetic pumps used in the regenerative SHE cell. The program was divided into two phases, with the Phase I work concentrating on materials characterization, the evaluation of alternative nondestructive evaluation methods, the estimation of stresses in the BASE material, and pump performance modeling. Proposed later phases will be concerned with fabrication and testing of improved, high-reliability BASE tubes. Only Phase I results are covered in the current study and all work was performed in close collaboration with the Environmental Research Institute of Michigan (ERIM), the location of current DOE-sponsored activities aimed at developing and evaluating a practical SHE.

The scope of Phase I work was partially defined by a number of credible causes that have been cited as the reason for observed fractures of BASE tubes in operating recirculating SHE systems. Among the postulated causes are thermal stresses due to both axial and radial temperature gradients during operation, thermal shock during filling of the system with sodium, and absorption of neutral sodium at high temperatures. There are, in addition, questions associated with the fundamental material properties of the ceramic β"-alumina, e.g., whether the processing of the material produces defects or voids that can form nucleation sites for subsequent crack initiation. Also, the effect of the microstructure of the β"-alumina on its fracture toughness and other materials properties needs to be understood. Several aspects of this question have been considered in the present work.

Based on the possible causes for tube failure noted above, the Phase I effort has included the following topics: a review of the literature relating to fabrication of β"-alumina; evaluation of the mechanical properties of commercially obtained BASE tubes used in present SHE modules; a study of processing methods for β"-alumina, including both alternative fabrication methods and various methods for sintering green tubes; a consideration of toughening of β"-alumina by additions of second-phase material; an evaluation of neutron diffraction, optical scanning, X-ray tomography, nuclear magnetic resonance, and X-ray diffraction as possible nondestructive evaluation methods for screening fabricated tubes; analytical studies of stresses due to fabrication and operation of the SHE and critical grain size determination for fracture; and testing of a small SHE electromagnetic pump to determine characteristic curves for a range of operating conditions. Each of these topics is discussed in a separate section of the report. When appropriate, conclusions for the individual areas are contained in the subsections of the report rather than in a general summary since not all of the topics covered are strongly interrelated.

2 Literature Review

Experience has shown that the major reason for failure of the sodium heat engine (SHE) is breakage of the BASE tubes.[1] It is not clear at this point, however, whether the failures result from inherent weakness of the BASE tubes or from operating procedures that inadvertently overstress the tubes. The program at Argonne National Laboratory (ANL) has examined both possible sources of premature failure. It has modeled the stresses that develop during operation of the SHE, and has characterized present-day BASE tubes to determine if they should be able to withstand the operating stresses. Nondestructive techniques will be evaluated as screening methods for eliminating tubes with large life-limiting flaws, and alternative processing techniques will be tested as a means to improve tube properties.

As the first step in characterizing present–day BASE tubes and developing alternative processing techniques, the literature on β"–alumina fabrication was surveyed. The survey provides a reference base to which we can compare the results of our mechanical testing on present–day commercial tubes, and it acquaints us with state–of–the–art processing of β"–alumina. For convenience, the survey has been organized in a sequence similar to that used in fabricating the BASE tubes: first, powder preparation is discussed, then the methods for shaping the powder into tubes are considered, followed by a discussion of the heat treatment of the tubes. After a review of the fabrication methods, the mechanical and electrical properties of β"–alumina are presented. Finally, work to enhance the mechanical properties of the BASE tubes by the addition of zirconia is discussed.

Before the tubes can be formed by any technique, a suitable powder must be obtained. A typical β"– Alumina composition is 8.7–8.9 wt.% Na_2O, 0.7–0.8 wt.% Li_2O, and 90.2–90.6 wt.% Al_2O_3, with the Li_2O stabilizer sometimes replaced or supplemented by small amounts of MgO. The first step in obtaining the powder is to mix the starting materials, typically αalumina, Na_2CO_3, and $LiNO_3$ (or $Li_2C_2O_4$), and then calcine them to produce the desired phase. The method by which the starting materials are mixed and calcined strongly affects the powder homogeneity, which has important consequences for the properties of the final material. Inhomogeneous distribution of starting materials can cause large grains and/or large voids in β"– lumina, two defects that cause tube failure.[2–4] Large grains and/or voids can also result from the introduction of impurities during processing, for example during extensive milling and screening of the powders. Thus, because the two main causes of defects in β"– Alumina are inhomogeneities and impurities in the powder,[5] improved properties might be expected by obtaining more homogeneous powder and reducing the level of impurities in the powder.

Improvements made over the last 15 years should lead to a more homogeneous β"– Alumina powder. In early work with β"– Alumina, the starting materials were mechanically mixed together in a single step and then calcined, either at a relatively low temperature of 800–1000°C to produce unconverted powder, or at 1250°C to produce partially converted powder.[6] Calcining the materials together in this way involves the addition of a very small concentration of Li_2O (<1 wt.%) to a large amount of Na_2O and Al_2O_3. Because the Li_2O concentration is so small, it is very difficult to obtain a homogeneous distribution of Li_2O.[6,7] An inhomogeneous distribution of Li_2O causes problems with conversion to the β" phase and leads to the formation of $LiAlO_2$, which can form low-melting eutectics in the presence of $NaAlO_2$, β"-alumina, or αalumina.[8,9] Such liquids can facilitate densification, but can also cause exaggerated grain growth during sintering and annealing. This must be avoided, because large grains often cause failure in BASE tubes.[2–4] In addition, the unwanted impurity phases degrade the electrical performance of β"-alumina.

The so-called "zeta process"[6] yields a more homogeneous distribution of Li_2O. In this process, $LiNO_3$ and αalumina are mixed in the appropriate proportions and calcined to form zeta lithium aluminate (Li_2O:$5Al_2O_3$). This is then used as the source of lithium rather than $LiCO_3$ or $LiNO_3$. The relatively large amount of Li_2O:$5Al_2O_3$ that is added helps to ensure that a more homogeneous distribution of lithium is obtained. As a result, conversion to β"-alumina proceeds more rapidly, and materials with relatively refined grain size are produced. β"-alumina typically has a duplex microstructure, but the coarse grains in zeta-processed materials are smaller than those in materials produced by single-step mixing and calcination. In zeta-processed materials, the size of coarse grains is 30–50 μm and that of the small grains is ≈2 μm, whereas single-step mixing and calcination typically produces materials in which the coarse grains are larger than ≈100 μm.[6,10] The strength of tubes made by the zeta process, as measured by diametral compression, is reported to be in the range of 24 to 42 kpsi.[10] Measurement of strength by burst testing of entire tubes gives a fracture strength of ≈19 kpsi for zeta-processed tubes, the lower value resulting because a larger volume of material is tested in burst tests.[3]

Although the zeta process improves the lithium distribution in β"-alumina, it involves two milling steps: first, milling of $LiNO_3$ and αalumina to form Li_2O:$5Al_2O_3$, then milling of Li_2O:$5Al_2O_3$, Na_2CO_3, and αalumina to form β"-alumina. In addition, blending, calcining, screening, and deagglomeration steps are needed; each of these steps increases the possibility that impurities become entrapped in the material. Burst testing and fracture analysis of zeta-processed tubes showed that the critical flaws were large voids at the center of or adjacent to large grains.[3] Furthermore, most of the defects were found to have high concentrations of iron, as well as other impurities such as calcium and silicon. Although high-purity materials were used in processing the materials, the multiple steps required in the zeta process can cause entrapment of impurities that produce critical flaws.

To decrease the number of processing steps and thereby reduce the level of entrapped impurities, spray drying was developed as an alternative single-step method for producing β"-alumina powder.[3,11-14] In the spray-drying technique, αalumina is dispersed in a solution containing the appropriate amounts of sodium and lithium salts, then sprayed from a heated nozzle to obtain an intimate, uniform mixture of the components. Fracture analysis of tubes produced from spray-dried powders[3] showed that the critical flaws were voids, just as in tubes produced from zeta-process powder. However, the voids in "spray-dried" tubes were smaller (≈82 μm vs. 123 μm), had only minimal levels of impurities, and had no large associated grains. The mechanical properties were also superior in tubes produced from spray-dried powders. The average fracture strength (by burst testing) of "spray-dried" tubes was 23.3 kpsi with a Weibull modulus of 10.4, while for "zeta" tubes, the average fracture strength was 19.1 kpsi with a Weibull modulus of 7.8. With the use of additives in the spray-drying process, the fracture strength of tubes decreased slightly to 22.3 kpsi, but the Weibull modulus increased to 13.2.[3]

The use of spray-dried powders reduces the level of impurities and impurity-related defects in BASE tubes, resulting in tubes with improved mechanical properties; however, optimization of the spray-drying process might yield further improvement. Fracture analysis of spray-dried tubes revealed that the concentration of sodium near voids was higher than that away from voids.[3] The voids could be due to inadequate compaction or an inhomogeneous distribution of the alkali salts, a problem that has been reported in several studies.[12,14] Upon sintering, high alkali concentrations can react and diffuse into the surrounding matrix, leaving a void or porous defect behind. Optimization of the spray-drying process to obtain a more homogeneous powder, and/or improved compaction of spray-dried powder, could therefore result in tubes with further improved mechanical properties.

After preparation of homogeneous β"-alumina powder, BASE tubes can be fabricated by a number of methods: extrusion,[15] slip-casting,[16] tape-casting,[17] electrophoretic deposition,[18,19] and isostatic pressing.[10,20] Of these methods, isostatic pressing has been used most widely. Isostatic pressing can be used to produce closed-end tubes and can be adapted to high production rates, as in the fabrication of automotive spark plugs.[11] Success with isostatic pressing requires a powder that flows easily into the die, compacts uniformly, and is dense enough that large compaction ratios are avoided, since this can lead to distortions of the green tube. Large amounts of powder acceptable for isostatic pressing can be produced by spray drying slurried powder to obtain relatively dense spherical agglomerates of β"–alumina with a uniform distribution of organic additives. Isostatic pressing might not be well suited for the production of thin–walled tubes (<0.7 mm), however, due to problems associated with filling the mold and removing of the green tube after pressing. For fabrication of thin–walled tubes, extrusion might be preferable. As with isostatic pressing, extrusion is also capable of high–volume production.[15]

After the fabrication of a green BASE tube by one of the above methods, an appropriate heat treatment schedule must be followed to obtain a dense, strong BASE tube with acceptable electrical resistivity (3–5 Ω–cm at 300°C for sodium sulfur battery application). BASE tubes are first bisque fired to slowly remove adsorbed species and any processing additives before heating to the sintering temperature. A bisque furnace can be placed in line with the sintering and annealing furnaces in a continuous process, or the bisque firing can be done in a separate furnace prior to sintering in a batch procedure. The continuous process offers the advantage that less handling of the green tube is necessary, so there is less opportunity to introduce flaws in the tubes. Other than logistics, this portion of the heat treatment appears to offer no particular problems in the processing of BASE tubes.

Bisque–firing is followed by sintering in the temperature range of 1550–1650°C. The sintering temperature must be high enough and the dwell time long enough to ensure high–density material (>98% of theoretical density), but the temperature must not be so high, or the dwell time so long, that exaggerated grain growth occurs. Low firing temperatures result in material with low density and whose strength is controlled by pore clusters; high firing temperatures produce a dense material whose strength is controlled by large grains.[21] Several sintering methods have been used to process BASE tubes: batch sintering, rapid zone sintering, and continuous pass–through sintering. With batch firing, high–quality electrolyte tubes can be produced at moderate production levels. Continuous sintering or rapid zone sintering would be more suitable for higher production levels, although zone sintering must be optimized before it can be used to produce tubes with acceptable lifetimes in sodium–sodium cells.[22]

The kinetics for conversion to the more conductive β" phase are sluggish compared to the densification kinetics; therefore, BASE tubes must be annealed after sintering in some rapid sintering schemes. Incomplete conversion to the β" phase has a dominant influence on the ionic conductivity of β"-alumina and its temperature dependence. Both resistivity and activation energy for resistivity decrease as conversion to the β" phase proceeds.[23] Incomplete conversion also leaves residual phases that can affect subcritical crack growth behavior and thereby the long-term lifetime of the material.[24] The postsintering anneal is carried out at some temperature (1400–1475°C) lower than the sintering temperature to allow for complete conversion to the β"-phase while avoiding exaggerated grain growth. Annealing a hot-pressed sample at 1400°C for 24 h has shown that it is possible to produce fine-grained, high-strength β"-alumina with acceptable resistivity.[25]

Because of the high temperatures used in processing BASE tubes, volatilization of the alkali components can be a problem if the proper precautions are not taken. Several schemes have been developed for preventing the loss of the alkali components.[22] Several of the techniques are based on the idea of encapsulating the BASE tube in one of the following materials: platinum, an αalumina tube pretreated with Na_2O or lined with a reuseable platinum liner, a larger BASE tube with similar Na_2O composition, or a chemically inert refractory container such as MgO or ZrO_2. Other schemes include packing the green tube in Na_2O-rich powder during firing, and rapid zone sintering. In zone sintering, volatilization is minimized without encapsulation, because an Na_2O-rich environment is established in the hot zone of the furnace, and the tubes remain in the hot zone for only a very short time.[22]

It has been shown that large grains and voids, caused by inhomogeneities and impurities in the β"-alumina powder, commonly cause failure of BASE tubes.[2–5] Table 1 summarizes the mechanical and electrical properties found in the literature on β"-alumina and shows that tubes with satisfactory strengths and fracture toughness can be fabricated. However, the scatter in these data suggest that without careful processing, tubes with much lower strengths and fracture toughness can also be produced. The fracture strengths (σ_F) range from 3 to 45 kpsi, with most values falling in the range of 20–30 kpsi, whereas fracture toughness (K_{IC}) ranges from 1.9 to 3.7 MPa-$m^{1/2}$. Electrical resistivity at 300°C shows much less scatter, with the majority of values in the range of 4–6 Ω–cm, which is considered acceptable for BASE tubes.

Several additional comments might be made about Table 1. The data from Ref. 25 clearly show the effect of grain size on the mechanical properties of β"-alumina: strength decreases rapidly with increasing grain

Table 1. Electrical and mechanical properties of β''-Al_2O_3

Ref. No.	Fabrication Method	Grain Size (μm)	K_{IC} (MPa-m$^{1/2}$)	σ_F (kpsi)	Weibull Modulus	ρ (Ωcm)
3	Zeta/IsoP	No GS given	1.9	19.0 (burst)	7.81	4.9
"	Spray Dry/IsoP	"	2.0	23.3 (burst)	10.36	3.9
"	Spray Dry (additives)/IsoP	"	–	22.3 (burst)	13.24	3.9?
6	Non-Zeta/Unconverted/IsoP	Large: 20–50 Matrix: <5	–	20–26 (4 pt. bend)	–	5–7
"	Non-Zeta/ Part. Converted/IsoP	Uniform ≈100	–	≈25 (4 pt. bend)	–	2.8
"	Zeta/IsoP	Large: 30–50 Matrix: <5	–	30 +/- 4 (4 pt. bend)	–	4
22	Zeta/IsoP/batch sinter	No GS given	–	37 (diametral)	–	4.3
"	Zeta/IsoP/continuous sinter	No GS given	–	39–45 (diametral)	–	4.4–4.7
"	Zeta/IsoP/zone sinter	Uniform. ≈10	–	–	–	25
10	Zeta/IsoP/Al_2O_3 "B"	Large: <100 Matrix: 5–10	–	42 (diametral)	–	4.1 – 4.4
"	Zeta/IsoP/Al_2O_3 "D"	Large: <100 Matrix: 5–10	–	24 (diametral)	–	4.6
25	Zeta/IsoP/sinter	Duplex Large ≈120	3.21 DCB[a]	18.0 (4 pt. bend)	–	–
"	Zeta/IsoP/sinter	≈ 35	3.2 DCB[a]	27.5 (4 pt. bend)	–	–
"	Partially Converted/IsoP/sinter	≈ 100	3.2 DCB[a]	13.5 (4 pt. bend)	-	-
"	Partially Converted/Hot Press	< 4	2.72 DCB[a] (A)	30.0 (4 pt. bend)	-	~5
"	Partially Converted/Hot Press	200–300	2.96 DCB(A)	13 – 22 (4 pt. bend)	–	
"	Partially Converted/Hot Press	< 4	3.5 DCB(C)	30.0 (4 pt. bend)	–	–
"	Partially Converted/Hot Press	200–300	3.7 DCB(C)	13 – 22 (4 pt. bend)	-	-
26	Zeta/IsoP/Sinter	1–2	–	–	–	4.8
"	Zeta/IsoP/Sinter	≈100	–	–	–	2.8
24	Non-zeta/0.25 Li_2O, 9.25 Na_2O/ IsoP/Sinter	≈3	2.3	30.5 (4 pt. bend)	–	12–14
"	Non-zeta/0.7 Li_2O, 8.7 Na_2O/ IsoP/Sinter	40% ≈3 60% ≈90	2.8	18.0 (4 pt. bend)	–	4 – 6
"	Non-zeta/Unk. Li_2O, 8.7 Na_2O/ Hot P	< 5	3.6	39.0 (4 pt. bend)	–	4 –5
4	Spray-dried/IsoP/zone sinter	Few: 200 Matrix: ≈2	–	27.0 – 44.0 (C-rings)	6–10	–
"	"	Few: 200 Matrix: ≈2	3.48	3.0 – 21.0(13) (burst)	–	–
5	Direct mix/IsoP/zone sinter	–	3.2	10.0 – 42.0 (C rings)	–	–
"	"	–	3.2	<3 –10 (burst)	–	–
21	Spray Dry/IsoP/zone sinter	–	2.9	33 –39 (C rings)	–	–
1	New "βetalyte" tubes (Thick Wall) Baked @ 900°C	–	–	19 – 28 (diametral)	–	–
"	Used "βetalyte" tubes (Thin Wall) Not baked out.	–	–	23 – 37 (diametral)	–	–

[a]DCB: Double cantilever beam technique; DCB(A) is with hot-pressing in direction of fracture plane; DCB(C) is with hot-pressing perpendicular to fracture plane.

size for grains larger than 120 µm. In fact, two fracture regimes were identified: for grains smaller than 120 µm, strength depended only weakly on grain size, but for larger grains, strength was a strong function of grain size.[26] Such behavior has been explained on the basis of the relative sizes of grains and cracks[27] and indicates that grain sizes larger than ≈100 µm must be avoided. The data of Ref. 25 also show the directional dependence of the mechanical properties for material produced by hot pressing. "DCB(A)" in Table 1 represents measurement of fracture toughness by the double–cantilever–beam method with the direction of hot pressing lying in the fracture plane, whereas "DCB(C)" represents measurement with the hot–pressing direction perpendicular to the fracture plane. By contrast, Ref. 28 shows that in the small–grain regime, resistivity is only slightly affected by grain size.

Also to be noted in Table 1, the data from Ref. 6 demonstrate that materials produced by the zeta process have comparable resistivity and slightly higher strengths than materials produced by the non–zeta processes, while the data from Ref. 3 show that tubes produced from spray–dried powder are probably better yet. Finally, the data of Ref. 22 show a high resistivity (25 Ω–cm) for tubes sintered by rapid zone sintering and then annealed at 1400°C. It was also reported in Ref. 22 that zone–sintered tubes were prone to massive early failure in tests of sodium–sodium cells. The high resistivity and early failure were attributed to the formation of a resistive layer due to a small loss of soda (≈0.2–0.3 wt.%) from the external surface. The high resistivity and massive failure are somewhat anomalous, however, because Ref. 22 also reported that the microstructure of zone–sintered samples was uniform and fine (grain size <≈10 µm) and that the resistivity was typically 4–5 Ω–cm after a postsintering anneal at 1400°C.

Many studies have focused on the addition of zirconia (ZrO_2) to improve the mechanical properties of β"–alumina.[29–39] ZrO_2 additions act in several ways to improve properties: first, ZrO_2 inhibits abnormal grain growth, thus preventing formation of one type of life–limiting flaw. Second, ZrO_2 has been reported to lower the sintering temperature of β"–alumina,[32] which might also help to avoid exaggerated grain growth. Third, the material is toughened if ZrO_2 is retained in the tetragonal phase.

For zirconia to be an effective toughening agent, it is important to control the zirconia grain size, because the tetragonal phase is retained only if the grain size remains below a critical value.[29] Retention of the tetragonal phase is required in the toughening process, because it is the tetragonal–to–

monoclinic transformation that requires additional work by the applied stress when the transformation is induced by a propagating crack. For a 15 vol.% ZrO_2/β''–alumina composite, the critical grain size is ≈1 μm.[30,31] Other requirements for effective toughening are that zirconia must be well dispersed and free from agglomerates; otherwise some untoughened regions can exist that are particularly susceptible to crack initiation.[37] This means that strict control of processing variables such as initial zirconia particle size and heat treatment schedule is essential for effective toughening. Table 2 demonstrates that toughening with zirconia additions has been more effective in some studies than in others; nevertheless, improved mechanical properties generally result from zirconia additions.

Through this literature survey, a consensus has been found on several points. First, the life–limiting flaws in BASE tubes are generally large grains and voids. Second, these flaws are thought to originate from inhomogeneities and impurities in the β"–alumina powder. For mechanically mixed materials, powders produced by the zeta process appear to be more homogeneous, judging by the improvement in properties of samples made by this process. However, mechanical mixing and the other processing steps associated with the zeta process may introduce impurities. The impurity levels in β"–alumina powders can be reduced by spray drying, a single–step processing method that produces β"–alumina materials with the best mechanical properties. Finally, additions of zirconia appear to significantly increase the strength and fracture toughness of β"–alumina, but strict control of the processing must be exercised to control the grain size of the zirconia and to prevent the introduction of zirconia agglomerates.

Based on this critical review of the literature, an effort was initiated in the area of powder preparation to obtain homogeneous, high–purity β"–alumina powders. A limited effort was also spent in making β"–alumina /ZrO_2 composite powders in an attempt to improve the mechanical properties of β"–alumina . These powders were used to explore the feasibility of processing β"–alumina tubes by extrusion or slip casting. Green β"–alumina tubes were sintered by both conventional and microwave methods. In parallel, a study of the mechanical properties and microstructures of commercially available β"–alumina tubes was also completed to assess the state of the art in mechanical properties of β"–alumina tubes. These studies on fabrication and synthesis and the mechanical/microstructural evaluations were performed to demonstrate the potential for improving the microstructure and mechanical properties of β"–alumina tubes. Residual strain (stress) measurements and nondestructive evaluation of the β"–alumina tubes were

Table 2. Mechanical properties of ZrO_2-toughened β''-Al_2O_3

Ref. No.	Fabrication Method	K_{IC} ($MPa\text{-}m^{1/2}$)	σ_F (kpsi)	Weibull Modulus	$\rho_{300°C}$ (Ωcm)
3	$ZrO_2(0\%Y_2O_3)$/Zeta/IsoP	2.5	–	–	6.8
"	"	2.3	–	–	12.3
"	$ZrO_2(1\%Y_2O_3)$/Zeta/IsoP	2.8	21.4	12.00	5.7
"	"	2.9	"	"	5.2
"	$ZrO_2(2\%Y_2O_3)$/Zeta/IsoP	2.5	25.7	6.91	5.1
"	"	2.4	"	"	4.9
"	$ZrO_2(3\%Y_2O_3)$/Zeta/IsoP	2.3	20.4	6.72	5.5
"	"	2.3	"	"	5.3
"	$ZrO_2(0\%Y_2O_3)$/Spray Dry/IsoP	3.6	–	–	6.5
"	$ZrO_2(1\%Y_2O_3)$/Spray Dry/IsoP	3.1	21.4	12.00	5.4
"	$ZrO_2(2\%Y_2O_3)$/Spray Dry/IsoP	2.7	25.7	6.91	4.9
"	"	3.0	"	"	4.6
"	$ZrO_2(3\%Y_2O_3)$/Spray Dry/IsoP	2.8	20.5	6.72	4.6
"	"	2.9	"	"	4.7
27	15 vol% ZrO_2 (1,2,3,4 mol% Y_2O_3)	4.5	52.5	–	7.7
37	15 vol% ZrO_2(2.2 mol% Y_2O_3)	5.0	52.5	–	6–8
36	8 wt% ZrO_2	4.0	52.5	16	–
28	20 vol% ZrO_2	4.35	58.0	–	9
29	15 wt% ZrO_2	5.0–8.0	33–45	–	6.4
"	25 wt% ZrO_2	–	55	–	"high"
30	15 vol% ZrO_2(2 mol% Y_2O_3)	5.0	–	–	–
31	15 vol% ZrO_2	4.1	50.0	–	8–9
33	12–15 vol% ZrO_2	3.8–4.2	–	–	–

made to locate critical flaws for the purpose of quality control. This portion of the study demonstrated the ability to screen defective β"-alumina tubes. A comprehensive stress analysis was completed to evaluate the failure modes of the tube, and the sodium pump in use at the Environmental Research Institute of Michigan was tested under a variety of conditions to evaluate the parameters controlling its performance. The final results for each of these areas are summarized in the following sections.

3 Mechanical and Microstructural Evaluation

3.1 Evaluation of Mechanical Properties

Mechanical properties (fracture toughness and strength) and microstructures of nine commercial β"-alumina tubes (seven from Ceramatec and two from Beta R&D) have been evaluated. Of the seven Ceramatec tubes, four were in as-fabricated condition and three had been exposed to liquid sodium. All of the Beta R&D tubes were in as-fabricated condition. More than 50 ring specimens (≈3 mm wide) were machined from each tube; their strength was then measured in a diametral mode.[40] The Ceramatec tubes were ≈15.2 mm in diameter, while the Beta R&D tubes were ≈33 mm in diameter. Strength of the rings from the four as-fabricated Ceramatec tubes ranged from 133 to 317 MPa, and a typical value of fracture toughness measured by indentation technique[41] was 1.8 ± 0.2 $\mathrm{MPa}\sqrt{\mathrm{m}}$. The average strength of each tube was 175 ± 16, 204 ± 14, 279 ± 26, and 238 ± 25 MPa. On the other hand, the strength of the two Beta R&D tubes ranged from 84 to 234 MPa, with the average value for each tube at 155 ± 34 and 190 ± 27 MPa. A graphical representation of strength for these tubes with standard deviation is shown in Fig. 1. The tubes represented by notations CX and CL are from Ceramatec, and those represented by H and T are from Beta R&D. Based on these data, it seems that Ceramatec tubes have slightly higher strength than Beta R&D tubes. The microstructure (Fig. 2) of Ceramatec tubes typically included large grains of ≈25 to 60 μm, whereas the Beta R&D tubes (Fig. 3) had relatively fine grains of ≈10–15 μm in length. Because the Beta R&D tubes have smaller grains, they were expected to have higher strength than the Ceramatec tubes. However, the measured strength shows the opposite trend, i.e., the Ceramatec tubes have higher strength. This discrepancy may be related to differences in grain microstructure (morphology).

A statistical analysis of the strength data was performed to construct Weibull plots of stress vs. probability of failure on a log scale (Fig. 4). From

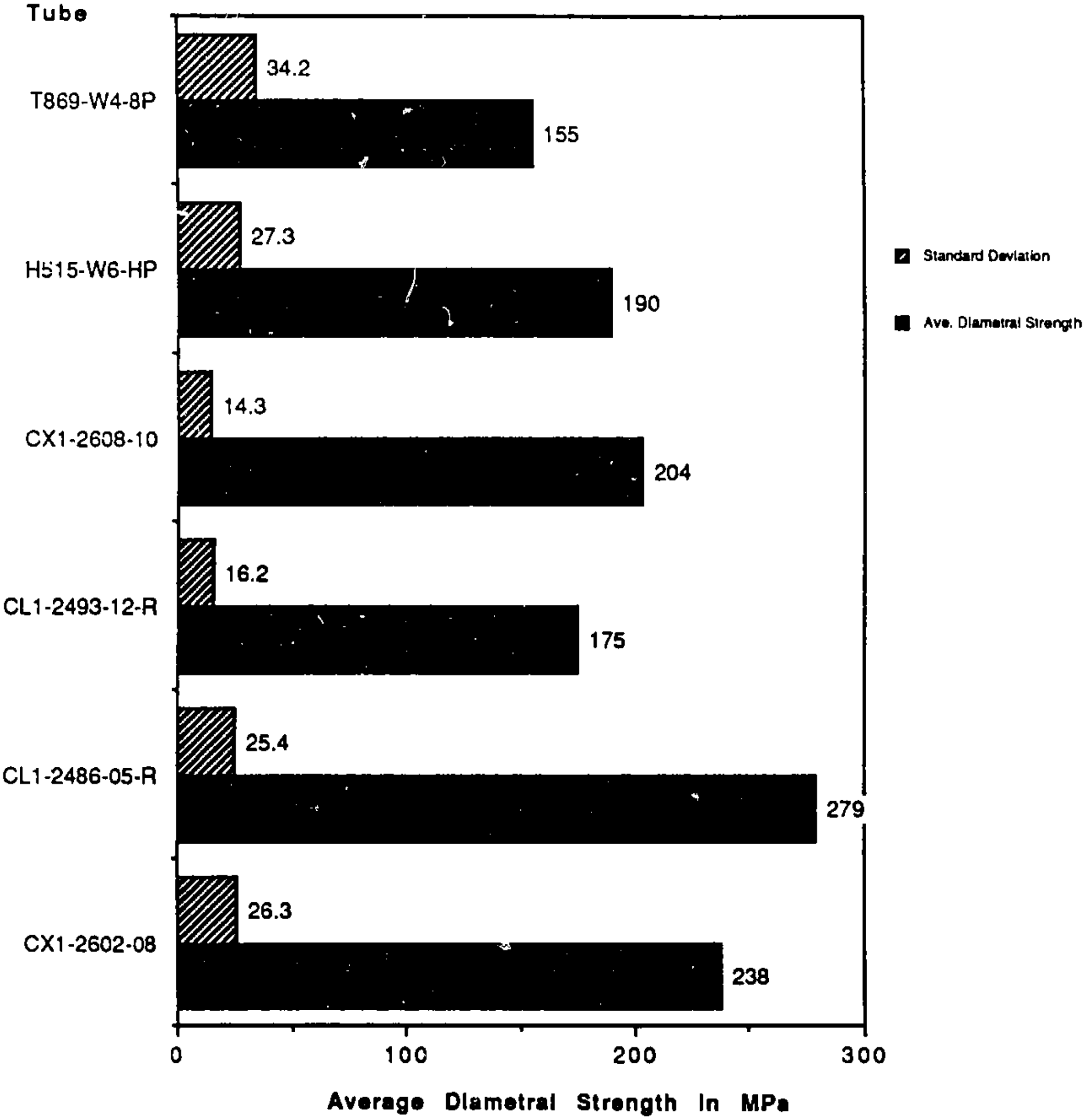

Fig. 1. Diametral strength of different tubes. CX and CL represent Ceramatec tubes; H and T represent Beta R&D tubes.

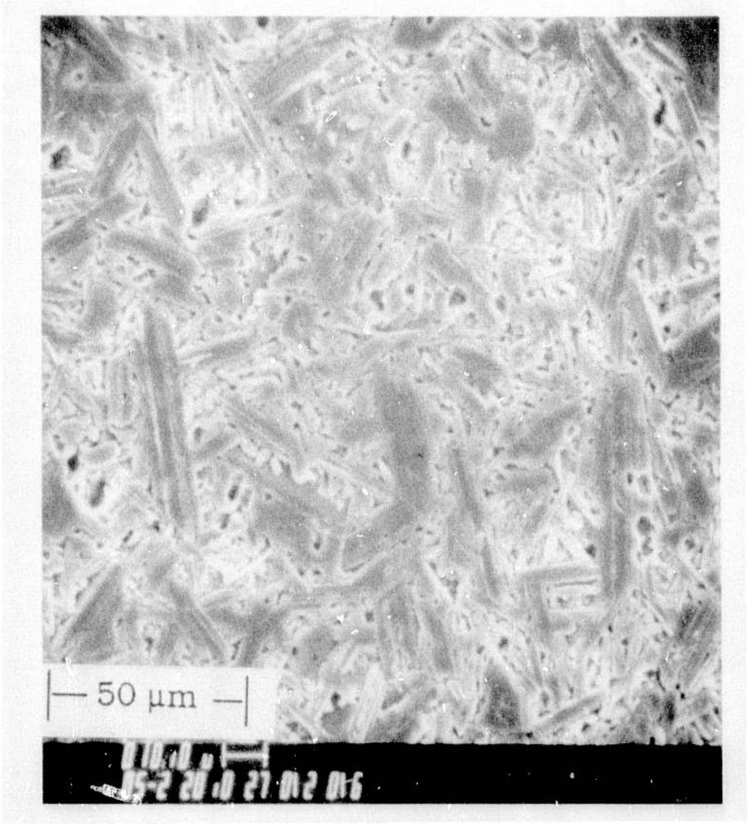

Fig. 2. Typical grain microstructure of Ceramatec tubes

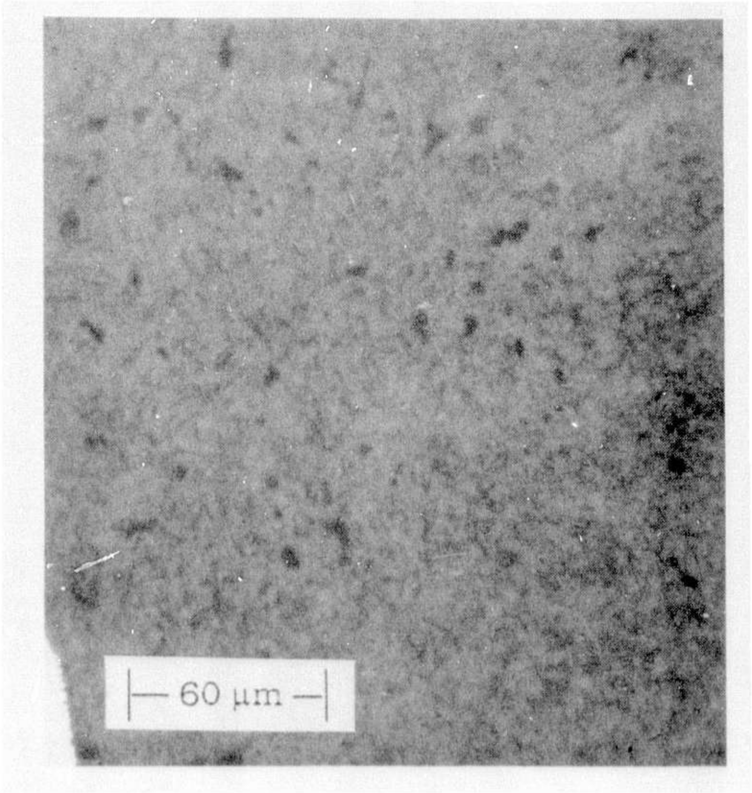

Fig. 3. Typical grain microstructure of Beta R&D tubes

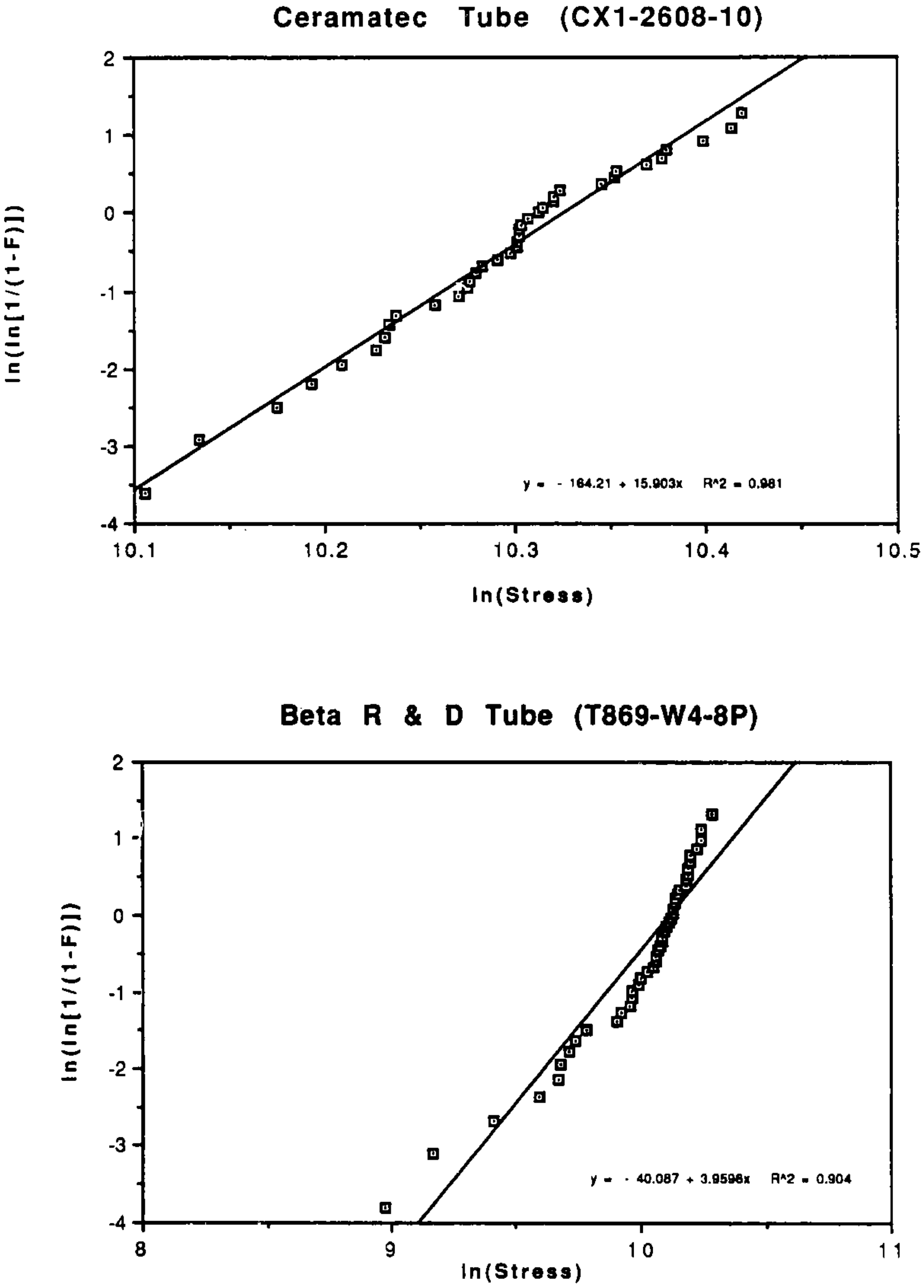

Ceramatec Tube (CX1-2608-10)

Beta R & D Tube (T869-W4-8P)

Fig. 4. Probability of failure (F) vs. stress plots on log-log scale for Ceramatec and Beta R&D tubes. Weibull modulus values were calculated from slope of straight lines in these plots.

the slopes of straight lines in these plots, the well-known Weibull moduli (m) were determined to be ≈10–16 for the Ceramatec tubes and ≈4–7 for the Beta R&D tubes. The variation of Weibull modulus for different tubes is shown in Fig. 5. The value of $m > 10$ represents a reasonable degree of reproducibility of strength data for Ceramatec tubes. A lower value of m for the Beta R&D tubes indicates a larger scatter in the strength data; a higher value is desirable.

The average strengths of the three Ceramatec tubes exposed to liquid sodium at approximately 900°C for 50–160 h were 326 ± 30, 224 ± 51, and 242 ± 21 MPa, respectively. The strength value (326 ± 30 MPa) of the first tube is questionable because of equipment problems. Based on the last two values, the strength of the exposed tube seems to be slightly less after exposure than that of the strongest tube in as-fabricated condition. It was also observed that for these tubes, exposure temperature did not seem to have noticeable effects on the strength values.

3.2 Summary of Mechanical and Microstructural Evaluation

The diametral strength of the Ceramatec tubes ranged from 133 to 317 MPa, and a typical value of fracture toughness measured by indentation was $1.8 \pm 0.2\ \mathrm{MPa}\sqrt{\mathrm{m}}$. Strength of the Beta R&D tubes was 84 to 234 MPa. Weibull moduli were ≈10–16 for the Ceramatec tubes and ≈4–7 for the Beta R&D tubes. Higher strength and Weibull modulus values suggest improved reliability for the Ceramatec tubes. Exposure of Ceramatec tubes to liquid sodium had no appreciable deleterious effects on strength.

4 Processing of β"- alumina Tubes

Green β"- alumina tubes were formed by isostatic pressing, extrusion, and slip casting. These tubes were then sintered by both conventional and microwave plasma methods.

4.1 Powder Processing

Several batches of β"- alumina powder were prepared by the zeta process,[6] in which Li_2O was added as Li_2O-$5Al_2O_3$ for uniform distribution of Li_2O. Li_2O–$5Al_2O_3$ was made by mixing appropriate amounts of Al_2O_3 and $LiNO_3$ and calcining the mixture at ≈1250°C for 4 h in air. Subsequently, appropriate amounts of Al_2O_3, Na_2CO_3, and Li_2O–$5Al_2O_3$ were mixed to obtain a stoichiometric composition of β"- alumina. The powder mixture

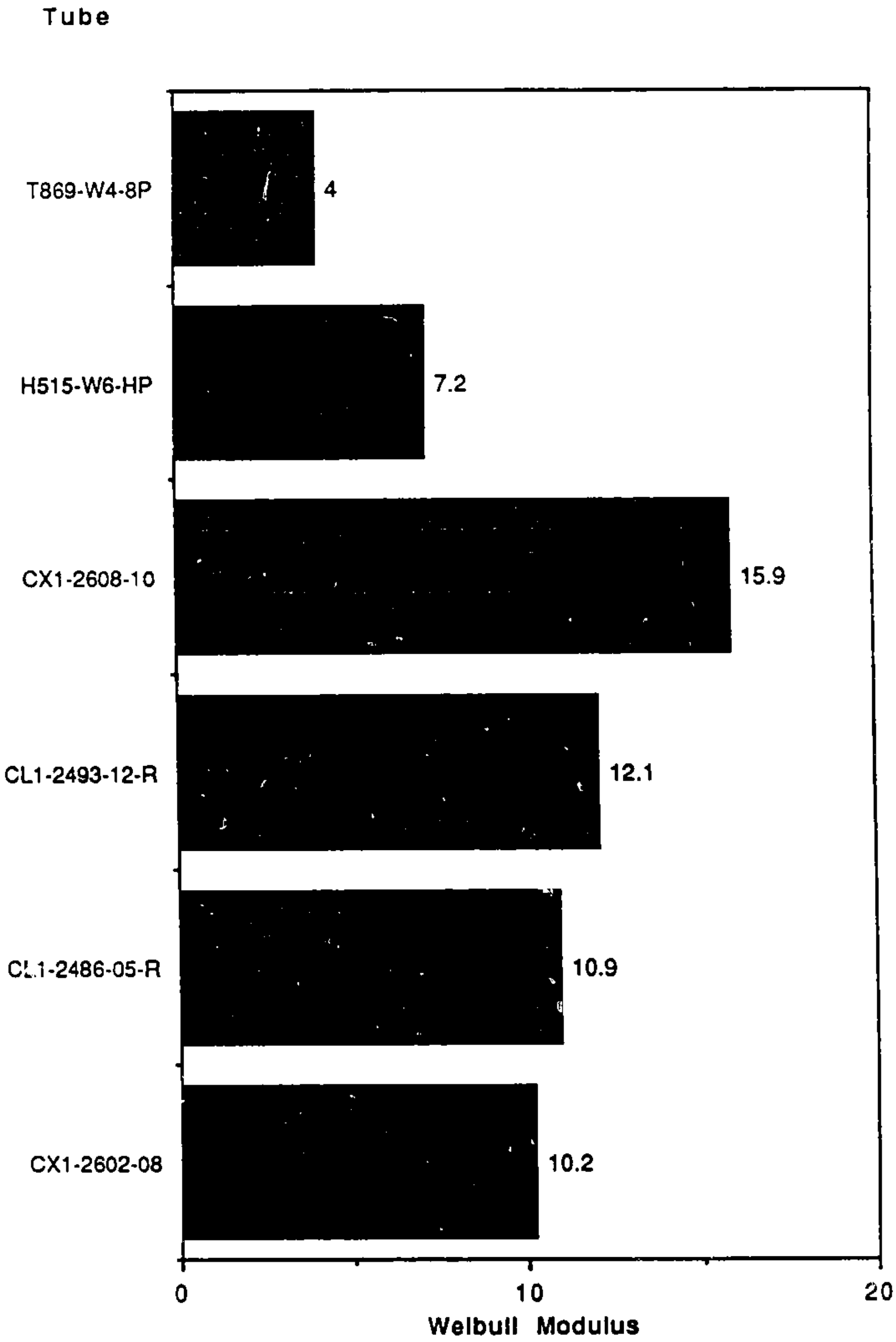

Fig. 5. Weibull modulus of strength data for different tubes. CX and CL represent Ceramatec tubes; H and T represent Beta R&D tubes.

was then calcined at 1250°C for 4 h. This powder was subsequently milled, and the average particle size was measured to be ≈6.2 μm before milling and 3.2 μm after milling. Phase purity of the powder was confirmed by X-ray analysis. Several 100–280 g batches of β"-alumina powder were made and were used to evaluate the feasibility of slip casting and extrusion of β"-alumina tubes.

4.2 Fabrication and Conventional Sintering of Green Tubes

Appropriate binder (3.9 wt. %), plasticizer (3.9 wt. %), and deflocculant (2.2 wt. %) were mixed with β"- alumina powder to make slips for casting and extrusion. Two extrusion runs were made to produce several feet of tube (≈0.25 in. in diameter). In addition, several slip-casting runs were made and two good-quality tubes (≈8 in. long and 0.5 in. in diameter) were slip cast. Currently, the extrusion and slip-casting parameters are being optimized. These tubes, as well as small pellets (0.5 in. in diameter pressed at ≈30000 psi), have been sintered at various temperatures for different lengths of time to achieve high density and fine-grained microstructures. Sintering temperatures ranged from 1595 to 1615°C and sintering time was 5 min to 2 h. These heat treatments resulted in densities of ≈95–98% with varying microstructures. A typical micrograph of extruded tube specimens sintered at 1595°C for 5 min is shown in Fig. 6. It was observed that increasing sintering time at a given temperature or increasing sintering temperature for a given length of time resulted in increased density. However, this increase was generally associated with a corresponding increase in grain size. Therefore, an effort was initiated to optimize the heat-treatment parameters to maintain appropriately fine microstructure. So far, a density of >98% theoretical with a fine microstructure of ≈3–12 μm has been achieved by sintering at 1605°C for 15 min. This high density with fine microstructure indicates that the heat-treatment procedures are close to optimum. Detailed mechanical evaluations, however, are required for confirmation.

With powder preparation optimized, high-quality β"-alumina powders can be produced routinely using zeta lithia as a source of lithia. This powder has fine average particle size of ≈3 μm and has been used to fabricate tubes by both extrusion and slip casting. Effects of the resulting relatively fine-grained (3–12 μm) microstructure on mechanical properties should be evaluated for optimization of heat treatment parameters. Tubes were also produced from this powder by isostatic pressing but were sintered by microwave plasma sintering, as described in the next section.

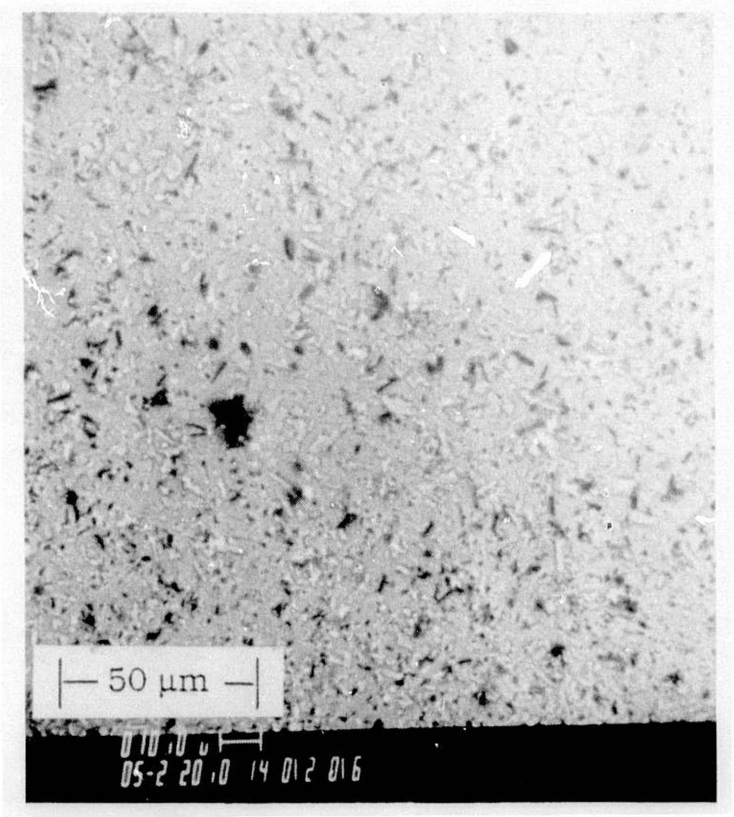

Fig. 6. Typical micrograph of extruded β"-alumina tube sintered at 1595°C for 5 min, showing fine uniform grain microstructure

4.3 Isostatic Pressing and Microwave Sintering

4.3.1 Rationale

Microwave sintering is considered by some as fast and uniform and to employ significantly lower temperatures than in conventional sintering. For these reasons, it appears to be highly attractive for sintering β"-alumina because soda loss could be minimized and the costly encapsulation required for conventional sintering could perhaps be eliminated.

However, temperature uniformity is very difficult to achieve during microwave heating of tubes because of the exponential temperature dependence of the effective electrical conductivity that governs the rate of conversion of microwave energy to heat. Thus, a local hot spot will become hotter and local temperature nonuniformity can become extreme.

A plasma will greatly simplify the temperature uniformity problem because heat is deposited on the surface from the hot plasma, and a local hot spot will absorb less heat than neighboring regions. Thus, stable heating can be attained easily.

Microwave plasma sintering holds the promise of using the best elements of both microwave and plasma heating. The heat input from the plasma will tend to counter the tendency to temperature nonuniformity of purely microwave heating. Partition of the microwave energy between plasma excitation and direct coupling to the specimen can be achieved by control of the plasma composition, pressure, and physical size. The net result will be more rapid and stable heating than possible with microwave heating alone; at the same time, the beneficial effects of microwave excitation may be realized, at least in part.

4.3.2 Temperature Gradients during Microwave Sintering

Because it has been reported that β"-alumina tubes often fail by cracks that form on their outer surface, it may be advantageous to design into the tube a residual stress gradient, with the surface in compression. Microwave heating provides a unique method of incorporating just such a stress gradient. Because microwave energy is transformed to heat throughout the tube wall, but the heat is dissipated from the outer surface, the inner surface will be hotter than the outer surface during sintering. Thermal contraction during cooling from the sintering temperature will place the outer surface in compression and the inner surface in tension. These residual stresses are absent in conventionally sintered tubes.

The magnitude of residual stress can be controlled by varying the temperature gradients with insulation or plasma heating. In the latter, the relative amount of microwave heating can be controlled by varying the microwave penetration of the plasma through regulation of pressure and plasma composition. In the extreme case of atmospheric pressure, little of the microwave energy penetrates through the plasma to the specimen, and the temperature gradient would be nearly zero.

Expected temperature gradients were explored by developing a simple finite–element computer program (on a spreadsheet) that allows computation of steady–state temperature profiles, given the temperature dependence of the thermal conductivities of both the specimen and insulation and the temperature dependence of the effective electrical conductivity that governs heating in a microwave field.

Although values for thermal conductivity and the activation energy of microwave loss in β"-alumina were not available, the selected estimates cannot be grossly in error. The thermal conductivity was assumed to be 2 W/mK (40% of the approximate value for α-alumina), while the activation energy of the conductivity was assumed to be 1 eV. The results shown in Table 3 were obtained for a tube of 15 mm outside diameter (OD) x 12 mm inside diameter (ID), with a center temperature of 1600°C (1873 K) and the use of various thicknesses of insulation. A lower thermal conductivity would increase the temperature difference and decrease the microwave power required.

It can be seen from these calculations that a considerable range of temperature differences is accessible in microwave heating. Of course, the temperature gradients in an atmospheric-pressure microwave plasma would be much lower, because most of the heating would be by the plasma.

4.3.3 Microwave Plasma Sintering Trials

A few microwave plasma sintering trials were conducted to densify β"-alumina tubes. The β"- alumina powder was mixed with a 5% polyethylene glycol (PEG) binder. Closed-end tubes approximately 12 mm in diameter by 65 mm long were isostatically pressed at 280 MPa. The binder was burned out by heating to 700°C in air for 1 h and held stationary in a TM_{012} tuned cylindrical cavity. Severe cracking was observed in all tubes. Based on extensive experience with plasma sintering of various α-alumina powders, the cracking probably can be avoided by further refinements in powder processing. Specifically, a finer particle size is required.

Eventually the quartz plasma tube failed. It was discovered that it had overheated, and soda lost from the specimens had reacted with it, causing it to fracture upon cooling.

4.3.4 Improved Microwave Plasma Sintering

Very recent findings have pointed the way to solving the problems mentioned above and significantly enhancing the probability of successful microwave plasma sintering of β"-alumina. The basic idea is to use an α-alumina tube, instead of the quartz tube, to contain the plasma. This would preclude the need to cool the tube, which is difficult to do well in micro

Table 3. Computed temperature at the surface of a tube, difference between interior and surface temperatures, and power required to heat a 15-mm OD x 12-mm ID tube during microwave sintering.

Insulation thickness (mm)	0	2.5	5	10
Surface temperature (K)	1738	1833	1846	1855
Temperature difference	135	39.5	27	18
Total microwave power (W/cm)	152	51	36	26

wave fields. We have learned that a large plasma volume is not required. The plasma tube need be only a few millimeters larger than the specimen. This will significantly reduce soda loss, since the inner surface of the plasma tube will become saturated quickly with soda and the plasma will become doped with soda, inhibiting further soda loss. We observed this inhibition some years ago in the RF-induction-coupled plasma sintering of β''-alumina.

A further benefit of the smaller plasma tube and resulting thinner plasma layer is greater flexibility in partitioning the microwave energy between the plasma and direct coupling with the specimen.

The temperature profile program was used to compute expected temperature profiles for an insulated α-alumina plasma tube. It was assumed that a plasma and β''-alumina tube were present within an alumina tube measuring 23 mm OD x 20 mm ID, surrounded by 7 mm of SALI (Zircar) alumina fiber insulation, which is the maximum amount that would fit within the quartz tube of the TM_{012} cavity. Various amounts of power applied to the plasma + specimen were specified. As before, the temperature of the inner wall of the tube was 1600°C. The results are presented in Table 4.

The computed surface temperatures of the insulation are within the limits of fused quartz, thus precluding the need to cool this tube.

Note that with the increase in power to the plasma, there is a dramatic reduction in the microwave heating of the insulation. This is because the lossy plasma requires a much lower microwave field intensity than the insulation to maintain a given level of power absorption.

Table 4. Computed temperature at the surface of the insulation and the power required to heat a 23 mm OD x 20 mm ID α-alumina plasma tube with 7 mm of SALI insulation at various amounts of power applied to the plasma + specimen

Plasma power (W/cm)	0	10	20	30
Surface temperature (K)	956	954	951	949
Total microwave power (W/cm)	44.1	43.6	43.2	42.8
Microwave power to insulation	44.1	33.6	23.2	12.8

4.3.5 Future Directions in Sintering

The insulated microwave plasma sintering system discussed above has substantial potential as a highly efficient and rapid method of sintering β"-alumina tubes. The following points are to be made:

- Temperature uniformity will be much greater than is possible with purely microwave heating. In fact, microwave heating of tubes, if possible at all, requires very slow heating.

- A controlled residual stress (outer surface in compression) can be built into the tube wall by sintering the tube under partial microwave and partial plasma heating.

- High speed processing is possible. Past experience with the RF–induction–coupled plasma has demonstrated that a linear translation rate of 20 mm/min is routinely achievable with properly designed powder. Higher rates may be possible in this microwave system because the high–temperature zone will be broader than in the RF plasma.

- Soda loss will be minimized because:

  –High–speed passage through the plasma will result in short residence time at high temperature.

  –A soda-rich surface will build up on the inner wall of the plasma tube as the first few β"–alumina tubes pass through.

Alternatively, a liner rich in soda can be inserted into the plasma tube.

–The lower anticipated firing temperature will result in a lower soda vapor pressure.

- Continuous processing is possible.
- Power requirements are very low. A maximum of 500 W should be more than sufficient to sinter β"-alumina tubes at the highest rate achievable without cracking (on the order of 20 mm/min or more).
- The cost of equipment will be very low. For experimental purposes, the magnetron and basic power supply could be obtained from an inexpensive microwave oven. A simple cylindrical cavity can be used to couple the microwave energy into the plasma and specimen.
- A relatively simple system could be designed to include closed–loop peak temperature control.

Experiments will be designed to explore the limits of this method. Variables to be considered are specimen translation rate, peak temperature, plasma composition, plasma pressure, and plasma dimensions (clearance between specimen OD and plasma tube ID). Powder design and evaluation for high–speed sintering, with required final properties, will be important. Soda loss and soda buildup in the system will be quantified. High–soda plasma tube liners (wall deposits, inserts, etc.) will be evaluated, if needed to minimize soda loss.

The reentrant cavity being designed at ANL would be ideally suited to the insulated plasma tube scheme. The low power requirements may make it feasible to use relatively inexpensive low–power 915–MHz generators, with a resulting increase in the dimensions of the cavity and size of tube that can be sintered.

4.4 Toughening by Second–Phase Additions

The effects of second–phase additions on fracture toughness of β"-alumina have been studied in an effort to improve the toughness of β"-alumina. β"- alumina powder was mixed with 10% tetragonal zirconia polycrystals (TZP), and pellets (1.3 cm in diameter) of the composite powder were isostatically pressed at ≈200 MPa. One composite pellet sintered at 1595°C for 5 min had a density of ≈96% theoretical and a fracture toughness of 3.8 ± 0.3 MPa. This represents an approximately two–fold increase in toughness of β"- alumina as a result of the 10% TZP addition. Microstructural evaluation indicates that the composite has a fine grain (<5 µm) microstructure with a few isolated large (>40 µm) grains. Further sintering studies are needed to optimize the microstructure. Additional improvement in toughness is expected with optimization of heat treatments and TZP contents. This result has important implications for the structural reliability of β"- alumina tubes.

5 NDE of Commercial Tubes

5.1 Neutron Diffraction

Neutron diffraction can be used to estimate the residual strains in BASE tubes and provide thermal expansion data as a function of crystallographic direction. Thermal expansion data can then be used to predict fabrication–induced residual strains and stresses. The advantages of neutron diffraction over more traditional methods of studying stress, such as X-ray diffraction, arise from some unusual characteristics of neutrons. The neutron can penetrate very deeply into or through many materials. Its penetrating ability is comparable to very–high–energy X-rays, but the neutron energies involved are relatively low, and little or no damage is done to the material. The neutron's capability to penetrate deeply facilitates the study of complex shapes and reduces the sensitivity to surface quality and microstructure, a problem with X-rays.

The neutron diffraction work described in this paper was carried out at the Intense Pulsed Neutron Source (IPNS) at ANL. In the IPNS, energetic pulses of protons delivered by an accelerator strike a uranium target in a shielded structure and knock neutrons out of the target. Through holes in the shielding, a collimated beam of neutron bursts emerges with the faster neutrons leading the slower. The neutrons move along the flight path and strike the sample under study, whereupon they are scattered in various directions. Banks of neutron detectors, which constitute a diffractometer, collect the scattered neutrons and provide the needed information.

The IPNS is useful because bulk strain measurements can be made as a function of temperature and the entire neutron diffraction spectrum is collected at once for various spatial directions. Computer programs necessary to carry out the analyses are readily available, with the resolution for measuring strain about 10^{-4}. Strain in the material is measured by observing the change in the separation of the planes on which the atoms are located. A simple equation, Bragg's law ($2d\sin\theta = \lambda$), determines the scattering angle θ at which a diffracted beam of wavelength λ will be very intense for a lattice spacing d.

Because there are many different planes and corresponding spacings, the scattered neutron spectrum -- intensity versus wavelength -- will show sharp peaks at certain wavelengths. If the interatomic spacing changes, i.e., there is a change in d, there will be a corresponding change in λ at which a given reflection occurs. The movement of the peaks $\Delta\lambda/\lambda$, either to left or right, is the measure of the strain we seek. Where there is a strain distribution for a specific crystallographic direction, as described here, the strain will show as a broadening of the line. Although the experimental arrangement seems complicated, after it has been properly set up an experiment at IPNS can be carried out rather easily.

Neutron diffraction experiments have been carried out on Ceramatec BASE tubes. In the experiments described here, Bragg's law is used first to determine the lattice spacing d for a particular *hkl* reflection averaged over the sample. The distribution in lattice spacing is then determined from the full width at half maximum (FWHM) of the various peaks. The FWHM of the diffraction peaks are used for the strain distribution analysis, as described in the following section. The diffraction pattern is presented in time-of-flight units (x-axis). Time of flight is related to neutron wavelength by $\lambda = ht/mL$, where λ is the neutron wavelength, h is Planck's constant, t is the time of flight for a neutron to reach a detector after leaving the neutron source, L is the flight path for the neutron from the source to the detector, and m is the neutron mass. Bragg's law can then be written as:

$$t = (2dmL/h)\sin\theta \tag{1}$$

where d is the lattice spacing and θ is the diffraction angle.

The widths of the Bragg peaks in the neutron diffraction spectrum were analyzed by the integral breadth method,[42] which assumes that the peak shapes and strain contributions are Gaussian. The contributions to the width of the Bragg peak are from instrumentation, variation in lattice spacing (strain), and/or particle size distribution. The FWHM is corrected for instrument broadening using

$$F^2_{adj} = F^2_{exp} - F^2_{std}, \qquad (2)$$

where F_{adj}, F_{exp}, and F^2_{std} are the adjusted, experimentally measured, and standard values of the FWHM acquired with a silicon standard. Particle size and strain can both contribute to broadening in the following way:[42]

$$F^2_{adj} = (1/2D\sin\theta)^2 + (4\langle e\rangle\tan\theta)^2, \qquad (3)$$

where D is the particle size and $\langle e\rangle$ is the FWHM of the distribution in lattice spacing, which is related to the variation in strain, in the material.

Because the diffraction angle is fixed and the wavelength varies, Eq. 3 can be shown to reduce to

$$(\Delta t/t)^2 = (h/2mLD\ \sin\theta)^2\ t^2 + 4\langle e\rangle^2, \qquad (4)$$

where it can be shown that $(\Delta t/t)^2 = (\Delta\lambda/\lambda)^2$, and a plot of $(\Delta t/t)^2$ vs. $(t)^2$, results in a line with intercept $4\langle e\rangle^2$ and a slope related to D, the particle size. Linewidth analysis[42] of an intact virgin (nonexposed) tube showed a distribution in lattice spacing of about 0.06% near the center of the tube. This represents a relatively small mean strain and indicates little variation of strain in the BASE tube examined.

An experiment was also carried out to measure the thermal expansion of the virgin Ceramatec tube material for 11 different crystallographic directions as a function of temperature from room temperature to 1000°C. The results are shown in Fig. 7. Analysis of this experiment showed that thermal expansion varies by about 50% for planes with spacing in the 1.3 to 2.3 Å range. Expansion in other crystallographic directions could be significantly larger because the reported average (bulk) expansion is about 8×10^{-6}/°C,[43] while the range measured by neutron diffraction is $6\text{-}8 \times 10^{-6}$/°C. This anisotropy could be the cause of significant localized residual stress in the tube after cooling from the fabrication temperature. These stresses, as described in the paper, can become even larger with the penetration of neutral sodium.

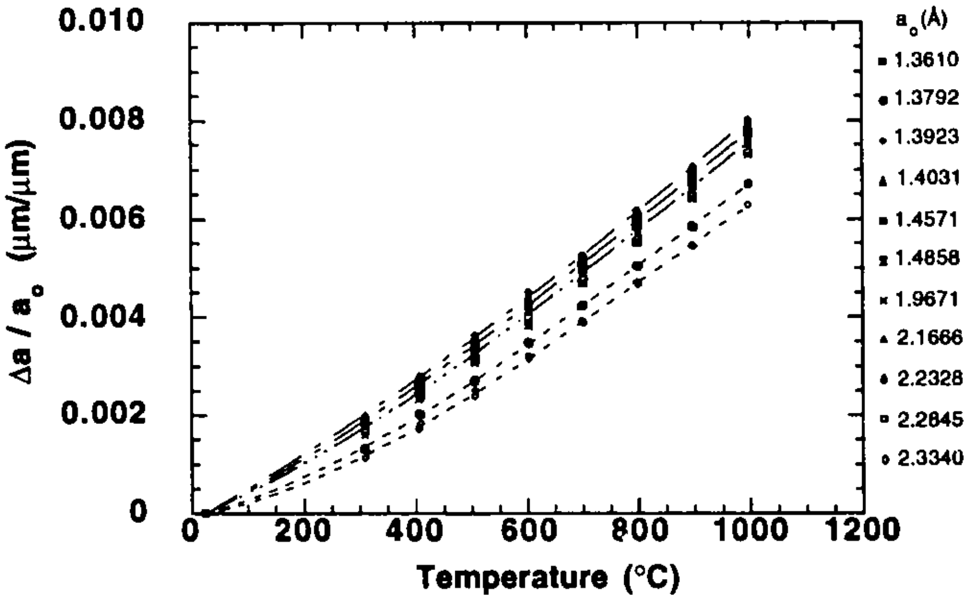

Fig. 7. Thermal expansion of virgin Ceramatec BASE tube material for 11 different crystallographic directions as a function of temperature from room temperature to 1000°C.

5.2 Optical Scanning of BASE Tubes

Through-transmission optical scanning by means of an intense neon light inserted in the BASE tubes has been used for rapid scanning of the outer-surface and near-surface regions of the tubes. The translucent nature of the BASE tubes makes this technique viable. Computer interfacing is used to enhance defect indications, allowing flaws as small as 25 μm to be imaged. Optically detected defects can be missed by the traditional X-ray methods used to inspect these tubes. X-ray tomography, on the other hand, may be useful for detecting variations in density.

Figure 8 is a schematic diagram of the optical scanning system. A pair of crossed polaroid filters allows the intensity of the light to be adjusted to optimize the image. A Macintosh computer is interfaced to an NEC CCD (Charged Coupled Device) camera, and the computer program "Image" is used for image reconstruction. Figure 9 shows images of a 12-mm-diameter Ceramatec tube with the neon light on and off. The defect not detectable with conventional radiography can be seen with the tube on. Destructive analysis indicates that the flaw region is an area near the surface with low density.

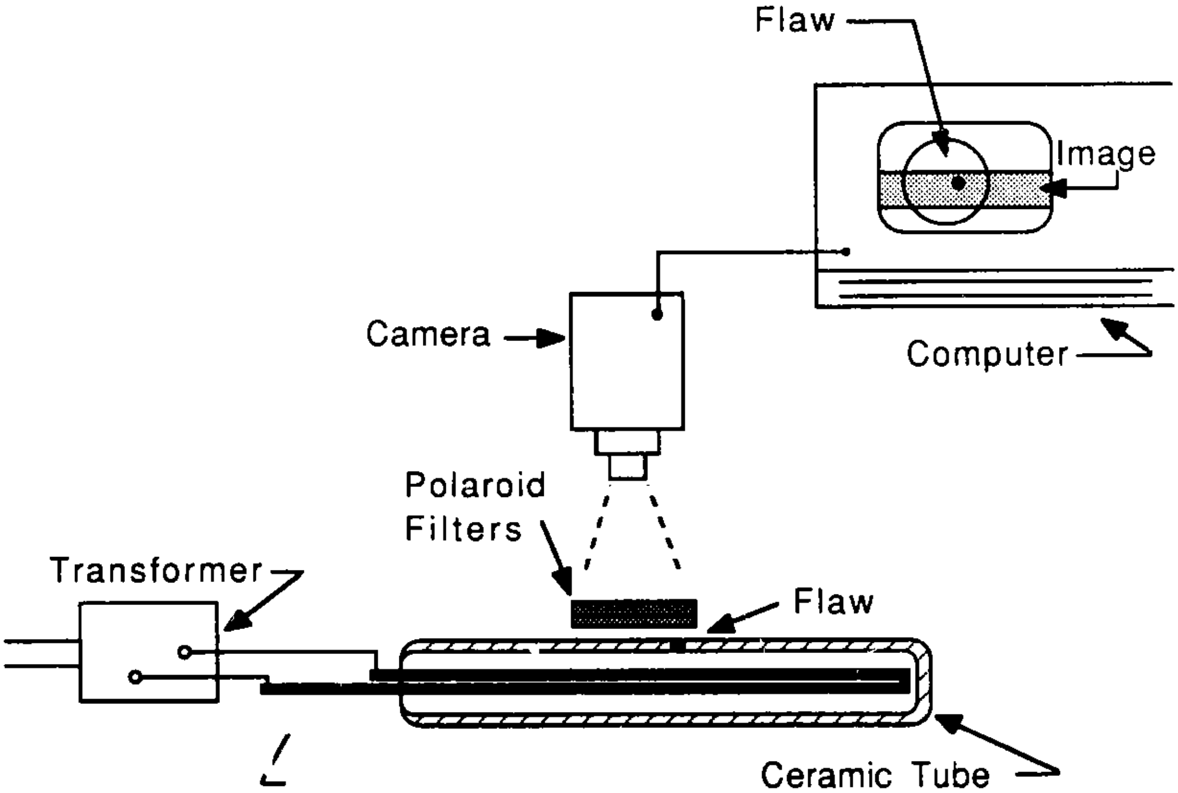

Fig. 8. Schematic diagram of the optical scanning system. A pair of crossed polaroid filters allows the light intensity to be adjusted for image optimization.

5.3 X-Ray Computed Tomography

X-ray computed tomography (CT) is an advanced nondestructive evaluation technique that can provide spatial variations of mass density within an object in three dimensions. Physical flaws such as inclusions, voids, and cracks in the object can be detected with a high spatial resolution (≈50 μm) because of the difference in density of the flaws with respect to the density of the object.

An as-received β"-alumina tube (ID No. CX1-2614-14) was inspected with a three-dimensional X-ray CT system designed and developed at Argonne. The system consists of a microfocus X-ray source and an image intensifier/CCD array camera–based detector. With a computer-controlled rotational stage, several two-dimensional X-ray projections of the object were obtained by rotating the object from 0 to 360 degrees. A three-dimensional image of the object is then reconstructed from the projection data with either the Feldkamp[44] or Radon code.[45]

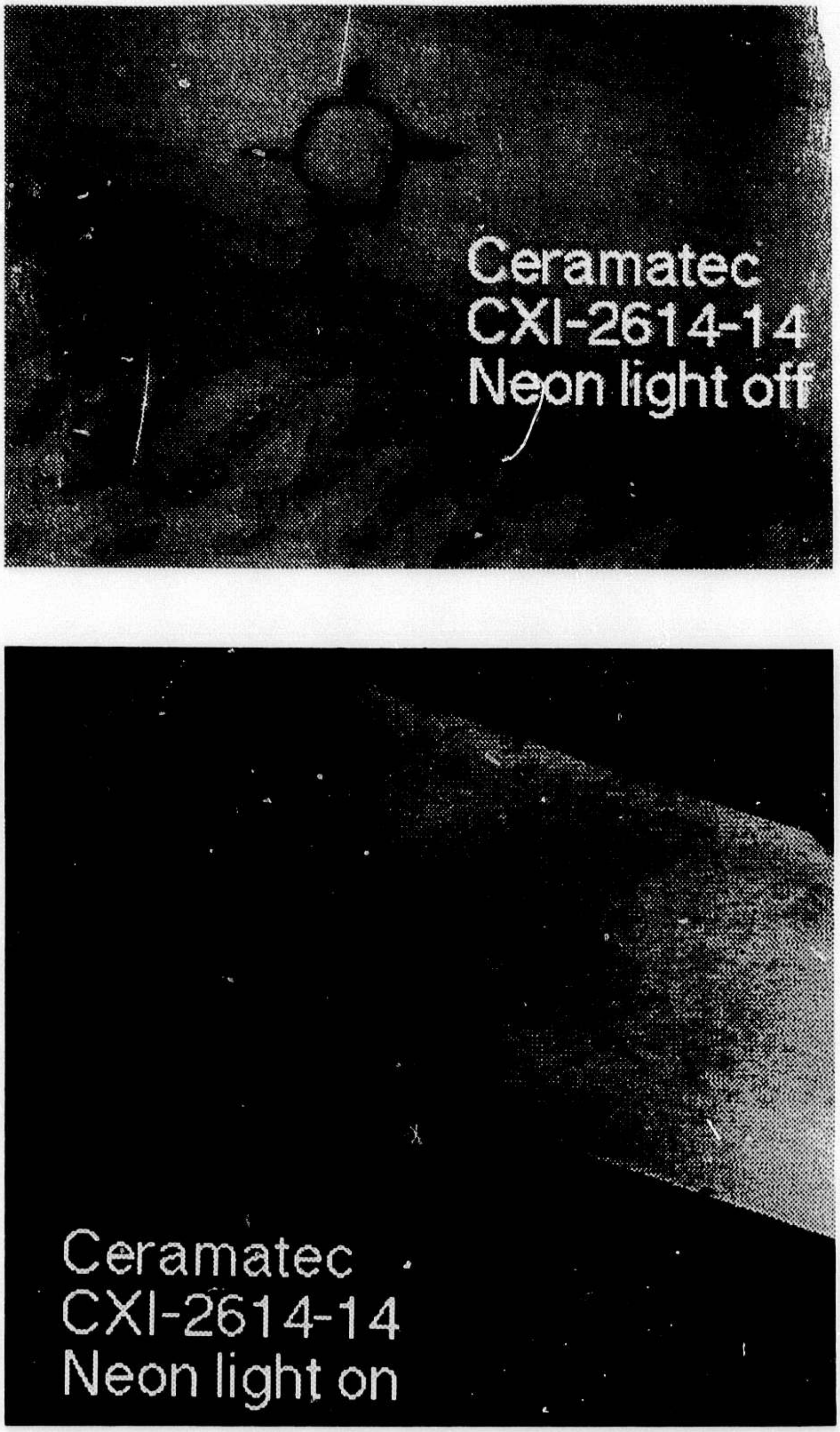

Fig. 9. Images of Ceramic tube with neon light on and off. Defect not detectable with conventional radiography can be seen with tube on. Destructive analysis indicates flaw region is a near-surface with low density. Tube diameter is ≈12 mm.

A middle section of the tube was examined over an axial length of 2 mm. With X-ray head voltage of 50 kV and a current of 0.7 mA, four tomographic slices of 0.5 mm thickness were obtained with an image resolution of 38 μm per pixel. Figure 10 shows an X-ray CT image of one. The tube appears to be devoid of physical flaws. The circular ring seen in the picture is an artifact caused by imbalanced detector elements. Figure 10 also shows two line profiles of the image intensity along horizontal and vertical lines through the axis of the tube. The asymmetry of the line shape about the tube wall may be due to beam hardening, which is an artifact related to preferential absorption of X-rays with respect to energy variation of the polychromatic source used. Beam hardening can be reduced by a filter element at the source; we used an 0.015-in. copper filter in our experiment.

To evaluate the uniformity of density distribution around the tube, the average image intensities over a small area about the mid-circumference of the tube were measured at angular positions of 0, 45, 90, 135, 180, 225, and 270, and 315 degrees. Figure 11 shows the density variations in gray levels around the tube for each of the four slices imaged. The largest density difference measured between any two locations is about 3%, which is about 1.4 times the standard deviation of the measurement error. In other words, the density is uniform within 1.4 sigma of the measurement error. To establish quantitative density measurements in a direct manner, work is underway to calibrate the system by using materials of known density.

5.4 Nuclear Magnetic Resonance

In general, NMR spectroscopic and imaging techniques can provide a wealth of information on both the chemical and physical characteristics of solid materials. In the specific case of β"-alumina tubes, application of these techniques can provide information on crystal structure, presence of paramagnetic impurities, presence of entrained metallic sodium, sodium distribution across the tube wall, extent of crystal lattice defects, and lattice strain. Additionally, given the ability to perform the NMR experiments as a function of sodium exposure, these techniques may provide critical information on the stability and mechanism of failure of the tubes. Initial solid-state NMR spectroscopic studies of β"-alumina tubes have provided significant information leading to improved understanding in the areas of strain, crystal lattice defects, and entrained impurities.

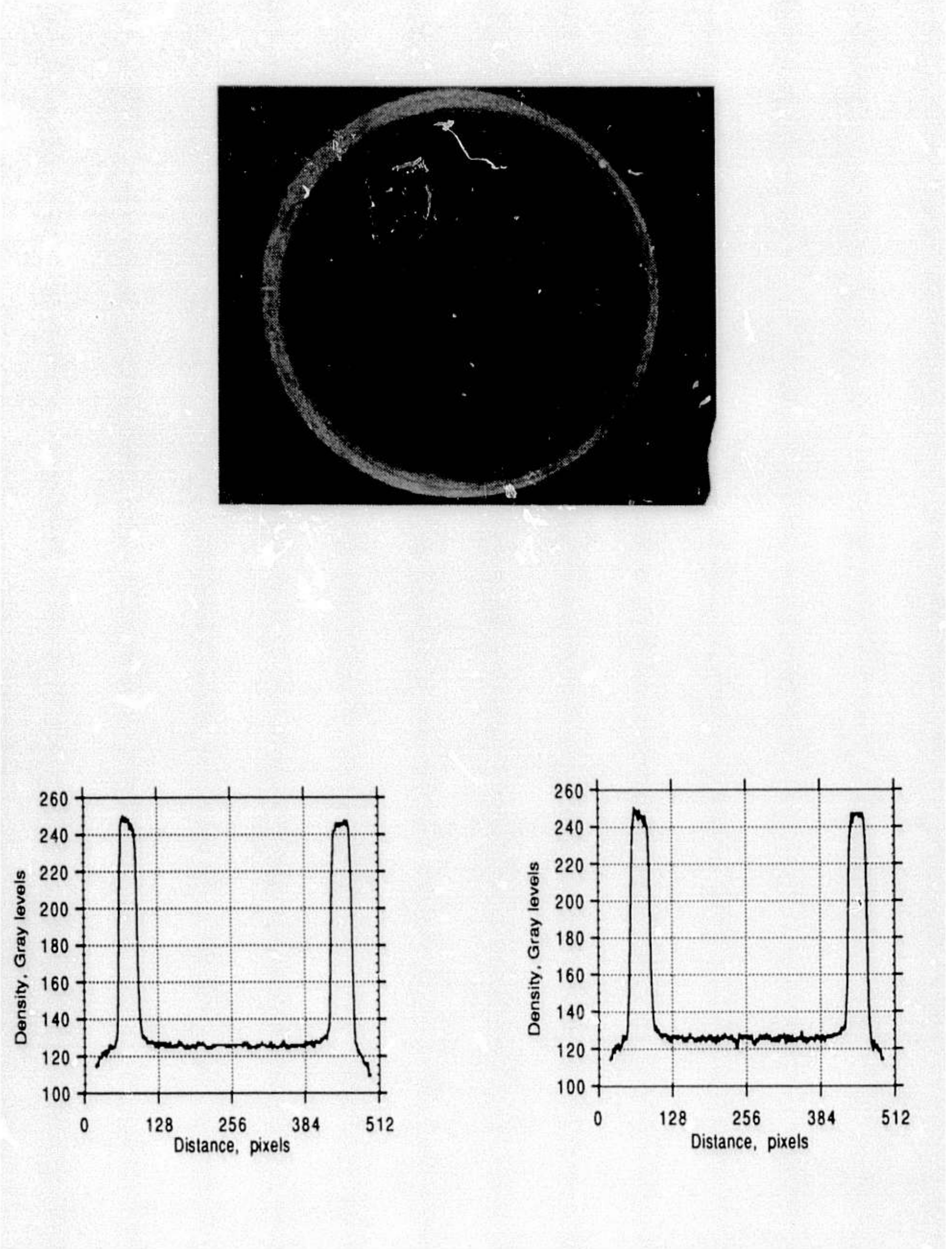

Fig. 10. X-ray tomography result showing two line profiles of image intensity along horizontal and vertical lines through origin of tube. Asymmetrical line shape may be due to beam hardening, which is an artifact related to preferential absorption of X rays with respect to energy variation of polychromatic source used.

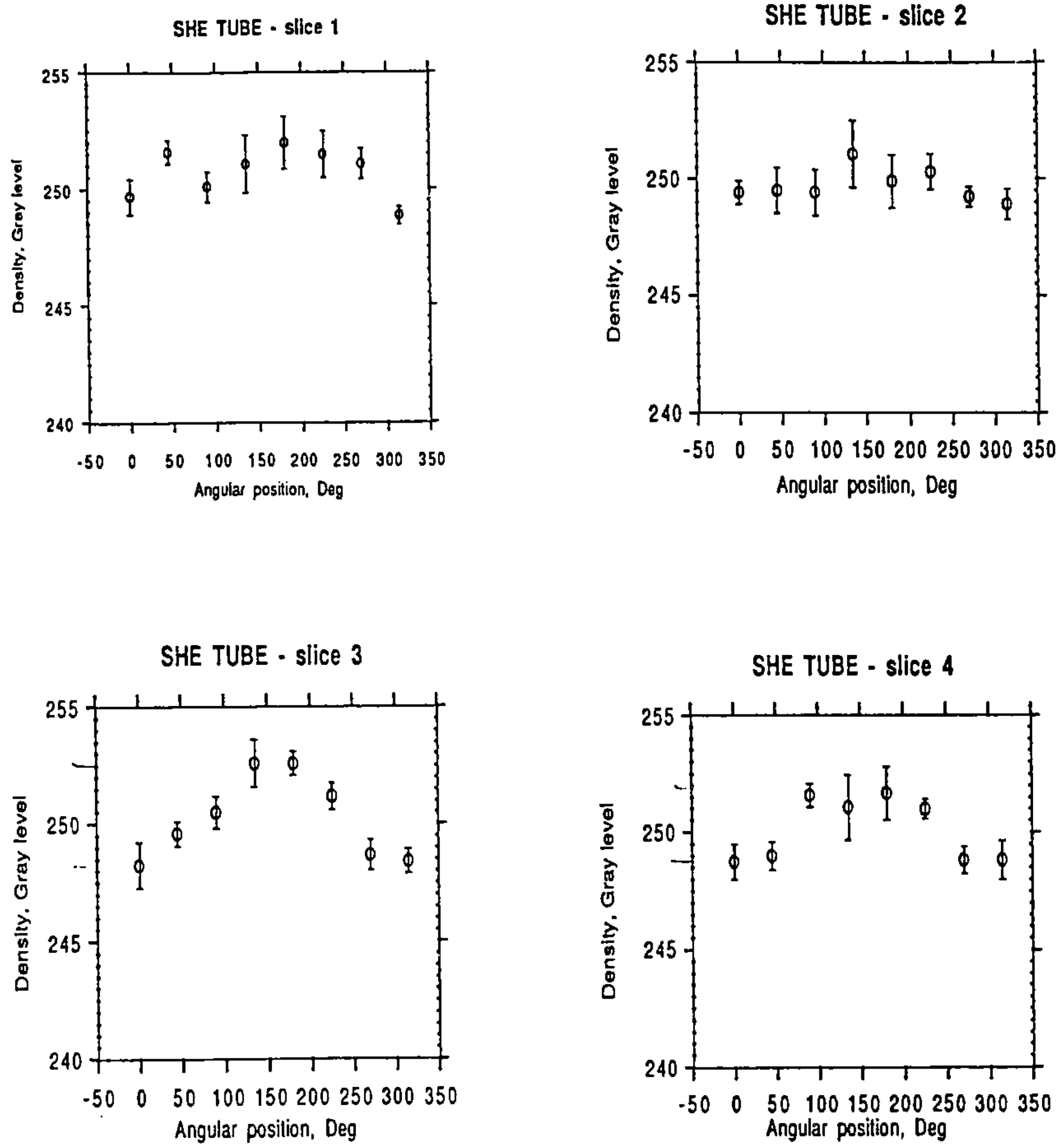

Fig. 11. X-ray tomography result showing density variations in gray levels around tube for each of four slices imaged. Largest density difference measured between any two locations is about 3%, which is ≈1.4 times the standard deviation of the measurement error. In other words, density is uniform within 1.4 sigma of measurement error.

Initial ^{23}Na NMR spectroscopic studies were performed at Michigan Technological University (MTU) on both virgin and exposed tubes. Static NMR spectra of the tubes were acquired at ambient temperature (17°C) and a magnetic field strength of 8.4 T (95.16 MHz ^{23}Na resonance frequency). A powder pattern (a static NMR spectrum of the polycrystalline material) was obtained from the virgin tube. The spectra obtained from the exposed and virgin tubes were nearly identical, indicating that exposure–induced deteriorations in the bulk crystal structure had not occurred in this specimen.

For quadrupolar nuclei, nuclei with a spin quantum number (*I*) greater than +1/2 and a nonspherical nuclear distribution, the NMR signal (lineshape) can be quite sensitive to the presence of lattice strain. This is due to coupling of the quadrupole nuclei to the distribution of electronic charge (the electronic field gradient [EFG]) surrounding it. Coupling to the EFG can be either static or dynamic and occurs in all cases except cubic lattice symmetry. The degree to which the nuclei couple to the EFG is dependent upon the individual nuclei's quadrupolar coupling constant. Lattice strain affects the electronic field gradient and gives rise to inhomogeneous broadening of the powder pattern. The net effect of quadrupolar coupling in the presence of strain is an inhomogeneous broadening of the NMR signal.

Both the ^{23}Na and ^{27}Al are quadrupolar nuclei with spin quantum number $I = 3/2$. Additionally, both ^{23}Na and ^{27}Al have relatively large quadrupolar coupling constants and have been shown to be sensitive to strain. For the specific case at hand, given the coupling ability of the ^{23}Na nuclei and the twisted spinel block crystal lattice structure of the β''-alumina material, the ^{23}Na experiment should be quite sensitive to strain. To establish the level of broadening, the NMR lineshapes for the unstrained lattices were simulated. The similarity of the experimental and theoretical results suggests that the intracrystalline strains for both the exposed and unexposed systems are quite small. An attempt to calculate an upper limit to the lattice strain may be made.

Crystal lattice defects and flaws generally produce short–order strain in the lattice. This strain is typically applied over the distance of a few atoms. The effect of these defects will be apparent in the NMR experiments if they are present in significant number of sites throughout the bulk structure. In these experiments, the lack of inhomogeneous broadening suggests that the bulk structure for both the virgin and the exposed tubes is relatively free of defects.

Intrinsic spin-lattice (T_1) relaxation measurements on the virgin and exposed tubes were also measured. The exposed tube had a slightly faster decay. This is possibly due to the crystal lattice being somewhat less rigid or to the presence of paramagnetic impurities induced during the exposure. Additional variable–temperature studies and multiple magnetic field experiments will be performed to help determine the active mechanism.

Work on additional specimens, both virgin and those with various sodium exposure times, will continue at ANL and MTU. This work will include high–speed studies of both ^{23}Na and ^{27}Al on ANL's "magic" angle spinning (MAS) probe. Additionally, ^{23}Na NMR imaging studies will be conducted to probe the sodium distribution in the tube wall.

5.5 X-Ray Diffraction

X-ray diffraction can provide measurements of surface stresses in many materials, although as can be seen in this report, the examination of ceramics may present problems. The technique, as in neutron diffraction, involves Bragg's Law. Changes in the lattice spacing $\Delta d/d$ of distinct lattice planes are measured. Penetration depths using commercially available X-ray diffraction systems for ceramics can reach about 100 μm. The basic idea is to relate the lattice strains to the stress state calculated according to the theory of elasticity. While complications can arise in the analysis of X-ray diffraction data (particularly for ceramics), the technique has been validated for many applications and is widely used. Although limited to measuring stresses on surfaces (while neutrons can provide a bulk average), X-ray diffraction is relatively inexpensive. Reference 46 describes X-ray diffraction in considerable detail.

Three organizations have been used to measure residual surface stresses in BASE tubes: Lambda Research Incorporated, the Technology for Energy Corporation (TEC), and the University of Denver. The results vary widely. TEC reports primarily tensile stresses, Lambda reports primarily compressive stresses, and the University of Denver, which reports strain, indicates very small values that suggest very small surface stresses. Table 5 summarizes their findings, while Appendices A–C present their results in detail.

Table 5. X-Ray Diffraction Results

Sample	Lambda (stress in ksi)	U. of Denver (strain)	TEC (stress in ksi)
CTI-2592-07*	-	-	-9 ± 3(circ)
	-	-	-1 ± 4(axial)
	-	-	(ground area as received)
	-	-	+26 ± 17(circ)
	-	-	+40 ± 25(axial)
	-	-	(ground area 5 days exposure to humidity)
	-	-	+33 ± 9 (circ)
	-	-	+16 ± 4(axial)
	-	-	(unground area as received)
	-	-	+12 ± 21(circ)
	-	-	-40 ± 29(axial)
	-	-	(unground area, 5 days exposure to humidity)
CXI 2598-16-1[a]	-	-	+73 ± 19(circ)
(50 hrsNa at 900°C)	-	-	+37 ± 25(axial)
CXI 2606-06-2[a]	-	-	-2 ± 4 (circ)
(160 hr Na at 900°C)	-	-	-2 ± 5 (axial)
CXI-2600-10[a]	-58 ± 4 (circ)	-	-
($2\Theta=121°$)	(5 days exposure to 60% humidity)	-	-
	-89 ± 16 (axial)	-	-
	(5 days exposure to 60% humidity)	-	-
CXI-2608-10[a]	-11 ± 18 ($2\Theta=103°$)	$\varepsilon_{11}=-0.05\%$ (circ)	-
	-44 ± 8 ($2\Theta=121°$)	$\varepsilon_{33}=+0.002\%$(normal)	-
		$\varepsilon_{13}=-0.009\%$(axial)	-
		($2\Theta=144°$)	
T867 V2 8P[b]	-	-	+10 ± 7(circ)
	-	-	+10 ± 6(axial)
	-	-	+4 ± 5(circ)
	-	-	+4 ± 3(axial)
	-	-	(3 days exposure to humidity

[a] Ceramatec tube.
[b] Beta tube.

Part of the variations result from the use of different diffraction peaks by the researchers. The Lambda Research facility appears to be more versatile and provides a broader selection of diffraction peaks for the stress analysis. Lambda was able to work with a peak that appears to be sharper than the one used by TEC. This may suggest that Lambda's results would be more reliable than those of TEC. The problem with a broad peak is that it is made of several peaks and during an X-ray diffraction scan there could be relative shifts between the peaks that can lead to false results. Another possibility for the variations is that the thermal expansion anisotropy of the material, shown by neutron diffraction studies to be significant, could lead to variation in strain with crystallographic direction. Because TEC and Lambda are examining different peaks, they arrive at a stress value by different crystallographic orientations, which may (due to anisotropy) have different values. The relatively large grain size (up to 50 μm) also complicates the analysis because the data are averaged over a smaller number of grains than may be required to obain a fair sampling. This is an inherent limitation of the X-ray technique when used with relatively large grain ceramics. Additional work will be required to establish the best procedure for X-ray diffraction and to validate the technique for BASE tubes.

5.6 Summary of NDE Methods

As a result of mechanical failures that terminate the operation of the test devices, the issue of β"-alumina solid electrolyte (BASE) durability is being addressed. Effective and economic nondestructive evaluation (NDE) methods and protocols are being sought to provide rapid evaluations of components. Analytical modeling is also being pursued to predict the fabrication-induced residual stresses that may contribute to tube failure.

Neutron diffraction experiments at Argonne National Laboratory have been carried out on Ceramatec BASE tubes to help determine the magnitude of bulk residual stresses (X-ray diffraction data used to determine residual stresses on the tube surface have been difficult to analyze). Linewidth analysis of an intact virgin tube showed a mean distribution in lattice spacing of about 0.06% in a region near the middle of the tube. An experiment was also carried out to measure the thermal expansion of the virgin Ceramatec tube material as a function of temperature from room temperature to 1000°C. Results showed that thermal expansion varies by at least 50%. This anisotropy could be the cause of significant residual stress in the tube after cooling from the fabrication temperature. These stresses can become even larger with the penetration of neutral sodium.

Nuclear magnetic resonance (NMR) studies were carried out to evaluate the possibility of detecting the presence of lattice defects and flaws. This analysis is carried out through the study of linewidths in the NMR spectrum. For a tube exposed to sodium, results suggest that the tube was relatively free of defects.

X-ray tomography has been applied to a section of a Ceramatec tube to determine if circumferential variations in density can be detected. The largest density difference measured between any two locations in one tube examined is about 3%, which is about 1.4 times the standard deviation of the measurement error. In other words, the density is uniform within 1.4 sigma of the measurement error. To establish quantitative density measurements in a direct manner, work is underway to calibrate the system using materials of known density.

Through-transmission optical scanning by means of an intense neon light inserted into the translucent BASE tubes has been used for rapid scanning of the outer-surface and near-surface region of the tubes. Computer interfacing has been used to enhance defect indications, allowing the imaging of flaws as small as 25 µm. Defects detected optically can be missed by traditional X-ray methods used to inspect these tubes. Destructive analysis of one tube suggested that an indicated flaw region is a low-density region near the outer surface. In addition to detection of flaws and regions of low density, regional variations in texture appear to be dete4ctable with this technique.

6 Stress and Fracture Analyses of β"–Alumina Tubes

Stresses in the β"-alumina tubes can be categorized into two groups. First, stresses are generated during fabrication and can arise due to differential shrinkage and creep during sintering and during subsequent cooldown to room temperature after sintering. Second, stresses are generated during operation of the sodium heat engine (SHE). Such stresses include those due to steady-state thermal gradient, neutral sodium penetration, and gradient in neutral sodium concentration. Because of the anisotropy of the thermal expansion coefficients, large grain stresses are generated in the β"-alumina tubes during a homogeneous temperature decrease. Similarly, because of the anisotropy of the lattice strains caused by neutral sodium penetration, grain stresses are also introduced by the homogeneous penetration of neutral sodium. Macroscopic stresses due to thermal gradients and gradients of neutral sodium concentration are superimposed on such grain stresses. Because the grain stresses change from grain to grain (depending on orientation), they are not directly comparable to the fracture stress obtained from the testing of macroscopic specimens. However, the grain stresses can act on flaws present on the grain boundaries to cause intergranular fracture.

Of the fabrication stresses, only those due to a cooldown after sintering have been analyzed in this present report. Of the steady-state operational stresses, those due to radial thermal gradient and neutral sodium penetration are considered. Stresses caused by transient loadings during startup or shutdown and edge effects (e.g., axial thermal gradient) have not been considered.

All stress and fracture mechanics analyses have assumed the linear elasticity theory and have used either finite-element methods, Eshelby's ellipsoidal inclusion theory,[47] or published results in the literature. In most cases, a generalized plane strain deformation is assumed. For the tube geometry, the outer diameter and the wall thickness are assumed as 15 and 1.2 mm, respectively.

6.1 Fabrication Stresses

6.1.1 Cooldown in Absence of Temperature Gradient

Although the thermal expansion coefficient for polycrystalline β"-alumina has been reported as 8 x 10^{-6}/°C,[48] recent neutron diffraction measurements (Fig. 7) have indicated that it is highly anisotropic and can be as low as 6 x 10^{-6}/°C in some crystallographic directions. Unfortunately, the thermal expansion coefficient in the c direction has not been measured but is expected to be greater than the polycrystalline value. Assuming that a single spheroidal anisotropic grain is buried inside an isotropic matrix, the stresses generated inside the grain can be computed with the inclusion theory of Eshelby [47]. The stresses were calculated with the following elastic constants: E = 190 GPa; ν = 0.20.

The variations of the a axis stress and c axis stress with grain aspect ratio (single-grain model) due to cooldown from 1000°C to room temperature are shown in Fig. 12 for two values of c-axis thermal expansion coefficient. The single-grain model ignores grain interaction effects that have been taken into account for a two-dimensional array of hexagonal

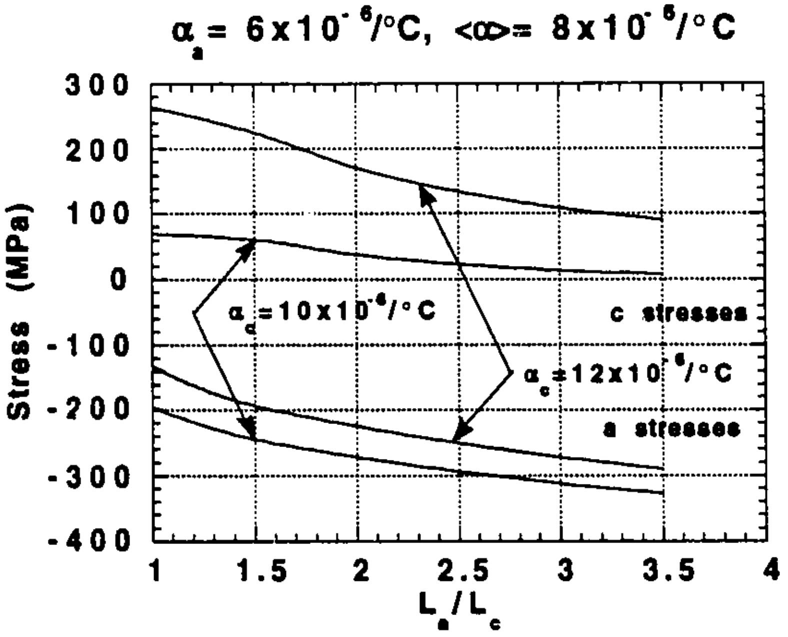

Fig. 12. Effects of aspect ratio of β"-alumina grains on internal grain stresses caused by anisotropic thermal strain during cooldown. Results are presented for two values of c-axis thermal expansion coefficient.

grains by Laws and Lee.[49] The corresponding mismatch strains due to anisotropic thermal expansion during cooldown that cause tensile stress on a hexagonal grain boundary are ≈2 x 10^{-3} and 4 x 10^{-3}, respectively. In the multiple-hexagonal-grain model, the corresponding tensile stresses at the middle of the grain are ≈100 and 200 MPa, respectively. The c-axis tensile stress is highly dependent on the thermal expansion coefficient and could be high for spherical (L_a/L_c = 1) or equiaxed hexagonal grains.

6.2 Steady-State Operational Stresses

6.2.1 Radial Thermal Gradient

The estimated temperature drop through the wall of the β"-alumina tubes during steady-state operation is ≈30°C, based on extrapolation of some very limited experimental data on the thermal conductivity of β"-alumina. If the actual thermal conductivity is lower by a factor of 2, the temperature drop could rise to 60°C. Fig. 13 shows the axial stress distributions through the tube wall for temperature drops of 30°C and 60°C. Maximum tensile stresses of 28 MPa and 56 MPa are predicted at the outer surface,

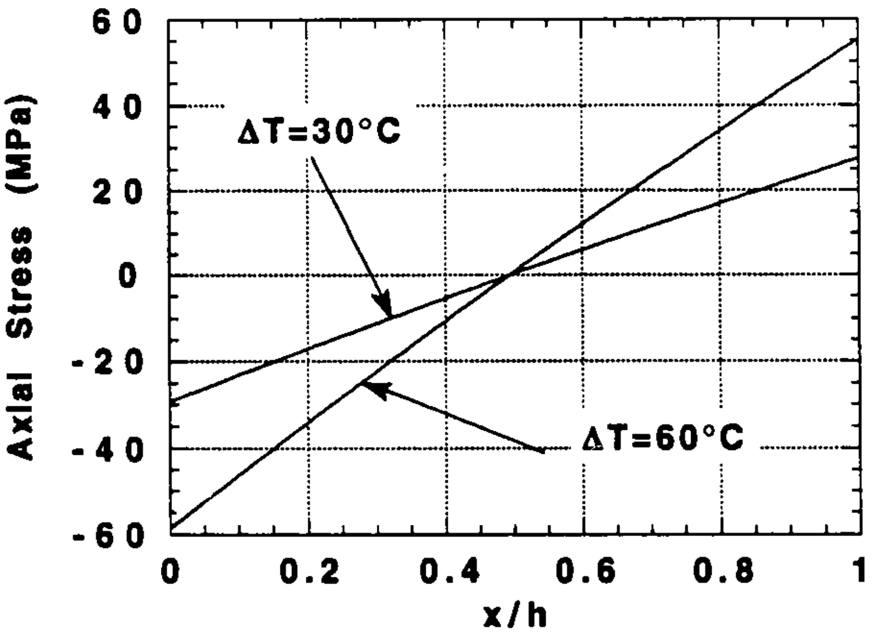

Fig. 13. Axial stress distribution in β"-alumina tube wall corresponding to 30°C and 45°C temperature drops through tube wall. Hoop stresses are approximately equal to axial stresses.

corresponding to the two temperature drops, respectively. These stresses are small compared to the fracture strength of the material.

6.2.2 Homogeneous Penetration of Neutral Sodium

It has been reported that the β"-alumina grains undergo a c-axis strain of 0.07% with negligible strains in the a direction due to homogeneous penetration of neutral sodium.[48] Because of the anisotropy of the strains, stresses are created in the β"-alumina tubes that are similar to those due to anisotropic thermal strains discussed in Sec. 5.1.1. Assuming isotropic grain orientations, the mismatch strain causing tensile stress at the grain boundary is $\Delta\varepsilon = 0.0007/3 = 0.000233$.

The results, presented in Fig. 14, show that the a-axis stresses are moderately tensile (but small compared to the fracture strength) if the aspect ratio (L_a/L_c) of the grains is large, i.e., the grains resemble pancakes.

A more accurate solution that takes into account multiple-grain (200-grain) interaction effects is available for a hexagonal grain array.[49] The

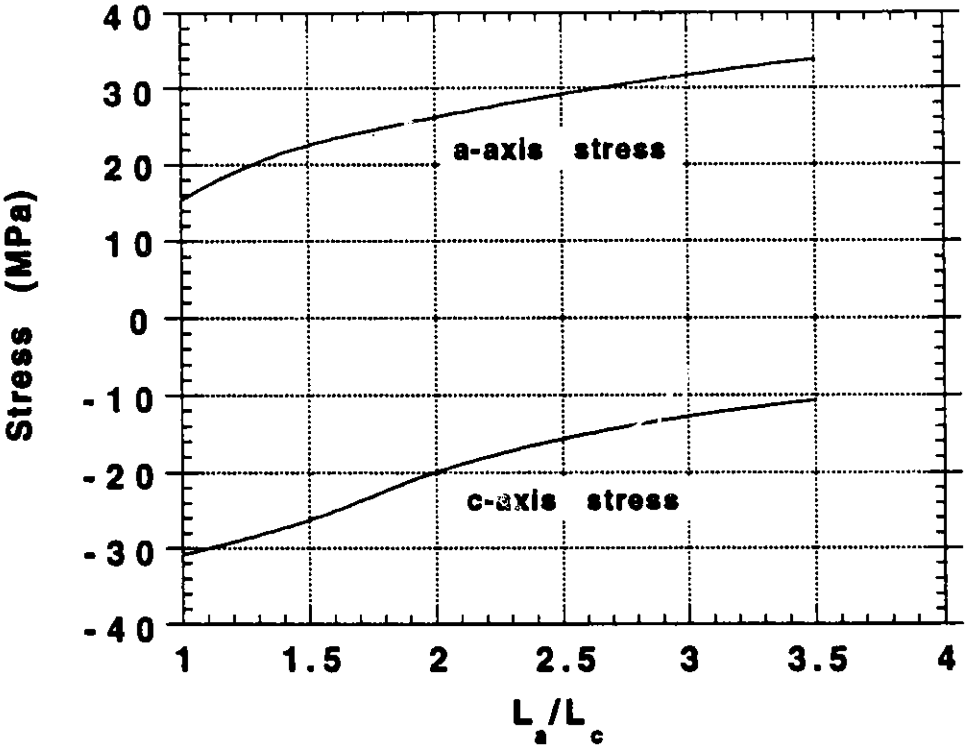

Fig. 14. Effects of aspect ratio of β"-alumina grains on internal grain stresses caused by anisotropic c-axis strain of 0.07% due to neutral sodium penetration

tensile stress at the middle of the grain is given by $\sigma = E\Delta\varepsilon/[4(1-\nu^2)]$, which gives a stress of ≈11.5 MPa. Two-grain and a four-grain model give stresses of ≈23 and ≈30 MPa, respectively. For comparison, the single-spherical-grain model gives σ_a = 12.5 MPa (Fig. 14).

6.2.3 Inhomogeneous Penetration of Neutral Sodium

Additional stresses are created in the β"-alumina tubes by inhomogeneous distribution of neutral sodium ranging from a maximum concentration at the inner surface to zero at the outer surface. The free c-axis strain of the β"-alumina grain corresponding to the maximum concentration of neutral sodium at the inner surface was assumed to be 0.07%. Three types of radial distribution of the c-axis strain were assumed, as shown in Fig. 15. For a random orientation of the β"-alumina, the anisotropic c-axis strain gives rise to a volumetric expansion strain equal to one-third of the c-axis

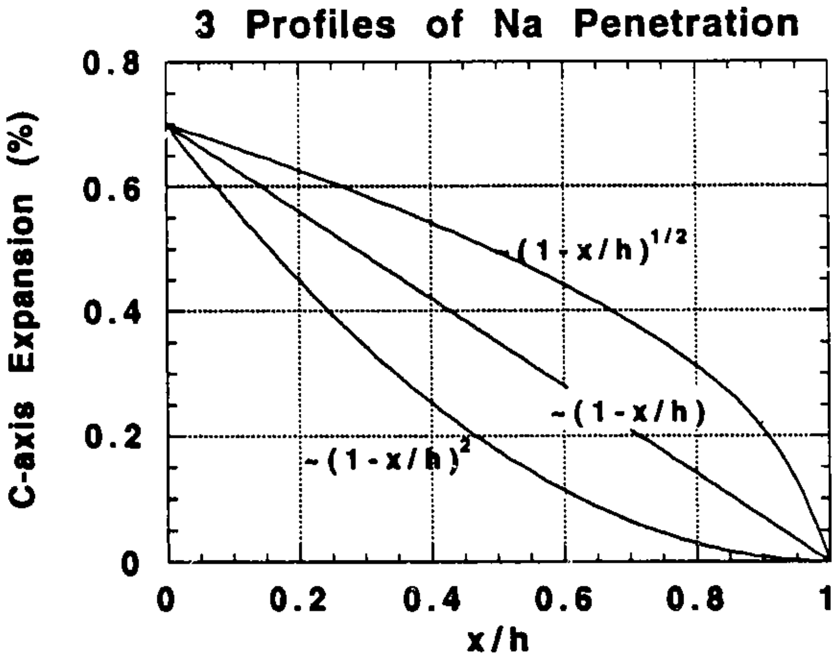

Fig. 15. Three c–axis expansion strain profiles corresponding to three sodium penetration profiles assumed for stress analysis

strain. The variation of the expansion strain with radius creates stresses in the tube similar to those from a temperature gradient through the tube wall.

The results corresponding to the three distributions of sodium are shown in Fig. 16. The inner surface is always under compression and the outer surface is always under tension. However, the maximum tensile stress at the outer surface can vary from 18 to 36 MPa, depending on sodium distribution. Thus, it is important to have some idea of the actual profile of the neutral sodium in the tube wall before a full determination of the stresses can be made.

6.3 Grain–Boundary Fracture

As mentioned earlier, the penetration of neutral sodium into '–alumina causes an anisotropic c–axis strain of 0.07% but only negligible strains in the *a* direction. A similar anisotropic strain is induced in the material during cooldown after sintering, due to anisotropic thermal expansion coefficients. The anisotropic strain of the grains due to neutral sodium penetration and anisotropic thermal expansion coefficients creates a logarithmic singularity in the normal stress at the triple–point junctions. Flaws situated near the

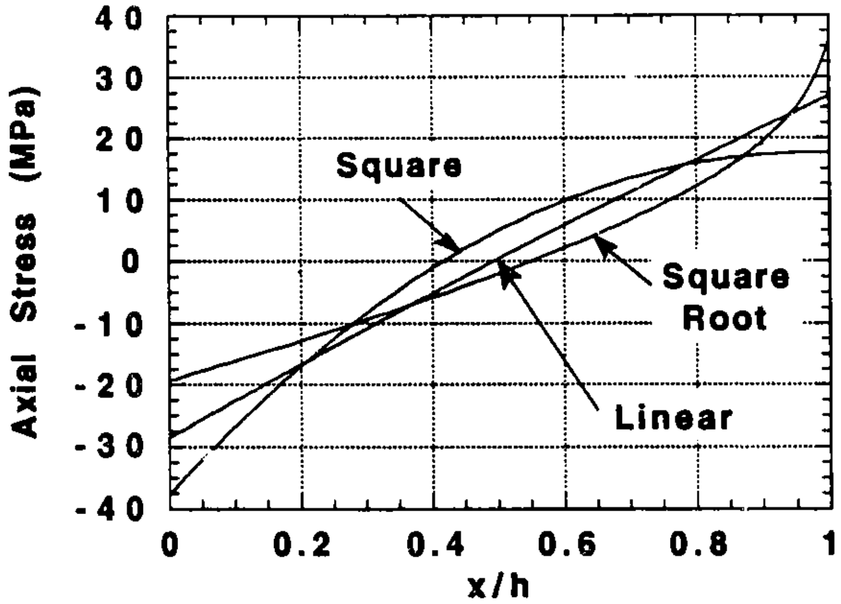

Fig. 16. Axial stress distribution in the β"-alumina tube wall corresponding to three sodium penetration profiles shown in Fig. 7. Hoop stresses are approximately equal to the axial stresses.

triple-point junctions can propagate unstably because of these stresses and cause grain-boundary fracture. Various models have been proposed to predict the cracking behavior of ceramic materials due to anisotropic thermal expansion coefficient. There is general agreement that there is a critical minimum grain size required for microcracking to occur, i.e., microcracking will not occur if the grain size of the ceramic material is less than a critical value. The universally accepted expression for the critical grain size (l_c) is of the following form:

$$l_c = Q \frac{G_{gb}}{E(\Delta\varepsilon)^2} \tag{5}$$

where G_{gb} is the grain-boundary toughness, E is the Young's modulus, $\Delta\varepsilon$ is the mismatch in strain ($\Delta\alpha\ \Delta T$) for thermal expansion strain plus that due to neutral sodium penetration), and Q is a constant. Various authors have proposed various values of Q on the basis of either experiments or analytical models. For our purposes, we have selected the following two models from Fu and Evans[50] and Laws and Lee:[49]

Fu and Evans

$$Q = \beta \ (1+\nu)^2 \tag{6}$$

where ν is the Poisson's ratio, and β, an empirical constant, is chosen as 3.5 to obtain approximate correlation with experiments.

Laws and Lee

$$Q = \frac{64(1-\nu^2)}{f^2(a/l_c)} \tag{7}$$

where f is a function of the ratio between crack size (a) and grain size (l_c).

Equations 5–7 can be applied to the present case by interpreting Δε to be the sum of the mismatch strain due to sodium penetration and thermal expansion anisotropy. For the sodium penetration case, the mismatch strain is the difference between the isotropic expansion strain of the material and the minimum grain expansion strain, which is zero. Thus,

$$\Delta\varepsilon \text{ (Na penetration)} = \frac{1}{3} \times 0.0007 = 0.00023.$$

For the thermal expansion case, the value of $\Delta\alpha \, \Delta T$ is taken as $2 \times 10^{-6} \times 1000$, i.e.,

$$\Delta\varepsilon \text{ (thermal)} = 0.002.$$

Thus, the stresses due to anisotropic strain are dominated by thermal effects rather than neutral sodium penetration effects.

Variations of the critical grain size with normalized flaw in the grain boundary are shown in Fig. 17. The model of Fu and Evans [50] predicts no dependence of critical grain size on the flaw size. Laws and Lee [49] analyzed various models, of which the four-grain model predicted the most stringent requirement for critical grain size. In this model, four regular hexagonal grains with the greatest mismatch in strain across the grain boundary under consideration are surrounded by an equivalent isotropic matrix. In the regular array, more than 200 regular hexagonal grains with fixed orientation are considered surrounding the grain boundary under consideration. In both cases, critical grain size increases rapidly with decreasing flaw size.

Evans [51] has proposed a value of $a/l_c = 0.1$ for a magnesium titanate system. Rice and Pohanka [52] have suggested a value of 0.02 for alumina. If

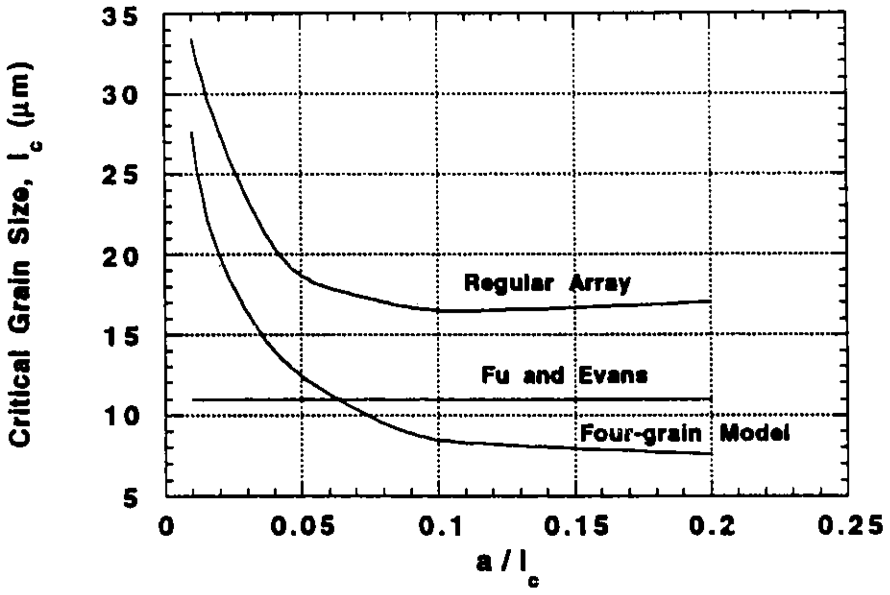

Fig. 17. Variation of critical grain size in β"-alumina with grain-boundary flaw size for grain-boundary toughness of 2 J/m²

this value is representative for the β"-alumina, the critical grain size should be about 20–30 mm. However, this value is based on the assumed grain-boundary toughness of 2 J/m^2. The current grain size of the β"-alumina tubes ranges from 30 to 100 μm. If the assumptions of the above analyses are reasonable, reduction of grain size can potentially remove one of the causes for failure of the β"-alumina tubes.

6.4 Conclusions

A summary of the estimated minimum and maximum stresses from various sources in the β"-alumina tubes are given in Table 6. Added together, the operational stresses vary from 100 to 170 MPa, which is still lower than the fracture strength of the material (≈200 MPa). However, these stresses may be sufficiently high to cause subcritical crack growth that leads to delayed fracture. This should be investigated in the future.

Relatively large internal grain stresses (100–200 MPa) are generated in the β"-alumina tubes during cooldown after sintering because of anisotropic thermal expansion coefficients. These large stresses can lead to intergranular fracture if the grain size is sufficiently coarse. Current grain size of the material varies from 30 to 100 μm. Based on the present analysis,

Table 6. Summary of Stresses in β''-Alumina Tubes (MPa)

Source of stress	Min	Max
Fabrication		
Cooldown from 1000°C to Room Temperature	100	200
Operational (Steady State)		
Uniform Na Penetration	25	25
Gradient in Na Penetration	20	40
Uniform Temperature of 800°C	20	40
Radial Thermal Gradient	30	60

intergranular fracture can be prevented by reducing the grain size to below 20–30 μm.

The grain stresses created during cooldown to room temperature after sintering (due to anisotropic thermal expansion coefficients) are much larger than those due to anisotropic expansion strains caused by neutral Na penetration.

7 SHE Pump Testing

Three DC-EM pump ducts and a permanent magnet assembly were received from ERIM in January 1991. The pump ducts were constructed from 0.125-in. OD, 0.006-in.-wall stainless steel tubing by flattening the tubes to allow a 0.002, 0.004, and 0.006-in. high flow channel over a length of about 7/16 in. Copper electrodes 11/32-in. wide were brazed to the duct's narrow sides at the middle of the flattened section. The permanent magnet had a measured field strength of 4700 G at a pole piece of about 0.25-in. diameter.

An arrangement was assembled to allow a flowrate and pump head test to be made using room-temperature sodium/potassium eutectic alloy (NaK) as the pumped fluid. The flow indication was very crude and probably accurate only to ±30%. Bourdon gages accurate to ±3% were used for pressure measurement.

Using the pump duct with the 0.006-in. high flow channel, head/capacity tests were run at direct currents of approximately 30, 43, 57, 67, 75, 85, and 95 A at flowrates ranging from zero to 31.5 mL/min. The highest pump head, attained at 95 A and zero flow, was 11.2 psi. At this same current, the head at 24 mL/min was 9.4 psi. The voltage drop between electrodes was 0.084 V, resulting in a pump efficiency of 0.36%. These tests were run at 1 atm system pressure.

The data allowed determination of the resistance of the bypassing current path around the high–flux field. Based on this calculated factor, the estimated current necessary to provide a pump head of 20 psi at 24 mL/min was found to be 202 A. A simple extrapolation of the pump head/current curve at 24 mL/min showed that a current of 190 A would be required to achieve 20–psi head. The SHE pump requirement is 20 psi at 24 mL/min.

The electrical resistivity of NaK at room temperature is about three times that of sodium at 250°C. Our judgment is that operation in sodium would be similar to that in NaK because performance depends heavily on the ratio of pump fluid resistance in the high–field region to the resistance of the bypassing current path through both the stainless steel and fluid. This ratio changes little with the geometries in consideration.

A test to study the sensitivity of the pump to low system pressure was performed. While pumping a 57 A, 24–mL/min, 5–psi head, system pressure was reduced slowly. No change was observed until a system pressure of -20-in. Hg was reached, when the flow suddenly dropped to about 10 mL/min and the head to 3 psi. The pump did not recover from this condition when starting conditions were resumed. Indeed, conditions were not improved with system pressures as high as 10 psig. The cause of this change is not known at present. The performance leads one to suspect that the pump duct narrowed due to a small deflection inward under vacuum (oil canning) and did not recover. However, computations show that the pressures are far too low to cause significant deflections in the pump.

While this flow reduction was not explained, it was possible to restart the pump and resume testing. This difficult recovery and its unpredictable nature could indicate possible plugging of the duct; however, this was not verified. It is known that such pumps are very sensitive to entrained gas, and this could be the cause. It is not understood why the plugging occurs at negative pressures (approximately 10-in. Hg absolute) and not at higher pressures.

Table 7 contains selected test data on the as-received 0.006-in. pump duct configuration using room–temperature eutectic NaK as the pumped fluid. Head-capacity flow tests were run at two different current levels by maintaining the current nearly constant and throttling the flow from the pump. The accuracy of the flowrate measurement is poor (±30%) except of course at zero flow. The bypass resistance is calculated from basic pump design factors and represents the resistance path for currents not passing through the NaK directly between the duct electrodes. For comparison, the effective NaK resistance directly across the electrodes is $1610 \times 10^{-6}\ \Omega$. Pump voltage was measured between the outer ends of the duct electrodes.

To improve pump performance, one must increase the bypass resistance and/or reduce the effective resistance. This is best achieved by matching the high–flux field as nearly as possible to the region of effective current. The as-received magnet pole pieces (1/4-in. dia.) extended beyond the pump duct in the direction parallel to current and were shorter than the electrodes in the direction parallel to flow. This wastes both magnetic flux lines and current. The pole pieces were reshaped into a rectangular configuration (5/32 by 3/8 in.) that more nearly optimized available flux and current. Table 8 gives pump test data using these pole pieces and a slightly reduced magnet air gap giving an average flux density of 5700 G. The improvement is due primarily to the higher bypass resistance and, to a lesser extent, to the higher flux density.

Although the current requirement of the pump is high, the voltage drop across the electrodes is surprisingly low, resulting in a relatively high efficiency for a pump this small. This leads to the conclusion that the pump could be powered directly from the heat engine output with some current–splitting circuitry and sufficient isolation from excessive leakage currents through the sodium inlet tubing to the pump.

It should be noted that Tables 5 and 6 give voltage values that are measured from the outer ends of the copper electrodes brazed to the pump duct and therefore include the voltage drops across both electrodes, braze joints, duct walls, NaK–to–duct wall contact, and pumped NaK. Voltage measurements across the pumped NaK are difficult because of the small duct size relative to the braze material and a significant voltage gradient across the

Table 7. EM pump data for as-received magnet assembly (4700 G), 1/4-in. dia., 0.006-in. duct

Current (A)	Voltage	Flowrate (mL/min)	Head (psi)	Eff. (%)	Bypass Resistance (10^{-6} Ω)
76.2	0.071	0	8.8	-	-
75.9	0.070	8	7.3	-	-
75.9	0.070	16	6.9	-	-
75.9	0.070	24	6.5	0.337	381
75.0	0.071	31.5	6.1	-	-
96.3	0.088	0	11.2	-	-
95.7	0.088	8	10.1	-	-
95.4	0.087	16	9.7	-	-
94.8	0.084	24	9.4	0.363	457
94.5	0.083	31.5	9.0	-	-

Table 8. EM pump data for modified magnet assembly (5700 G), 5/32 x 3/8 in. pole pieces, 0.006-in. duct

Current (A)	Voltage	Flowrate (mL/min)	Head (psi)	Eff. (%)	Bypass Resistance (10^{-6} Ω)
78	0.069	0	12.7	-	-
78	0.069	8	12.3	-	-
76.5	0.069	16	12.1	-	-
76.5	0.069	24	12.0	0.627	654
76.5	0.069	31.5	11.7	-	-
102.9	0.095	0	17.9	-	-
99.9	0.090	8	16.8	-	-
97.5	0.090	16	16.4	-	-
96	0.088	24	15.9	0.518	706
96	0.088	31.5	15.5	-	-

braze material. Our estimate of the duct-only voltage drop is about 50% of the values given in Tables 5 and 6. This will increase the efficiency values given in the tables by a factor of 2.

Calculations made to determine the effects of changing the pump duct height indicate that narrower pump ducts will increase the head developed by the pump. The relationship between duct height and developed head is shown in Fig. 18. The curve represents a calculation of the head developed at an NaK flowrate of 24 mL/min at room temperature over a range of duct heights. One actual data point at 0.006-in. height, 5700 G magnetic field strength, and 96 A total current was used to produce a pump head of 15.9 psi at 24 mL/min. The bypassing resistances within the pump were calculated and adjusted over the range of duct-height change to allow prediction of performance shown.

The objective of the EM Pump program has been to improve the basic EMM pump design. This has been achieved by a combination of pump testing and design analysis. A useful design relationship for DC-EM pumps is found in a 1953 article published in Nucleonics ("Direct-Current Electromagnetic Pumps," by A. H. Barnes).[53] The design relationship is based on a pump equivalent circuit and addresses the several parallel resistance paths. Equation 8 of the article is given as:

$$Q = \frac{10^8 s}{B}\left[I\left(\frac{R_w R_b}{R_w + R_b}\right) - \frac{10Ps}{B}\left(R_e + \frac{R_w R_b}{R_w + R_b}\right)\right]$$

where Q = flowrate (cm^3/sec),

s = width of pump tube in magnetic field direction (cm),

B = magnetic flux density (G),

I = total current to pump (A),

R_w = resistance of current path through duct walls (Ω),

R_b = resistance of current path through pumped fluid in the regions of weak magnetic field (Ω),

R_e = resistance of current path through pumped fluid in the effective pumping region of high magnetic field (Ω), and

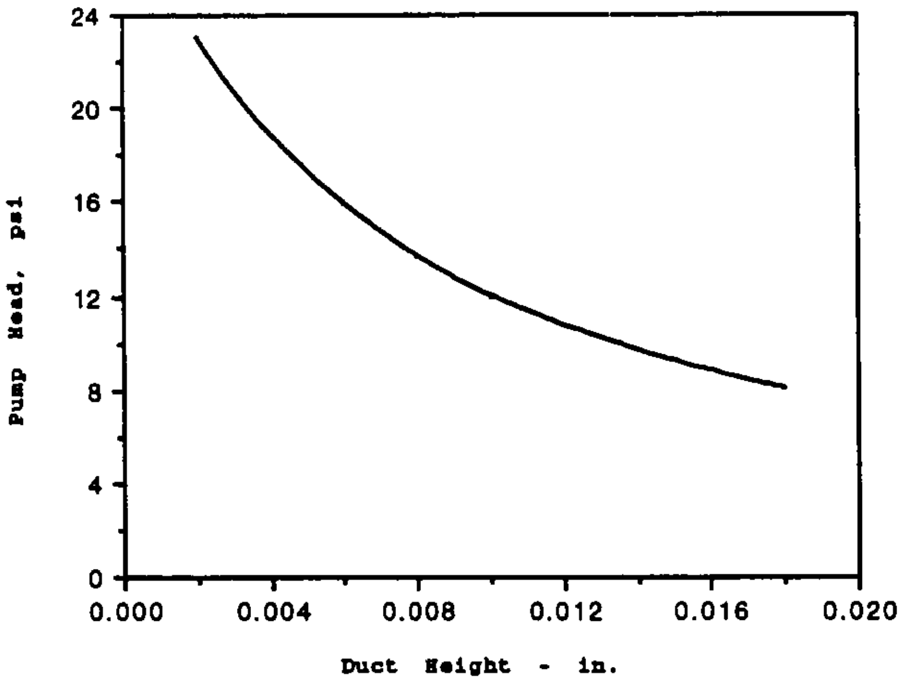

Fig. 18. Predicted pump head developed at 5700 G, 96 A, 24 mL/min

P = developed head of pump (dynes/cm^2).

This equation has been used to design large DC-EM pumps, but is limited because it requires an estimation of R_b. Such estimations are generally based on calculations from test data from similar pumps of known geometry. In this method, it is difficult to isolate R_w from R_b, so they are combined as R_B. Also, this equation can be useful in studying the effects of small design changes and in learning the optimum values of magnetic flux density and current. Substituting R_B and rearranging Eq. 8 in the article gives:

$$P = \frac{BI}{10s}\left(\frac{R_B}{R_e+R_B}\right) - Q\left[\frac{B^2}{s^2\left(R_e+R_B\right)10^9}\right].$$

This equation is now arranged in the form

dynamic head = head at zero flowrate - flowrate X slope of the head vs. flowrate curve.

By introducing data taken while pumping room–temperature eutectic NaK and calculating a value for R_e, we can determine R_B for the particular geometry of the duct, magnetic field strength, and pole–piece configuration. For a duct 0.006 in. high, 3/16 in. wide, and 11/32 in. long, we calculate Re to be 1610 x 10^{-6} Ω. One set of data taken on the pump duct as-received from ERIM but with modified pole pieces is as follows:

P = 15.9 psi

Q = 24 mL/min.

B = 5700 G

s = 0.006 in.

I = 96 A

R_e = 1610 x 10–6 Ω

These values result in a value of R_B = 730 x 10^{-6} Ω. The right-hand term in the equation has only a small effect and can be dropped when making comparative studies of small design changes. This elimination results in a value of R_B = 707 x 10^{-6} Ω.

The above design relationship should be useful in examining the effects of altering parameters such as magnetic field strength and current without changing pump geometry. A simple calculation shows that a field strength of 1 T and total current of 58.5 A would produce the same pumping performance. The minimum current achievable would be 28.5 A and would require a field strength of 3.84 T.

8 Conclusions

Because the Phase I program covers a wide variety of topics that are not closely correlated, general conclusions are difficult to formulate. Each report section above has a separate summary and, therefore, that material has been collected below to form a set of tentative conclusions for the total Phase I activity.

The literature survey performed at the start of this program revealed a consensus on several points. First, the life–limiting flaws in BASE tubes are generally large grains and voids. Second, these flaws are thought to originate from inhomogeneities and impurities in the β"–alumina powder.

For mechanically mixed materials, powders produced by the zeta process appear to be more homogeneous, judging by the improvement in properties of samples made by this process. However, mechanical mixing and the other processing steps associated with the zeta process may introduce impurities. The impurity levels in β"-alumina powders can be reduced by spray drying, a single-step processing method that produces β"-alumina materials with the best mechanical properties. Finally, additions of zirconia appear to significantly increase the strength and fracture toughness of β"-alumina, but strict control of the processing must be exercised to control the grain size of the zirconia and to prevent the introduction of zirconia agglomerates.

An evaluation of the mechanical and microstructural properties of the BASE tubes was based on a detailed study of nine commercially obtained samples; seven from Ceramatec and two from Beta R&D. The diametral strength of the Ceramatec tubes ranged from 133 to 317 MPa, and a typical value of fracture toughness measured by indentation was 1.8 ± 0.2 $\mathrm{MPa}\sqrt{\mathrm{m}}$. Strength of the Beta R&D tubes was 84 to 234 MPa. Weibull moduli were ≈10–16 for the Ceramatec tubes and ≈4–7 for the Beta R&D tubes. Higher strength and Weibull modulus values suggest slightly improved reliability for the Ceramatec tubes. Exposure of Ceramatec tubes to liquid sodium had no noticeable deleterious effects on strength.

A brief scoping study of alternative processing methods for fabrication of BASE tubes involved forming green state tubes through isostatic pressing, extrusion, and slip casting. These tubes were then sintered by both conventional and microwave plasma methods. It was shown that with an optimized powder preparation, high-quality β"-alumina powders can be produced routinely using zeta lithia as a lithia source. Fine grained tube microstructure (3–12 μm) can be obtained and, with proper heat treatment, improved mechanical properties should be possible. A limited number of microwave sintering experiments were performed to explore uniformity issues related to sintering temperatures; however, there was insufficient time available to do more that illustrate the feasibility of the process and indicate future directions for development.

A major effort during Phase I was the evaluation of alternative nondestructive evaluation (NDE) methods for examining the BASE tubes and predicting their reliability. Neutron diffraction was used to estimate bulk residual strains and provide expansion data as a function of crystallographic direction. Linewidth analysis of a virgin tube showed a relatively small mean strain and little spatial strain variation. Thermal expansion for 11 different crystallographic directions as a function of temperature were obtained showing that thermal expansion varies by about 50% for planes in the 1.3 Å to 2.3 Å range. This anisotrophy, particularly if it is increased by sodium penetration, could be a cause of large localized residual stresses.

Through transmission optical scanning by means of an intense neon light proved to be the most efficient and reliable method for scanning the surface and near surface of tubes. X–ray tomography was used to evaluate the uniformity of the tube density distribution. The largest variation was approximately 3% in the tube examined – about 1.4 times the standard deviation of the measurement error. A limited number of NMR studies on virgin and exposed tubes indicated that exposure to sodium did not produce any obvious deterioration in the bulk crystal structure of the tube.

A series of X–ray diffraction studies was performed to determine surface stresses in BASE tubes. Wide variations were observed in the results, probably due to the inherent problem of using this method on specimens with a large grain size. It is clear that a protocol for the use of X–ray diffraction as an NDE method would require a considerable effort to determine statistical data and correlate the results with other methods. At present, the scatter between results is too large to make this method a practical screening process.

Fabrication and operational stresses were considered in an extensive series of analyses. Considered were the steady–state operational stresses due to a radial thermal gradient and penetration of neutral sodium. Also analyzed were cooldown stresses after sintering. Added together, operational stresses are in the 100 to 170 MPa range, below the fracture strength of the material (≈200 MPa). These could, however, cause subcritical crack growth leading to delayed failure. Relatively large internal grain stresses (100–200 MPa) are generated during cooldown. It was concluded that intergranular fracture could be prevented by reducing grain size to below 20–30 μm. Neutral sodium penetration seems to not cause significant anisotropic expansion strains.

The small EM pump used in the regenerative SHE was operated in a specially designed test loop to obtain pump performance data. A slight redesign of the pump was recommended. This involved a reshaping of the pole pieces to better utilize the magnetic field and reduce current requirements. A useful pump design relationship was presented for the device. This should be useful in examining the value of alterations in field strength and current without alteration of pump geometry.

References

1. *Research Program on a One kW Sodium Heat Engine (SHE) System*, Final Technical Report (May 4, 1986 to September 30, 1989), Contract No. DE-AC02-83CE40651, Ford Motor Company, Dearborn, MI (Oct. 1, 1989).

2. E. K. Beauchamp, *β''-Alumina Electrolyte Failure in Sodium/Sulfur Batteries*, Sandia National Laboratories Report SAND86-0019, Contract No. DE-AC04-76DP00789 (July 1986).

3. B. J. McEntire, R. H. Snow, J. L. Huang, L. Viswanathan, and A. V. Virkar, *Characterization of Processing Flaws in Beta''-alumina*, Adv. Ceram., 22, 335–349 (1988).

4. S. R. Tan, G. J. May, J. R. McLaren, G. Tappin, and R. W. Davidge, *Strength Controlling Flaws in Beta Alumina*, Trans. J. Brit. Ceram. Soc., 79, 120–127 (1980).

5. S. R. Tan and G. J. May, *The Dependence of the Fracture Stress of Beta-Alumina on Microstructural Defects*, J. Mater. Sci. Lett., 12, 1058–1061 (1977).

6. G. E. Youngblood. A. V. Virkar, W. R. Cannon, and R. S. Gordon, *Sintering Processes and Heat Treatment Schedules for Conductive, Lithia-Stabilized β''- Al_2O_3*, Bull. Am. Cer. Soc., 56(2), 206–212 (1977).

7. R. S. Gordon, B. J. McEntire, M. L. Miller, and A. V. Virkar, *Processing and Characterization of Polycrystalline β''-Alumina Ceramic Electrolytes*, Processing of Crystalline Ceramics, H. Palmour III, R. F. Davis, and T. M. Hare, eds., Plenum Press, New York, 405–420 (1978).

8. *Research on Electrodes and Electrolyte for the Ford Sodium-Sulfur Battery*, Annual Report (June 30, 1974 to June 29, 1975), Contract NSF (RANN)-C805, University of Utah, Salt Lake City, UT (July 1975).

9. *Research on Electrodes and Electrolyte for the Ford Sodium-Sulfur Battery*, Semiannual Report (June 29, 1975 to December 31, 1975), Contract NSF (RANN)-C805, University of Utah, Salt Lake City, UT (Feb. 1976).

10. M. L. Miller, B. J. McEntire, G. R. Miller, and R. S. Gordon, "A Prepilot Process for the Fabrication of Polycrystalline β''- Al_2O_3 Electrolyte Tubing," Am. Cer. Soc. Bull., 58(5), 522–526 (1979).

11. D. W. Johnson, Jr., S. M.. Granstaff, Jr., and W. W. Rhodes, *Preparation of* β''- Al_2O_3 *Pressing Powders by Spray Drying*, Bull. Am. Cer. Soc., 58(9), 849–855 (1979).

12. S. R. Tan, *The Preparation of Sodium Beta Alumina by the Isostatic Pressing and Zone Sintering of Spray-Dried Powders*, Conf. on High Temperature Solid Oxide Electrolytes, 2, Upton, NY, Brookhaven National Laboratory (Aug. 16–18, 1983).

13. R. Stevens and J. G. P. Binner, *Review - Structure, Properties, and Production of Beta Alumina*, J. Mater. Sci., 19, 695–715 (1984).

14. E. M. Vogel, D. W. Johnson, Jr., and M. F. Yan, *Homogenization, Phase Formation, and Sintering of Spray-Dried Beta"-Alumina*, Bull. Am. Cer. Soc., 60(4), 494–500 (1981).

15. R. A. Pett, F. D. Runkle, G. J. Tennenhouse, and A. N. Theodore, *Extrusion of Thin-Walled* β''*-Alumina Tubes*, Am. Cer. Soc. Bull., 61(9), 992–995 (1982).

16. M. Rivier and A. D. Pelton, *A New Slip-Casting Technique for the Laboratory Fabrication of* β*-Alumina and Other Ceramics*, Am. Cer. Soc. Bull., 57(2), 183–185 (1978).

17. R. Durstine, *Fabrication of Beta-Alumina Tubes from Cast Ceramic Tapes*, Proc. International Conf. on Fast Ion Transport in Solids, Electrodes, and Electrolytes, p. 79, Lake Geneva, WI (1979).

18. R. W. Powers, "The Electrophoretic Forming of Beta-Alumina Ceramic," J. Electrochem Soc., 122(4), 490–500 (1975).

19. J. H. Kennedy and A. Foissy, *Fabrication of Beta-Alumina Tubes by Electrophoretic Deposition from Suspensions in Dichloromethane*, ibid., 482–486.

20. I. W. Jones and L. J. Miles, *Production of β-Alumina Electrolyte*, Proc. Brit. Cer. Soc., 19, 161–178 (1971).

21. J. R. G. Evans, R. Stevens, and S. R. Tan, *A Study of the Sintering of β-Alumina: Microstructure and Mechanical Properties*, Br. Ceram. Trans. J., 83, 43–49 (1984).

22. B. J. McEntire, G. R. Miller, and R. S. Gordon, *Sintering of β''-Alumina Electrolyte Tubing*, Bull. Am. Cer. Soc., 63(6), 792–802 (1984).

23. G. E. Youngblood, G. R. Miller, and R. S. Gordon, *Relative Effects of Phase Conversion and Grain Size on Sodium Ion Conduction in Polycrystalline, Lithia-Stabilized β''-Alumina*, J. Am. Cer. Soc., 61(1–2), 86–87 (1978).

24. J. P. Singh, A. V. Virkar, D. K. Shetty, and R. S. Gordon, *Microstructural Effects on the Subcritical Crack Growth in Polycrystalline β''-Alumina*, in Fracture Mechanics of Ceramics, vol. 8: Microstructure, Methods, Design, and Fatigue, R. C. Bradt, A. G. Evans, D. P. H. Hasselman, and F. F. Lange, eds., Plenum Press, New York (1986).

25. A. V. Virkar, G. J. Tennenhouse, and R. S. Gordon, *Hot-Pressing of Li_2O-Stabilized β''-Alumina*, J. Am. Cer. Soc., 57(11), 508 (1974).

26. A. V. Virkar and R. S. Gordon, *Fracture Properties of Polycrystalline Lithia-Stabilized β''-Alumina*, J. Am. Cer. Soc., 60(1–2), 58–61 (1976).

27. J. P. Singh, A. V. Virkar, D. K. Shetty, and R. S. Gordon, *Strength-Grain Size Relations in Polycrystalline Ceramics*, J. Am. Cer. Soc., 62(3–4), 179–183 (1979).

28. A. V. Virkar, G. R. Miller, and R. S. Gordon, *Resistivity-Microstructure Relations in Lithia-Stabilized Polycrystalline β''-Alumina,"* J. Am. Cer. Soc., 61(5–6), 250–252 (1977).

29. F. F. Lange, B. I. Davis, and D. O. Raleigh, *Transformation Strengthening of β''-Al_2O_3 with Tetragonal ZrO_2,"* J. Am. Cer. Soc., 66(6), C50–C52 (1983).

30. Y. Sheng, P. Sarkar, P. S. Nicholson, *The Mechanical and Electrical Properties of ZrO_2-$Na\beta''$-Al_2O_3 Composites*, J. Mater. Sci., 23, 958–967 (1988).

31. L. Viswanathan, Y. Ikuma, and A. V. Virkar, *Transformation Toughening of β''-Al_2O_3 by Incorporation of Zirconia*, J. Mater. Sci., 18, 109–113 (1983).

32. J. G. P. Binner and R. Stevens, *Improvement in the Mechanical Properties of Polycrystalline Beta–Alumina via the Use of Zirconia Particles Containing Stabilizing Oxide Additions*," J. Mater. Sci., 20, 3119–3124 (1985).

33. D. J. Green, "Transformation Toughening and Grain Size Control in β''–Al_2O_3/ZrO_2 Composites," J. Mater. Sci., 20, 2639–2646 (1985).

34. Y. Sheng and P. S. Nicholson, *Microstructural Development of a ZrO_2–$Na\beta''$–Al_2O_3 Composite*, J. Mater. Sci., 23, 982–986 (1988).

35. J. G. P. Binner, R. Stevens, and S. R. Tan, *Toughening of Hot–Pressed Beta–Alumina Using Zirconia Additions Prepared from Zirconate, Tartrate, and Carbonate Precursor Materials*, J. of Microscopy, 140(2), 183–194 (1985).

36. J. R. G. Evans, R. Stevens, and S. R. Tan, *Thermal Shock of β–Alumina with Zirconia Additions*, J. Mater. Sci., 19, 4068–4076 (1984).

37. D. Olson and L. C. De Jonghe, *Zirconia–Toughened Sodium Beta''–Alumina Solid Electrolyte*, J. Mater. Sci., 21(12), 4221–4226 (1986).

38. S. N. Heavens, *Strength Improvement in Bet–Alumina by Incorporation of Zirconia*, J. Mater. Sci., 23(10), 3515–3518 (1988).

39. D. J. Green and M. G. Metcalf, *Properties of Slip–Cast Transformation–Toughened β''–Al_2O_3/ZrO_2 Composites*, Bull. Am. Cer. Soc., 63(6), 803–820 (1984).

40. E. A. Ripperger and N. Davids, "Critical Stress in Circular Ring," Trans. Amer. Soc. Civ. Engr., Paper No. 2308, pp. 619–635 (1948).

41. A. G. Evans, *Fracture Toughness: The Role of Indentation Techniques*, pp. 112–135 in Fracture Mechanics Applied to Brittle Materials. S. W. Freiman, ed., American Society for Testing and Materials Special Technical Publication 678 (1978).

42. C. N. J. Wagner and E. N. Aqua, *Adv. in X-Ray Analy.* 7, pp. 46-65 (1964).

43. *Research Program on a One kW Sodium Heat Engine (SHE) System*, Final Technical Report (May 4, 1986 to September 30, 1989), Contract No. DE-AC02-83CE40651, Ford Motor Company, Dearborn, MI (Oct. 1, 1989).

44. L. A. Feldkamp, L. C. Davis, and J. W. Kress, J. of Opt. Soc of Amer. 1, 612 (1984).

45. P. Grangeat, G. Hatchadourian, P. Le Masson, and P. Sire, *Logical Radon, Notice Descriptive Des Algorithmes et des Programmes*, Version 2.1 du 13-04-1990, LETI/DSYS/SETI/90-180 PS, Grenoble, France (May 11, 1990).

46. I. C. Noyan and J. B. Cohen, *Residual Stress: Measurement by Diffraction and Interpretation*, Springer-Verlag (1987).

47. J. D. Eshelby, *The Determination of the Elastic Field of an Ellipsoidal Inclusion, and Related Problems*, Proc. Royal Soc., A, 241 pp. 376-396 (1957).

48. T. K. Hunt, *Final Technical Report on Research Program on a One KWe Sodium Heat Engine (SHE) System*, Prepared for U.S. Dept. of Energy, Assistant Secretary for Conservation (Oct. 1989).

49. N. Laws and J. C. Lee, *Microcracking in Polycrystalline Ceramics: Elastic Isotropy and Thermal Anisotropy*, J. Mech. Phys. Solids, 37, No. 5, pp. 603–618 (1989).

50. Y. Fu and A. G. Evans, *Some Effects of Microcracks on The Mechanical Properties of Brittle Solids – I. Stress, Strain Relations*, Acta Metall., 33, pp. 1515–1523 (1985).

51. A. G. Evans, *Microfracture from Thermal Expansion Anisotropy – Single Phase Systems*, Acta Metall., 26, pp. 1845–1853 (1978).

52. R. W. Rice and R. C. Pohanka, *Grain-Size Dependence of Spontaneous Cracking in Ceramics*, J. Am. Ceram. Soc., 62, pp. 559–563 (1979).

53. A. H. Barnes, *Direct-Current Electromagnetic Pumps*, Nucleonics (Jan. 1953).

Appendix A:

X-Ray Diffraction Results Supplied by Lambda Research

X-RAY DIFFRACTION ANALYSIS

Paul Prevey, Director of Research

Lambda Research Incorporated
1111 Harrison Rd.
Cincinnati, Ohio

This report, provided by Lambda Research, is reproduced in its entirety.

**LAMBDA
RESEARCH**
1111 HARRISON AVENUE CINCINNATI, OHIO 45214-1801 PHONE: 513/621-3933 FAX: 513/621-3935

Argonne National Laboratory
9700 South Cass Avenue
Building 212
Room E213
Argonne, IL 60439

FEASIBILITY STUDY OF THE SURFACE RESIDUAL STRESS MEASUREMENTS BY X-RAY DIFFRACTION ON CERAMATEC BETA"-ALUMINA TUBES

REPORT: 0046-0002 ATTN: Dr. David S. Kupperman
DATE: 03/08/91 AUTHORIZATION: 03410035

INTRODUCTION

Two beta"-alumina tubes were received from Argonne National Laboratory for the purpose of determining the feasibility of making surface residual stress measurements. The tubes, identified as CXI-2600-10 and CXI-2608-10, were reportedly manufactured from beta"-alumina. Specimen CXI-2600-10 had an O.D. of nominally 0.6 in., an I.D. of 0.5 in. and was nominally 12 in. long; one end of the tube was closed. Specimen CXI-2608-10 was approximately 2.0 in. long and was used to develop a technique for making residual stress measurements in the beta"-alumina.

Laboratory Technician: Ronald E. Jones
Ronald E. Jones
Quality Assuranace Manager:
Perry W. Mason
Director of Research:
Paul S. Prevey

This report shall not be reproduced, except in full, without the approval of Lambda Research, Inc. The results reported apply only to the specific sample/s submitted for analysis. Lambda Research operates a quality system in accordance with ISO/IEC Guide 25. Lambda Research is accredited by the American Association for Laboratory Accreditation in the mechanical field of testing, as listed in the current A2LA Directory of Accredited Laboratories.

TECHNIQUE

A technique was first developed for residual stress measurements in the beta"-alumina tubes using Specimen CXI-2600-10. The technique development consisted of obtaining a diffraction pattern of the beta"-alumina and selecting diffraction peaks suitable for residual stress measurement Several repeat residual stress measurements were then made to determine which diffraction peak gave the best results.

The crystal structure of the beta"-alumina was assumed to be rhombohedral with lattice parameters referred to hexagonal axes of A = 5.6101 and C = 33.461. The structure is based upon prior private communications with General Motors Research Laboratories on similar material received from the same source. Miller indices assigned to the diffraction peaks sighted here are based upon a best estimate of proper indexing of that structure. No such structure is found in the JCPDS Files.

Two diffraction peaks were considered for x-ray diffraction residual stress measurement using a copper K-alpha technique. The first peak considered, which occurred at nominally 103 deg., was found to produce an unacceptably high standard deviation and was, therefore, abandoned. The second peak, occurring at 120.4 deg. and attributed to the (4,2,.,10) planes was selected as the best available technique for x-ray diffraction residual stress measurement. Virtually all other available diffraction peaks appeared to be either of low intensity or to be obviously compound diffraction peaks, subject to interference.

X-ray diffraction residual stress measurements were made in the longitudinal and circumferential directions, at the surface only, on tube specimen CXI-2608-10. The measurements were made in the marked area (on the cylindrical side of the tube), approximately 2.3 in. from the open end at the specific times after exposure to the atmosphere as shown in Table III. The purpose of the measurements was to determine any changes in residual stress caused by water absorption. The tube was not removed from the plastic shipping bag that contained the desiccant prior to residual stress measurement.

The samples were rocked through an angular range of +-2.5 deg. around the mean psi angles during measurement to integrate the diffracted intensity over more grains, minimizing the influence of the grain size.

X-ray diffraction residual stress measurements were performed using a Six-Angle Sine-Squared-Psi technique employing the diffraction of chromium K-alpha radiation from the apparent (4,2,.,10) planes of the hexagonal crystal structure of beta alumina at a Bragg angle of approximately 121.0 deg. The Six-Angle Sine-Squared-Psi technique was performed to determine whether or not the lattice spacing was a linear function of sine-squared-psi as required for the plane-stress linear elastic macroscopic residual stress model. The diffraction peak angular positions were determined for positive psi tilts of 0, 18.4, 26.6, 33.2, 39.2, and 45.0 deg. The diffraction peak angular positions at each of the psi tilts employed for measurement were determined from the position of the K-alpha 1 diffraction peak separated from the superimposed K-alpha doublet assuming a Cauchy diffraction peak profile in the high back-reflection region.(1) The diffracted intensity, peak breadth, and position of the K-alpha 1 diffraction peak were determined by fitting the assumed Cauchy profile by least squares regression after correction for the Lorentz polarization and absorption effects, and for a linearly sloping background intensity.

Details of the diffractometer fixturing are outlined below:

Incident Beam Divergence:	3.0 deg. long. direction 1.0 deg. circ. direction
Detector :	Si(Li) set for 90% acceptance of the chromium K-alpha energy
Psi Rotation :	0.0, 18.4, 26.6, 33.2, 39.2, and 45.0 deg.
E/(1 + v) :	3.39×10^7 psi
Irradiated Area :	2.5mm x 7mm (0.01 in. x 0.3 in.) (long axis in the direction of measurement) for the longitudinal direction 7mm x 2.5mm (0.3 in. x 0.1 in.) (short axis in the direction of measurement) for the circumferential direction

The value of the elastic constant E/(1 + v) required to calculate the macroscopic residual stress from the strain measured normal to the (4,2,.,10) planes of the beta"-alumina was calculated using bulk values for E and v, available from previous examinations of similar material. No attempt was made to empirically determine the x-ray elastic constant of the beta"-alumina employed in the manufacture of tubes.

Because only surface measurements were made in this investigation, it was not possible to correct the results for the effects caused by the penetration of the radiation employed for residual stress measurement into the subsurface stress gradient. The magnitude of this correction can be quite significant, particularly on machined or ground surfaces, and can even change the sign of surface results.

RESULTS AND DISCUSSION

The x-ray diffraction patterns obtained on Specimen CXI-2608-10 during the technique development are shown graphically in Figure 1 and tabulated in Table I.

The figure presents the data as a plot of x-ray intensity vs. the diffraction angle. The diffracted intensity, measured at each step scanning increment, is plotted individually. The "B" series of figures represent an enlarged view of the "A" scale to facilitate the identification of minor diffraction peaks.

Table I shows the data generated on the diffractometer, detectable peaks are identified by an assigned number at the left of the table. The next two columns show the diffraction angle, "2-theta," and the interplanar spacing, "d," after correction for systematic angular error using the NBS silicon standard. In the fourth column, "I/Io," the net peak maximum intensities are listed on a relative scale, with the most intense peak given a value of 100. The fifth column, "Net I % S.D.," displays the percentage standard deviation of the net peak intensity. Peaks with a standard deviation above 50% are not reported.

Several repeat residual stress measurements made on Specimen CXI-2608-10 during the technique development are shown in Table II. The longitudinal and circumferential residual stress measurements made at the surface of Specimen CX-2600-10, as a function of time of exposure to the atmosphere, are presented in Table III. Compressive stresses are shown as negative values, tensile as positive, in units of ksi (10^3 psi).

Figures 2 through 7 and Tables IV through IX indicate the degree of linearity of the lattice spacing of the planes as a function of sine-squared-psi for each stress measurement. The preferred orientation present in the material is quantified by the function, F, the normalized (4210) pole density obtained from measurements of the diffraction peak intensity using the Field-Merchant technique of texture determination during stress measurement. Unity of the function F throughout the range of psi would indicate a totally random sample with uniform peak intensity at all psi angles.

The error shown for each residual stress measurement is one standard deviation resulting from random error in the determination of the diffraction peak angular positions and in the empirically determined value of E/(1 + v) in the <4210> direction. An additional semi-systematic error on the order of +-2 ksi may result from sample positioning and instrument alignment errors. The magnitude of this systematic error was monitored using a powdered metal zero-stress standard in accordance with ASTM specification E915, and found to be -0.9 ksi and +0.3 ksi during the course of this investigation.

CONCLUSIONS

The first set of measurements made to establish the repeatability of the measurement technique on Specimen CXI-2608-10 show average values of -11.1 +-18.18 ksi and -43.8 +-7.67 ksi for 2-theta angles of approximately 103 deg. and 121 deg., respectively. Since the standard deviation was much lower for the diffraction peak at a 2-theta of approximately 120 deg., it was used for all subsequent residual stress measurements. The peak widths ranged between 0.5 deg. and 0.6 deg.

The residual stresses are entirely compressive for the beta"-alumina tube, CXI-2600-10, for the measurements made immediately after removal from the desiccant, after several hours out of exposure to the ambient atmosphere, and after five days of exposure. The measurements are least compressive in the circumferential direction as compared to the axial direction. The stresses range from -129 ksi to -37 ksi. The standard deviations are on the order of +-5 ksi for the circumferential direction, and between +-11 and +-26 ksi for the axial direction. The date each stress measurement was made, as well as the start time and finish time, the temperature and the humidity, are shown in Table III.

The results appear to show that the circumferential stress becomes somewhat more compressive with time. No trend is evident in the axial data. The error is larger in the axial direction, perhaps due to the wider angular divergence of the incident beam used for the axial measurement.

REFERENCES: [6sf.100290.fm]

(1) P.S. Prevey, ADV. IN X-RAY ANAL., Vol. 29, 1986, pp. 103-112.

(2) P.S. Prevey, ADV. IN X-RAY ANAL., Vol. 20, 1977, pp. 345-354.

page 1

LAMBDA RESEARCH INC.
CINCINNATI OHIO

QUALITATIVE PHASE ANALYSIS

Specimen CX-1 2608-10 1/.2NSLS/M
Data File: 046002.q01 9012E21KO Wavelength = 1.54178 (A)
Corrected Using NBS SRM 640 Maximum Intensity = 761 cps

Range No 1 20.00 -->140.00 deg. at .02 deg. steps for 1.0 s

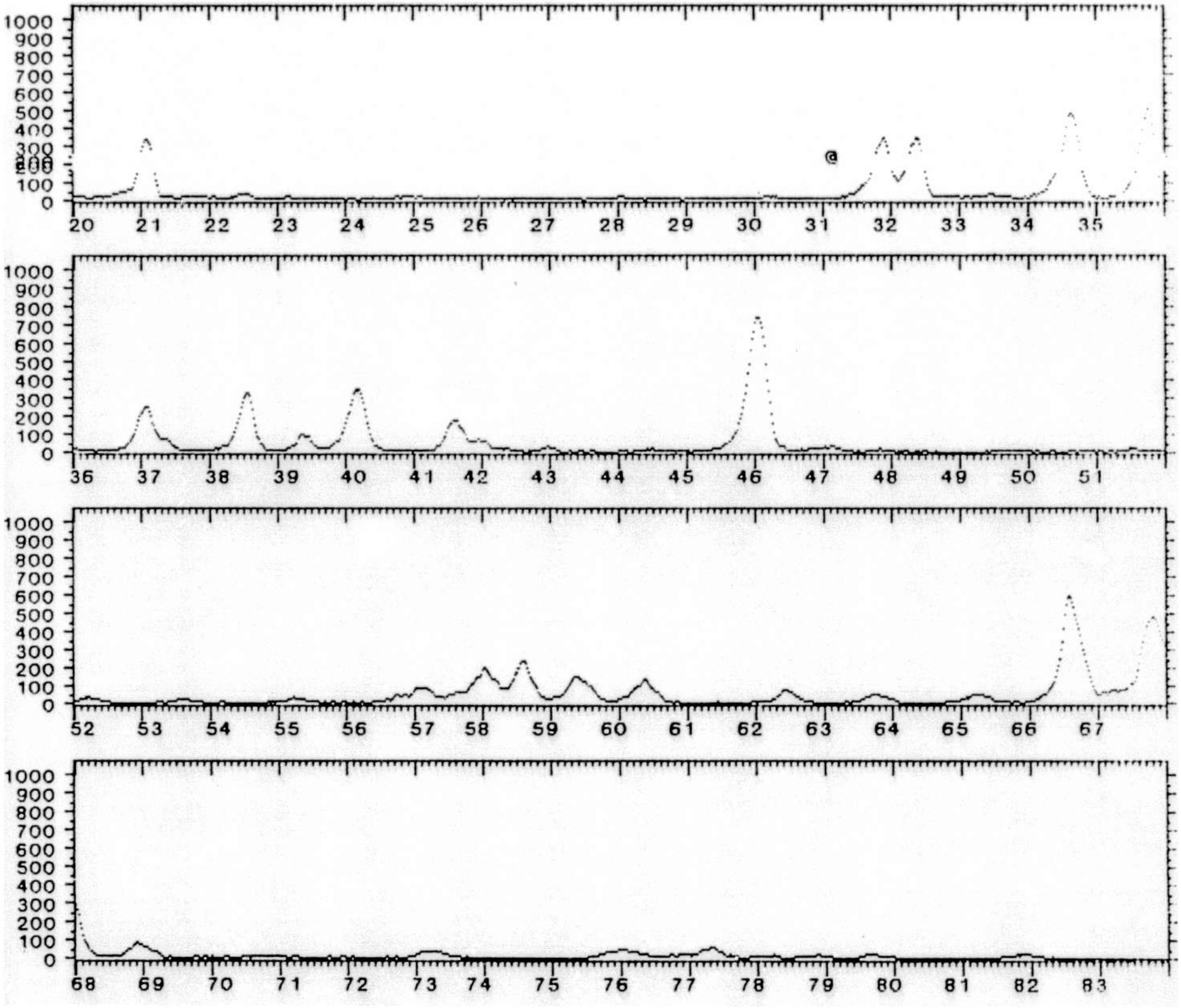

Figure 1A

LAMBDA RESEARCH INC.
CINCINNATI OHIO

QUALITATIVE PHASE ANALYSIS

Specimen CX-1 2608-10 1/.2NSLS/M
Data File: 046002.q01 9012E21KO Wavelength = 1.54178 (A)
Corrected Using NBS SRM 640 Maximum Intensity = 761 cps

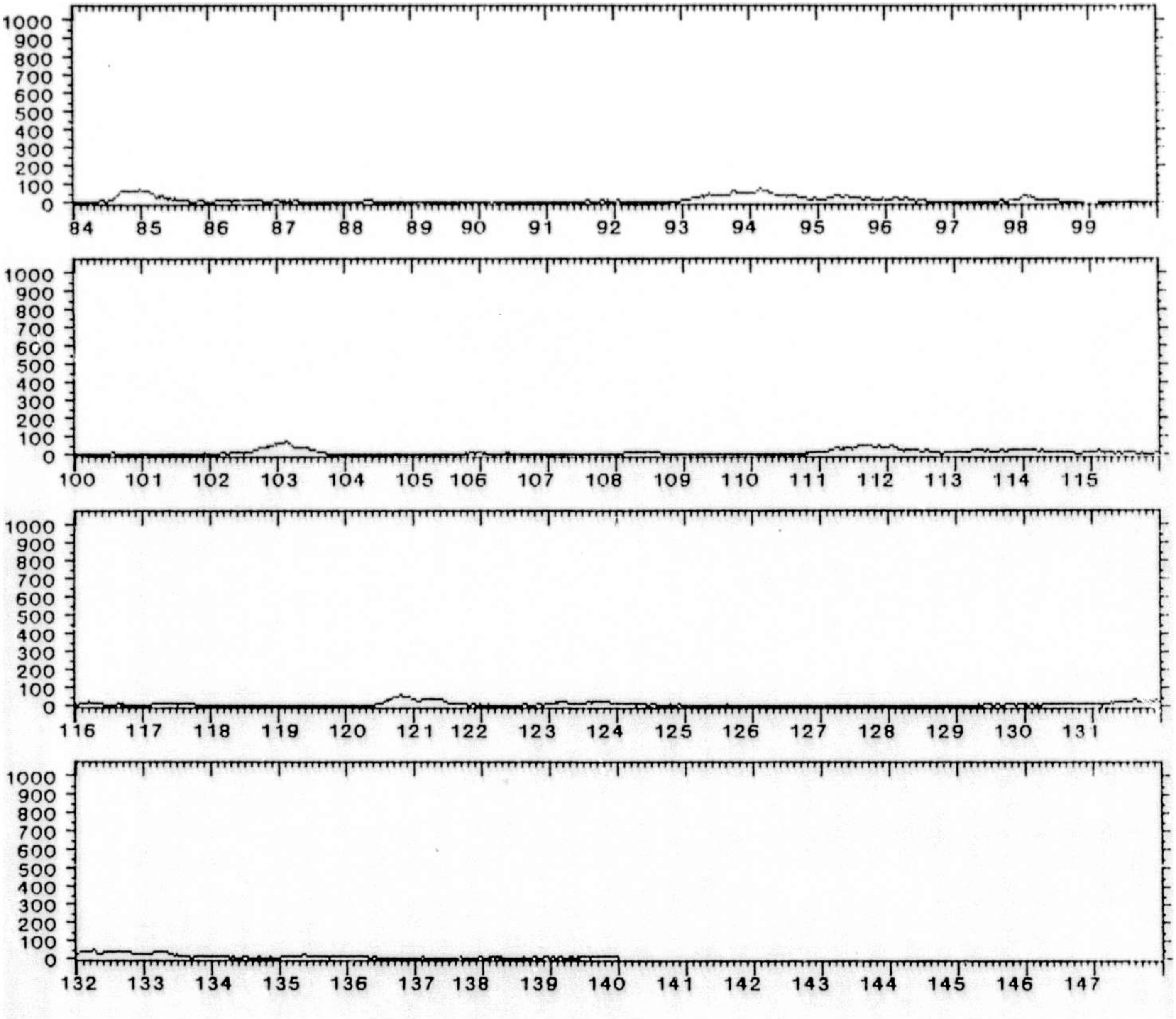

Figure 1A (Cont.)

LAMBDA RESEARCH INC.
CINCINNATI OHIO

QUALITATIVE PHASE ANALYSIS

Specimen CX-1 2608-10 1/.2NSLS/M
Data File: 046002.q01 9012E21KO Wavelength = 1.54178 (A)
Corrected Using NBS SRM 640 Maximum Intensity = 761 cps

Range No 1 20.00 -->140.00 deg. at .02 deg. steps for 1.0 s

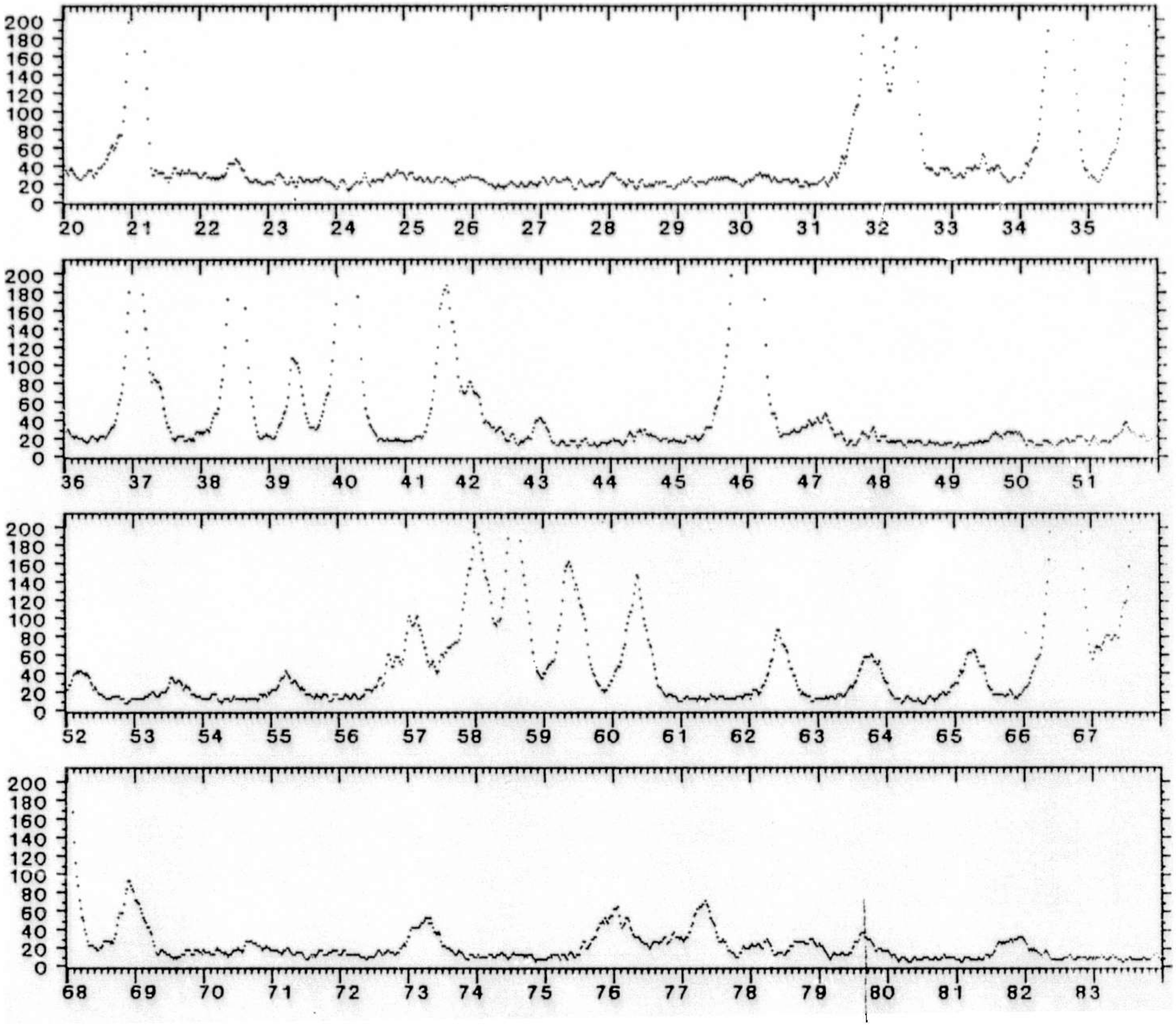

Figure 1B

LAMBDA RESEARCH INC.
CINCINNATI OHIO

QUALITATIVE PHASE ANALYSIS

```
        Specimen CX-1 2608-10                    1/.2NSLS/M
Data File: 046002.q01          9012E21KO          Wavelength = 1.54178 (A)
Corrected Using NBS SRM 640                   Maximum Intensity =    761 cps
```

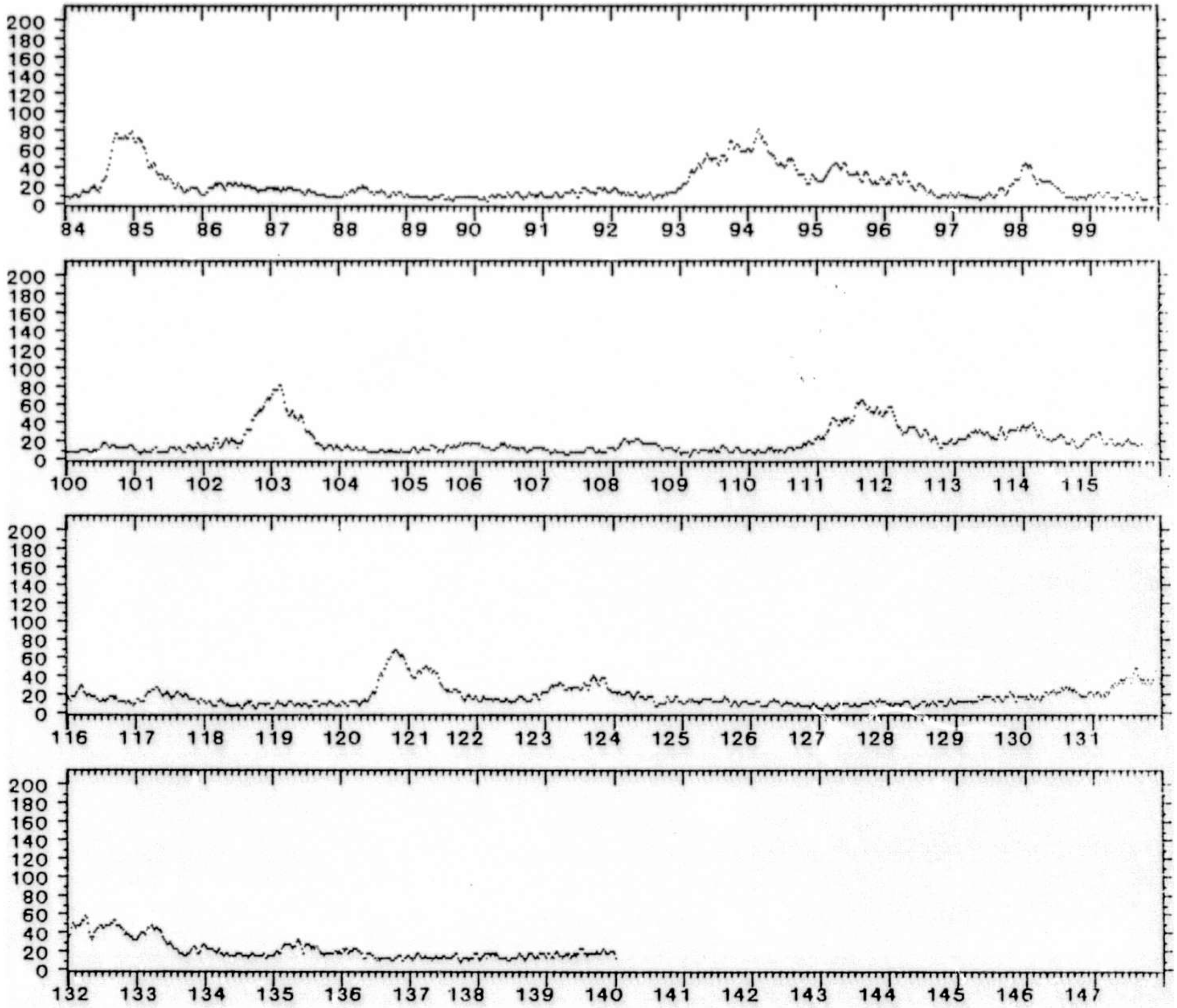

Figure 1B (Cont.)

Lambda Research, Inc.

046002.i03 **SSPSI3.12** **02/07/91**

SIN(PSI)^2 X-RAY DIFFRACTION STRESS ANALYSIS **4**

0046002.i03 BAIO2 Tube 2.5 in. From End Loc. Surf. Cir. Im. 9102C01KS

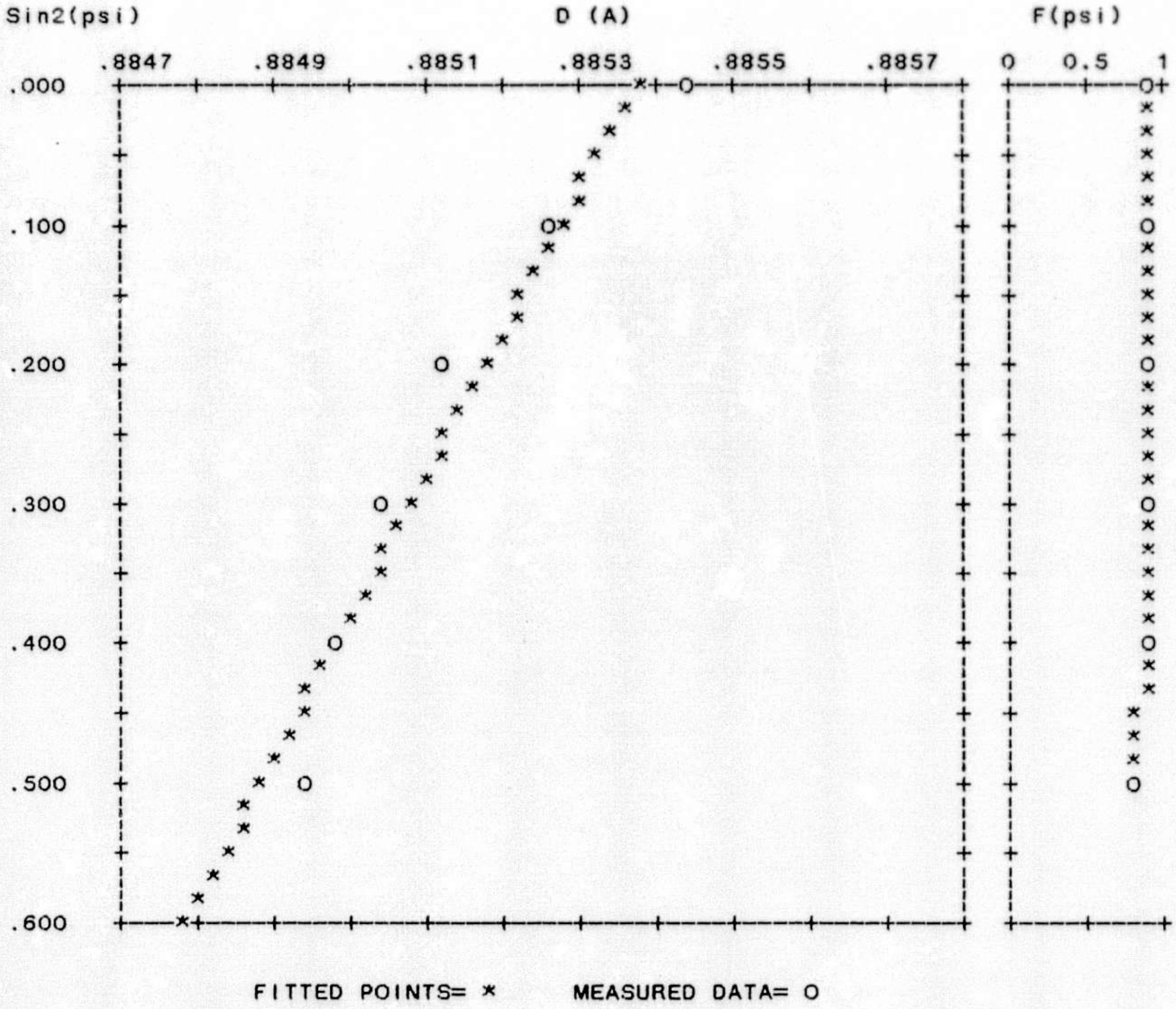

D(0) = .88535 (A) D(.5) = .88489 (A) STRESS = -37.6 +- 4.1 (ksi)

Figure 2

```
                          Lambda Research, Inc.
046002.i03                     SSPSI3.12                          02/07/91

          SIN(PSI)^2 X-RAY DIFFRACTION STRESS ANALYSIS                       6

0046002.i03      6AlO2 Tube 2.5 in. From End Loc. Surf. Cir. 1hr.      9102C01KS
```

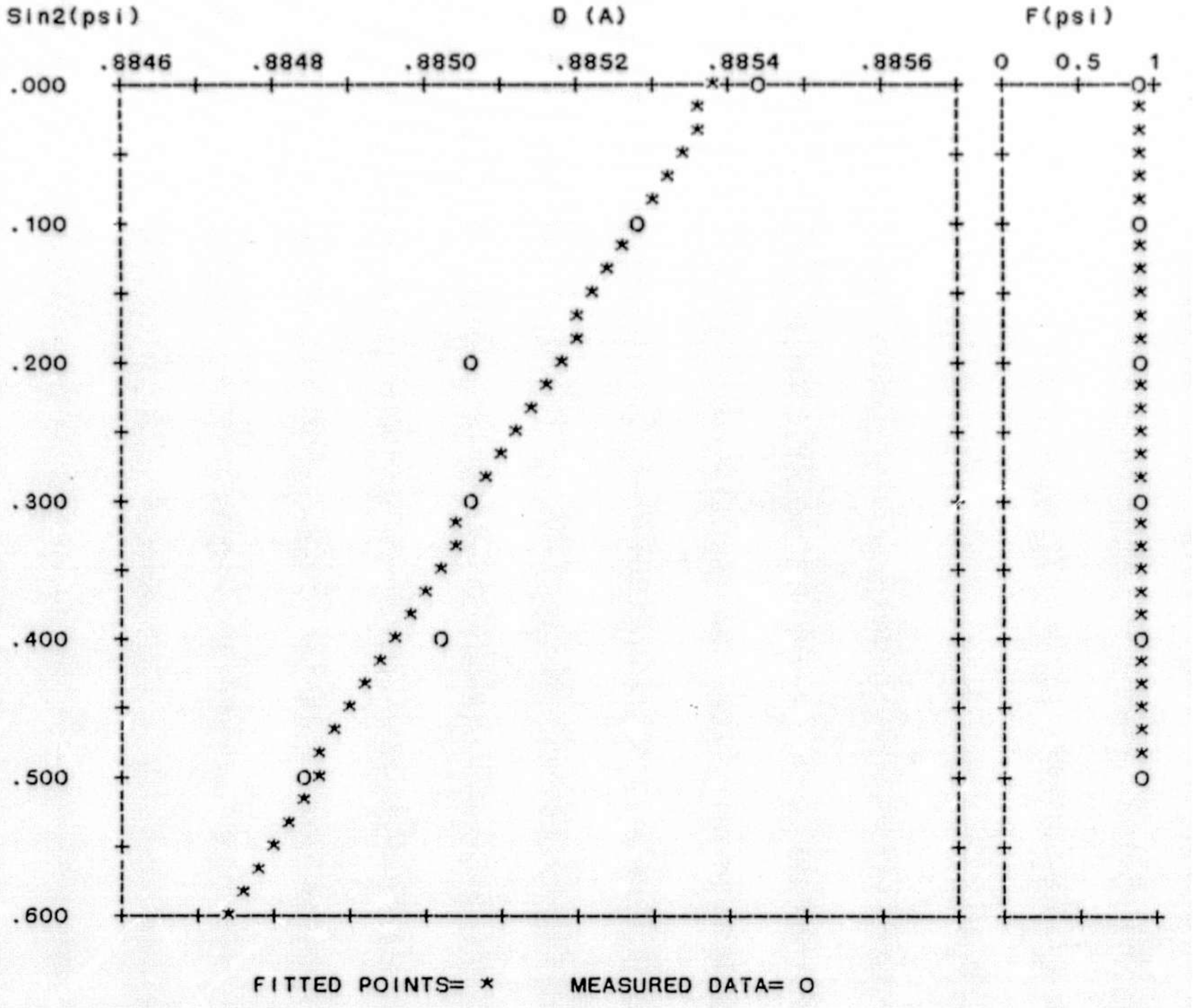

```
D(0) =  .88540 (A)     D( .5) =  .88486 (A)     STRESS =   -41.0 +-  4.9 (ksi)
```

Figure 3

```
                         Lambda Research, Inc.
046002.i03                    SSPSI3.12                      02/07/91

          SIN(PSI)^2 X-RAY DIFFRACTION STRESS ANALYSIS                 12

046002.i03     8AlO2 Tube 2.5 in. From end Loc. Surf. Axial 5day     9102C06RJ
```

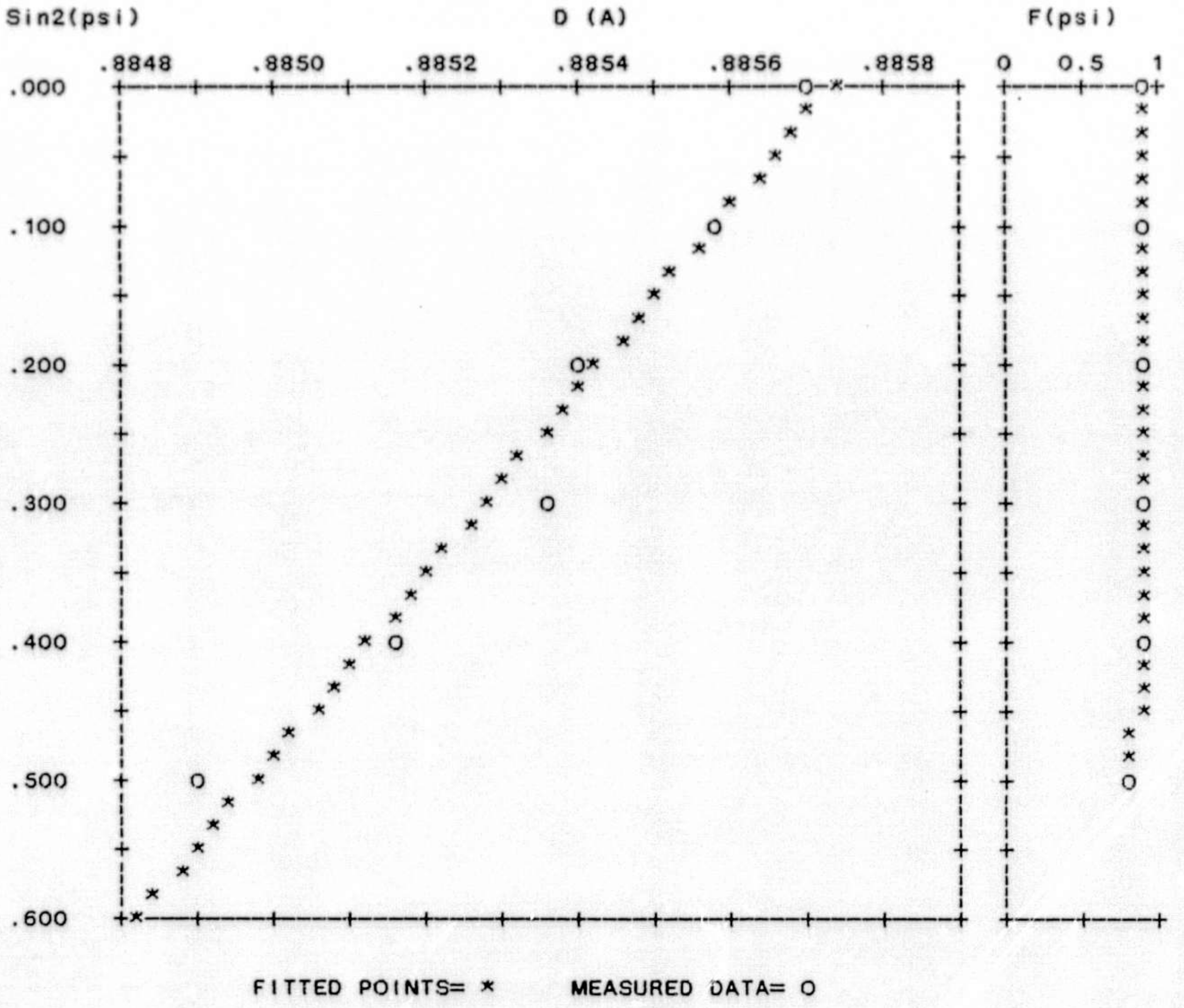

```
D(0) =  .88574 (A)     D( .5) =  .88498 (A)     STRESS =   -57.9 +-  4.4 (ksi)
```

Figure 4

```
                         Lambda Research, Inc.
046002.i03                    SSPSI3.12                       02/07/91

        SIN(PSI)^2 X-RAY DIFFRACTION STRESS ANALYSIS                  2

046002.i03      BAlO2 Tube 2.5 in. From End Loc. Surf. Axial lm.      9102C01KS
```

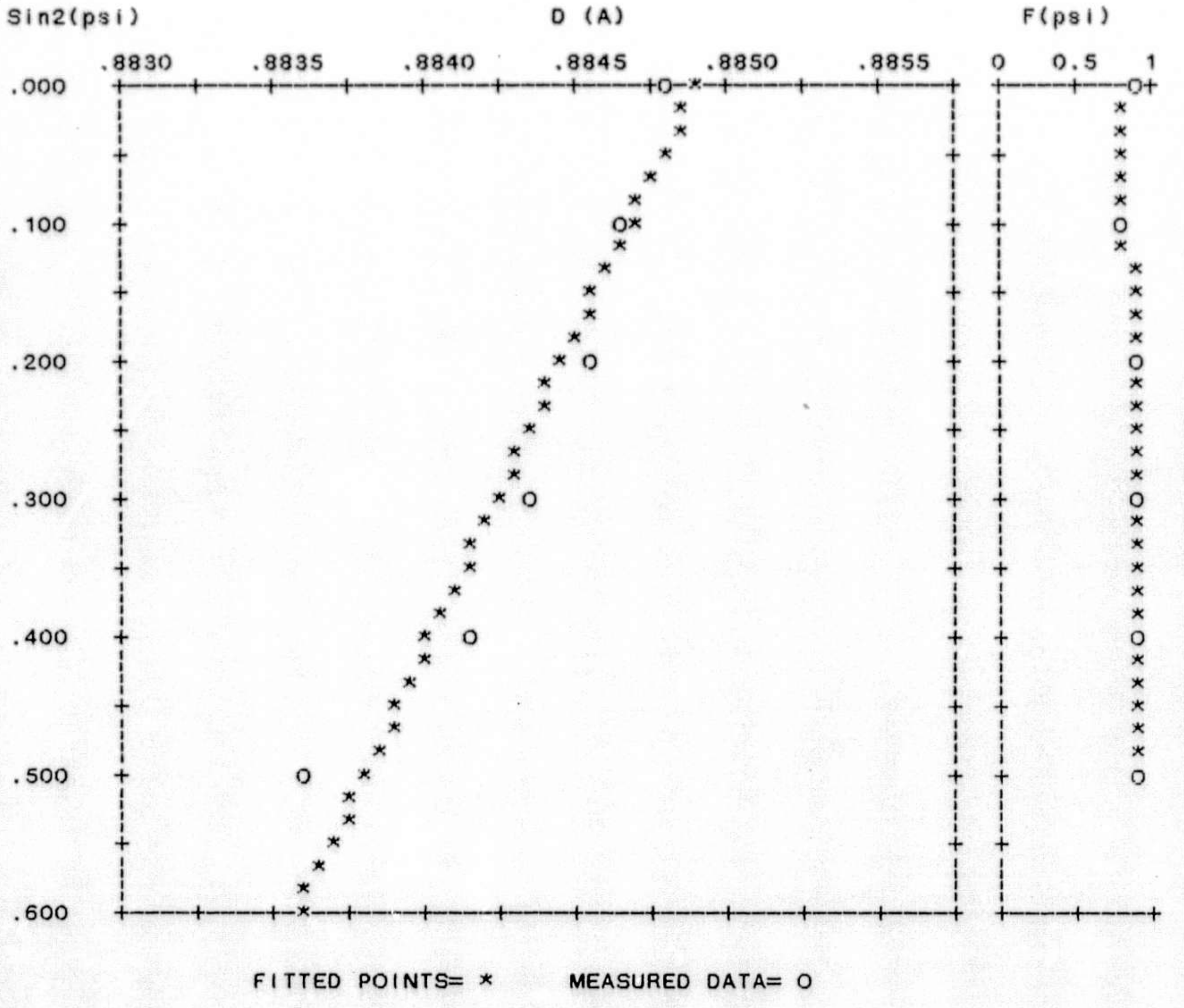

```
D(O) =   .88493 (A)      D( .5) =  .88383 (A)      STRESS =    -84.1 +- 11.1 (ksi)
```

Figure 5

```
                         Lambda Research, Inc.
046002.i03                    SSPSI3.12                    02/07/91

         SIN(PSI)^2 X-RAY DIFFRACTION STRESS ANALYSIS                8

0046002.I03    BAIO2 Tube 2.5 In. From End Loc. Surf. Axial 1hr.    9102C01KS
```

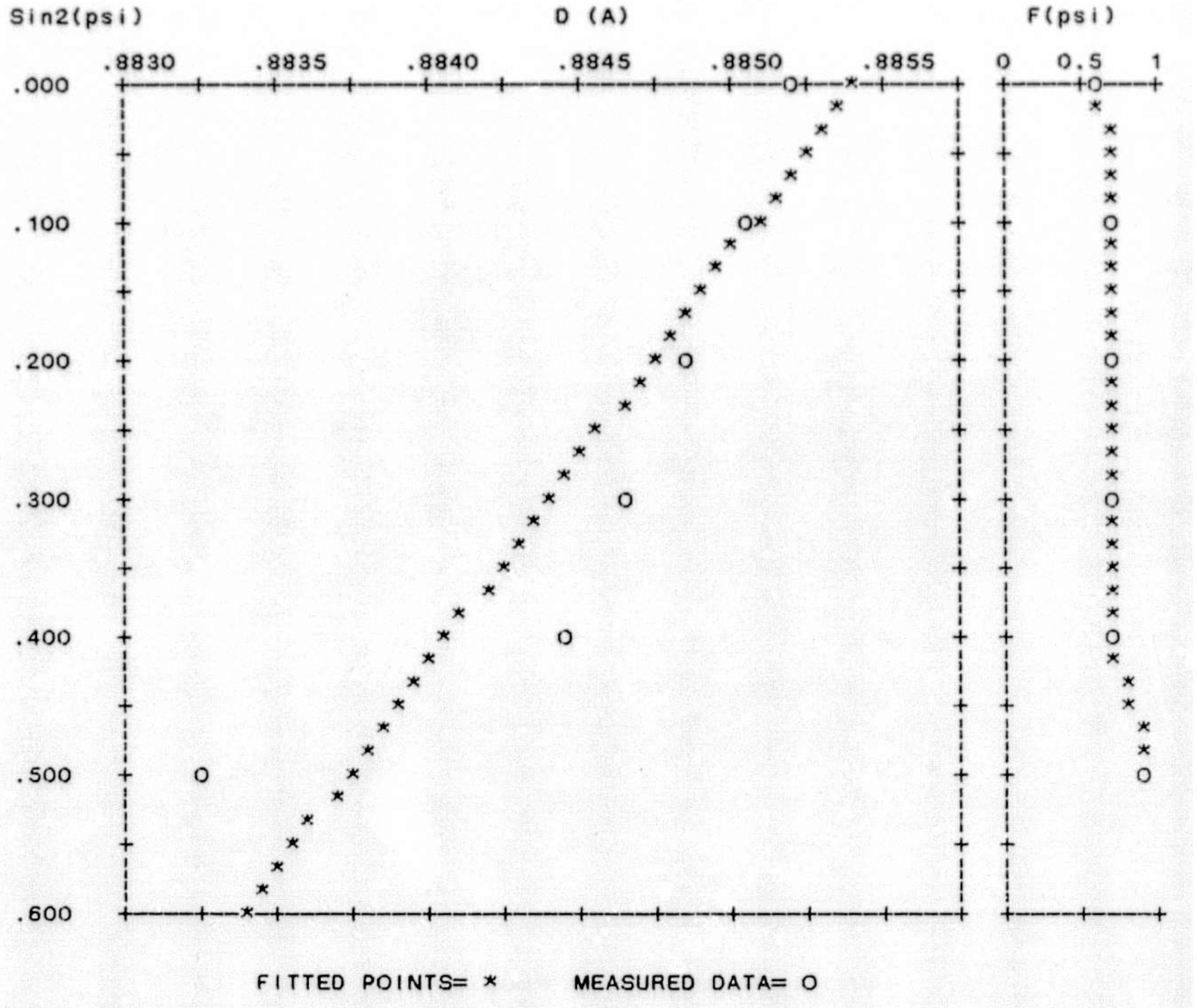

```
D(0) =  .88544 (A)      D( .5) =  .88376 (A)      STRESS =  -128.8 +- 26.0 (ksi)
```

Figure 6

```
                    Lambda Research, Inc.
046002.i03                SSPSI3.12                    02/07/91

        SIN(PSI)^2 X-RAY DIFFRACTION STRESS ANALYSIS            10

046002.i03    8AI02 Tube 2.5 in. From End Loc. Surf. Axial 5day   9102C06RJ
```

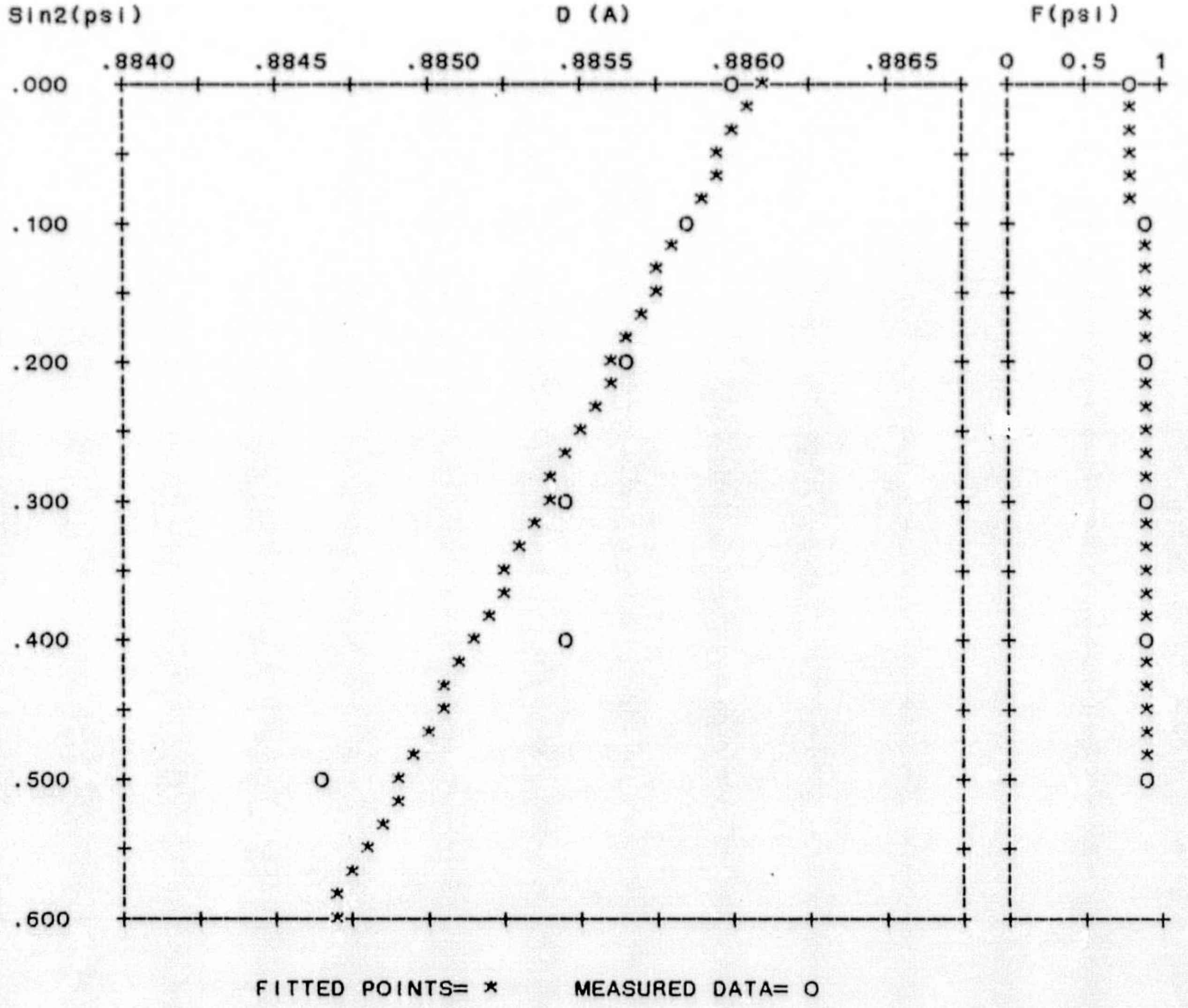

```
D(O) =  .88611 (A)     D( .5) =  .88494 (A)     STRESS =   -89.2 +- 16.1 (ksi)
```

Figure 7

Lambda Research, Inc.
046002.q01 QUALTAB3.04.FOR 12/21/90

QUALITATIVE PHASE ANALYSIS

Specimen CX-1 2608-10 1/.2NSLS/M

Data File: 046002.q01 9012E21KO Wavelength = 1.54178 (A)
Alignment Correction Using NBS SRM 640 Maximum Intensity = 761 cps

Peak No.	2-Theta (deg.)	d(A)	I/Io	Net I %S.D.	Intensity (cps) Peak	B.G.	Net	Width (deg.)
Range No: 1	20.00 -->140.00 deg. using .02 deg. steps for 1.0s							
1	21.05	4.220	43	6	349	31	318	.26
2	22.49	3.953	3	48	48	29	18	.24
3	31.86	2.809	46	6	359	22	337	.24
4	32.34	2.768	46	6	357	22	336	.24
5	33.36	2.686	2	43	39	21	18	.42
6	34.60	2.592	65	5	499	20	479	.32
7	35.74	2.512	68	5	520	20	500	.28
8	37.04	2.427	34	7	265	19	246	.26
9	38.52	2.337	44	6	339	19	321	.28
10	39.30	2.293	13	12	111	18	93	.26
11	40.12	2.248	47	6	364	18	347	.30
12	41.58	2.172	23	8	188	17	171	.28
13	46.00	1.973	100	4	749	15	733	.34
14	47.10	1.929	4	25	47	15	32	.42
15	51.51	1.774	3	32	38	15	23	.26
16	52.19	1.753	4	26	46	15	30	.34
17	53.53	1.712	3	35	36	15	21	.30
18	55.19	1.664	4	27	43	15	28	.34
19	57.13	1.612	12	12	103	15	88	.28
20	57.99	1.590	26	8	206	15	191	.30
21	58.57	1.576	33	7	254	15	239	.28
22	59.35	1.557	20	9	164	15	149	.40
23	60.33	1.534	18	10	149	15	134	.34
24	62.41	1.488	10	14	90	15	75	.31
25	63.76	1.460	6	19	61	14	46	.44
26	65.24	1.430	7	17	67	14	53	.32
27	66.56	1.405	82	4	613	14	599	.38
28	67.80	1.382	67	5	505	14	492	.44
29	68.88	1.363	11	13	93	13	80	.40
30	70.64	1.333	2	39	30	13	17	.28
31	73.25	1.292	6	19	54	12	42	.46
32	76.05	1.251	7	16	66	12	54	.44
33	77.33	1.234	8	15	73	12	61	.30
34	78.24	1.222	3	34	31	12	19	.23
35	78.90	1.213	3	32	32	11	21	.46
36	79.64	1.204	4	25	40	11	29	.24
37	81.96	1.176	3	28	35	11	24	.52
38	84.99	1.141	10	14	81	11	70	.57
39	93.78	1.056	8	15	70	10	61	.18
40	94.18	1.053	10	13	83	10	74	.22
41	96.30	1.035	3	29	32	10	23	.16

TABLE I

```
                       Lambda Research, Inc.
046002.q01               QUALTAB3.04.FOR                   12/21/90

                    QUALITATIVE PHASE ANALYSIS                       page 2
        Specimen CX-1 2608-10                  1/.2NSLS/M

Peak   2-Theta                     Net I        Intensity (cps)        Width
 No.    (deg.)       d(A)   I/Io   %S.D.    Peak     B.G.     Net     (deg.)
 42     98.09       1.021     5     21        46       10      36        .26
 43    103.15        .984    10     13        84       10      75        .54
 44    108.24        .951     2     49        22       10      12        .60
 45    111.71        .931     8     16        66       11      56        .24
 46    114.09        .919     3     29        34       11      23        .36
 47    115.07        .914     3     33        30       11      19        .24
 48    116.25        .908     3     33        31       11      19        .26
 49    117.35        .902     2     37        28       11      17        .26
 50    120.88 Ka1    .886     8     16        70       12      59        .36
 51    121.32 Ka2    .886     5     20        52       12      40        .24
 52    123.26        .876     3     32        33       12      21        .22
 53    123.76        .874     4     26        41       13      28        .30
 54    130.73        .848     2     48        28       14      14        .42
 55    131.69        .845     5     23        48       15      34        .40
 56    132.29        .843     5     21        55       15      40        .14
 57    132.75        .841     5     22        53       15      38        .30
 58    133.27        .840     4     24        48       15      33        .34
 59    135.31        .833     2     50        29       16      13        .58
```

TABLE I (Cont.)

Lambda Research
Cincinnati, OH

SURFACE RESIDUAL STRESS
BETA"-ALUMINA TUBE CXI-2608-10

2-Theta(deg.)	Repeat	Stress(ksi)	Peak Width(deg.)
103	1	+ 3.3	0.56
	2	-25.7	0.54
	3	-31.0	0.52
	4	-13.2	0.48
	5	+11.3	0.47
	AVG.	-11.1 +-18.18	0.51 +-0.04
121	1	-37.6	0.64
	2	-36.9	0.59
	3	-49.9	0.61
	4	-53.9	0.62
	5	-40.6	0.60
	AVG.	-43.8 +-7.67	0.61 +-0.02

TABLE II

Lambda Research
Cincinnati, Ohio

BETA"-ALUMINA TUBE CXI-2600-10

	DATE	START TIME	FINISH TIME	TEMP. (DEG.)F	HUMIDITY	STRESS (KSI)
CIRCUMFERENTIAL DIRECTION						
Immediately	2/1/91	11:35 AM	12:42 PM	73	51%	- 37.6 +- 4.1
Hours	2/1/91	12:42 PM	1:45 PM	74	51%	- 41.0 +- 4.9
5 Days	2/6/91	10:30 AM	11:42 AM	76	62%	- 57.9 +- 4.4
AXIAL DIRECTION						
Immediately	2/1/91	10:25 AM	11:35 AM	73	51%	- 84.1 +-11.1
Hours	2/1/91	1:50 PM	2:52 PM	74	51%	-128.8 +-26.0
5 Days	2/6/91	8:15 AM	10:25 AM	75	63%	- 89.2 +-16.1

TABLE III

```
                         Lambda Research, Inc.
 046002.i03                    SSPSI3.12                      02/07/91


          SIN(PSI)^2 X-RAY DIFFRACTION STRESS ANALYSIS                 3


0046002.i03      8AIO2 Tube 2.5 in. From End Loc. Surf. Cir. Im.      9102C01KS


   PSI    2 THETA    TIME    COR. TIME      D(A)      VERTEX      F(P)  SIN(P)^2
   ----------------------------------------------------------------------------

    .00    120.48    81.58    331.58
           120.73    47.94    122.65
           120.98    44.56    110.12
           121.26    50.11    132.05
           121.53    57.87    167.99      .88545   120.895      .953     .000

  18.43    120.43    80.79    292.83
           120.66    53.15    122.66
           120.88    43.08     87.94
           121.28    46.87    100.72
           121.68    64.21    177.39      .88527   120.935      .980     .100

  26.56    120.53    76.16    198.65
           120.81    50.64     94.98
           121.08    46.23     83.00
           121.38    52.04    100.25
           121.68    66.15    153.39      .88513   120.968     1.000     .200

  33.21    120.48    90.52    225.31
           120.78    62.75    110.47
           121.08    53.13     85.31
           121.36    59.17    101.74
           121.63    70.59    139.18      .88505   120.987      .968     .300

  39.23    120.48   103.33    228.14
           120.73    76.08    121.77
           120.98    61.77     86.71
           121.31    65.08     95.13
           121.63    79.57    136.32      .88500   120.998      .946     .400

  45.00    120.53   120.88    224.56
           120.73    91.99    124.94
           120.93    74.43     87.22
           121.38    80.05    100.46
           121.83   110.91    197.24      .88494   121.011      .841     .500



  E/(1+V)=  33884.  +-    0. (ksi)         STRESS =   -37.6 +-  4.1(ksi)


  D(0) =  .88538 +-  .00003 (A)    D( .5) =  .88489 (A) SSQR = .119E-07
```

TABLE I V

```
                         Lambda Research, Inc.
046002.i03                   SSPSI3.12                          02/07/91

          SIN(PSI)^2 X-RAY DIFFRACTION STRESS ANALYSIS                  5


0046002.i03      8AI02 Tube 2.5 in. From End Loc. Surf. Cir. 1hr.     9102C01KS


   PSI    2 THETA    TIME   COR. TIME      D(A)     VERTEX     F(P)  SIN(P)^2
   ---------------------------------------------------------------------------

    .00    120.48    65.29   268.27
           120.68    40.94   109.03
           120.88    36.41    91.11
           121.21    39.92   105.21
           121.53    48.24   145.01      .88544   120.896     .967    .000

  18.43    120.43    75.31   264.37
           120.68    48.84   110.16
           120.93    40.52    82.34
           121.28    45.04    97.43
           121.63    57.17   148.18      .88530   120.930    1.000    .100

  26.56    120.48    82.58   238.69
           120.71    59.55   123.77
           120.93    47.86    87.22
           121.31    51.60    98.79
           121.68    66.91   156.97      .88508   120.979     .991    .200

  33.21    120.43    95.17   261.33
           120.68    68.44   129.76
           120.93    54.37    88.87
           121.33    58.44   100.69
           121.73    76.87   167.45      .88507   120.981     .977    .300

  39.23    120.43   111.55   270.16
           120.68    79.76   130.69
           120.93    62.79    88.05
           121.26    63.90    91.47
           121.58    76.99   126.68      .88503   120.990     .966    .400

  45.00    120.53   115.89   220.62
           120.76    82.63   107.72
           120.98    65.49    73.78
           121.33    69.60    82.49
           121.68    87.09   124.45      .88485   121.031     .897    .500



  E/(1+V)=  33884.  +-    0. (ksi)          STRESS =   -41.0 +-  4.9(ksi)


  D(0) =  .88540 +-  .00004 (A)    D( .5) =  .88486 (A) SSQR = .169E-07
```

TABLE V

```
                          Lambda Research, Inc.
046002.i03                    SSPSI3.12                          02/07/91

           SIN(PSI)^2 X-RAY DIFFRACTION STRESS ANALYSIS                   11


046002.i03       8AIO2 Tube 2.5 in. From end Loc. Surf. Axial 5day      9102C06RJ


    PSI    2 THETA    TIME    COR. TIME      D(A)      VERTEX      F(P)  SIN(P)^2
    ---------------------------------------------------------------------------

     .00    120.40     61.49    255.59
            120.64     38.86    104.49
            120.88     32.99     81.36
            121.18     37.78    100.35
            121.48     46.67    144.47      .88572   120.834      .933    .000

   18.56    120.44     73.21    221.87
            120.72     49.30    106.58
            121.00     45.30     93.75
            121.26     51.39    114.98
            121.52     62.57    163.90      .88559   120.862      .907    .101

   26.56    120.40     87.78    256.43
            120.66     61.78    126.97
            120.92     50.04     90.94
            121.30     56.94    112.45
            121.68     76.25    195.07      .88540   120.905      .973    .200

   33.21    120.36     98.05    269.99
            120.62     68.86    128.31
            120.88     53.99     86.62
            121.22     56.41     93.50
            121.56     71.99    143.23      .88537   120.913     1.000    .300

   39.23    120.44    101.62    226.93
            120.70     74.34    119.19
            120.96     61.68     87.84
            121.28     64.89     96.32
            121.60     79.39    139.33      .88517   120.958      .939    .400

   45.00    120.60    123.44    197.65
            120.78    101.19    133.77
            120.96     86.00    101.85
            121.30     86.91    105.25
            121.64    108.00    158.41      .88492   121.016      .876    .500



   E/(1+V)=  33884.  +-    0. (ksi)          STRESS =    -57.9 +-   4.4(ksi)


   D(0) =  .88574 +-  .00004 (A)    D( .5) =  .88498 (A) SSQR = .141E-07
```

TABLE VI

```
                         Lambda Research, Inc.
046002.i03                    SSPSI3.12                         02/07/91

            SIN(PSI)^2 X-RAY DIFFRACTION STRESS ANALYSIS                  1


046002.i03     8AI02 Tube 2.5 in. From End Loc. Surf. Axial Im.     9102C01KS


   PSI    2 THETA    TIME   COR. TIME     D(A)     VERTEX      F(P)  SIN(P)^2
   ---------------------------------------------------------------------------

    .00   120.55     57.42   245.22
          120.75     39.89   115.60
          120.95     32.58    83.32
          121.33     33.81    88.48
          121.70     43.34   135.53     .88482   121.038     .904    .000

  18.43   120.41     82.75   317.18
          120.83     56.46   137.42
          121.25     48.28   105.92
          121.53     54.12   128.83
          121.81     65.25   184.58     .88468   121.072     .878    .100

  26.56   120.34     73.59   243.25
          120.80     52.05   114.38
          121.25     45.60    91.65
          121.60     49.02   104.63
          121.95     61.44   164.70     .88459   121.092    1.000    .200

  33.21   120.27     79.41   255.52
          120.73     59.81   128.86
          121.18     50.48    94.53
          121.63     52.82   103.99
          122.09     66.87   173.57     .88437   121.143     .975    .300

  39.23   120.13     98.06   325.28
          120.76     69.87   132.47
          121.39     61.40   104.75
          121.78     64.49   116.78
          122.16     77.76   179.62     .88418   121.185     .962    .400

  45.00   120.20     78.99   218.90
          120.90     57.90    94.06
          121.60     49.71    71.15
          121.92     53.71    84.67
          122.23     60.66   114.10     .88363   121.313     .889    .500


  E/(1+V)=  33884  +-    0. (ksi)          STRESS =    -84.1 +- 11.1(ksi)


  D(0) =  .88493 +-  .00009 (A)    D( .5) =  .88383 (A) SSQR = .890E-07
```

TABLE VII

```
                         Lambda Research, Inc.
046002.i03                    SSPSI3.12                        02/07/91

        SIN(PSI)^2 X-RAY DIFFRACTION STRESS ANALYSIS                  7


0046002.i03    8AIO2 Tube 2.5 in. From End Loc. Surf. Axial 1hr.    9102C01KS


   PSI    2 THETA   TIME   COR. TIME     D(A)     VERTEX     F(P)  SIN(P)^2
   ------------------------------------------------------------------------

    .00   120.48    48.74   200.99
          120.68    33.96    97.02
          120.88    27.98    71.16
          121.28    30.43    81.38
          121.68    41.49   142.70     .88525   120.941     .687    .000

  18.43   120.33    48.93   178.20
          120.71    34.36    83.65
          121.08    28.61    61.74
          121.46    32.27    75.84
          121.83    41.85   126.52     .88505   120.986     .736    .100

  26.56   120.38    51.19   154.50
          120.71    40.12    91.52
          121.03    34.39    69.86
          121.36    34.80    71.73
          121.68    40.55    95.42     .88486   121.029     .753    .200

  33.21   120.13    57.09   192.15
          120.63    42.04    90.52
          121.13    35.14    65.41
          121.48    36.01    69.08
          121.83    41.79    93.31     .88469   121.069     .787    .300

  39.23   120.18    73.77   217.22
          120.66    56.71   110.88
          121.13    49.96    87.21
          121.48    49.04    85.33
          121.83    55.07   109.75     .88447   121.119     .739    .400

  45.00   120.08    76.42   199.58
          120.86    53.57    80.78
          121.64    43.21    68.16
          123.14    69.92   191.36
          124.64    69.71   218.66     .88328   121.394    1.000    .500



  E/( 1+V)=  33884.  +-    0. (ksi)        STRESS =  -128.8 +- 26.0(ksi)


  D(0) =  .88544 +-  .00021 (A)    D( .5) =  .88376 (A) SSQR = .486E-06
```

TABLE VIII

```
                        Lambda Research, Inc.
046002.i03                    SSPSI3.12                        02/07/91

            SIN(PSI)^2 X-RAY DIFFRACTION STRESS ANALYSIS                 9


046002.i03       BAlO2 Tube 2.5 in. From End Loc. Surf. Axial 5day   9102C06RJ


   PSI    2 THETA    TIME   COR. TIME      D(A)      VERTEX      F(P)  SIN(P)^2
   ----------------------------------------------------------------------------

    .00   120.29    56.32   236.90
          120.53    39.11   112.53
          120.77    32.21    82.34
          121.13    36.40   100.30
          121.49    47.47   163.80      .88602   120.765      .813    .000

  18.43   120.38    68.11   188.96
          120.61    56.76   134.43
          120.83    51.61   114.79
          121.16    53.21   121.38
          121.49    65.53   178.61      .88586   120.800      .916    .100

  26.56   120.16   101.06   311.39
          120.62    75.97   169.53
          121.08    68.74   143.11
          121.32    73.56   162.38
          121.56    83.19   207.58      .88566   120.847      .923    .200

  33.21   120.20    85.45   226.95
          120.66    68.50   140.94
          121.12    63.46   123.47
          121.48    68.64   145.04
          121.84    81.37   213.75      .88547   120.889      .946    .300

  39.23   120.28    86.93   188.24
          120.62    74.76   136.39
          120.96    70.93   124.35
          121.40    73.46   135.55
          121.84    83.85   184.91      .88548   120.888     1.000    .400

  45.00   120.52   138.49   250.62
          120.94   127.31   209.78
          121.36   121.25   192.51
          121.66   125.99   213.01
          121.96   135.94   260.47      .88465   121.077      .939    .500



  E/(1+V)=  33884.  +-    0. (ksi)          STRESS =   -89.2 +- 16.1(ksi)


  D(0) =  .88611 +-  .00013 (A)    D( .5) =  .88494 (A) SSQR = .186E-06
```

TABLE IX

```
                         Lambda Research, Inc.
046002.i01                   SSPSI3.12                       01/18/91

         SIN(PSI)^2 X-RAY DIFFRACTION STRESS ANALYSIS                 1


046002.i01          8A102 Spec. CX-11 O.D. Loc. Surf. Long.        9101C16RJ


   PSI   2 THETA   TIME    COR. TIME     D(A)     VERTEX     F(P)  SIN(P)^2
   ------------------------------------------------------------------------

    .00   102.50   219.48   883.68
          102.71   151.63   433.32
          102.92   119.15   298.79
          103.13   121.39   307.81
          103.34   158.46   472.77     .98482   102.912     .754    .000

  10.00   102.36   234.22   953.00
          102.64   140.38   337.14
          102.92    97.37   196.65
          103.13    96.50   194.61
          103.34   125.39   285.04     .98471   102.928    1.000    .030

  20.00   102.22   307.56  1260.24
          102.50   224.73   568.93
          102.78   158.93   307.72
          103.13   145.49   270.23
          103.48   214.37   536.98     .98489   102.902     .778    .117

  25.00   102.36   319.58   954.39
          102.64   235.96   486.18
          102.92   162.15   261.52
          103.20   148.33   230.86
          103.48   195.66   357.35     .98410   103.017     .901    .179

  30.00   102.22   436.59  1660.55
          102.57   282.94   521.47
          102.92   215.71   325.66
          103.27   228.43   363.19
          103.62   306.31   657.81     .98465   102.936     .744    .250

  35.00   102.22   495.93  1580.21
          102.57   358.41   608.90
          102.92   243.36   297.72
          103.27   246.65   307.12
          103.62   351.68   606.80     .98431   102.987     .712    .329



  E/(1+V)=  33884.  +-    0. (ksi)        STRESS =   -49.7 +- 27.7(ksi)


  D(0) =  .98480 +-  .00015 (A)    D( .3) =  .98432 (A) SSQR = .313E-06
```

SIN(PSI)^2 X-RAY DIFFRACTION STRESS ANALYSIS 2

046002.i01 BA102 Spec. CX-11 O.D. Loc. Surf. Long. 9101C16RJ

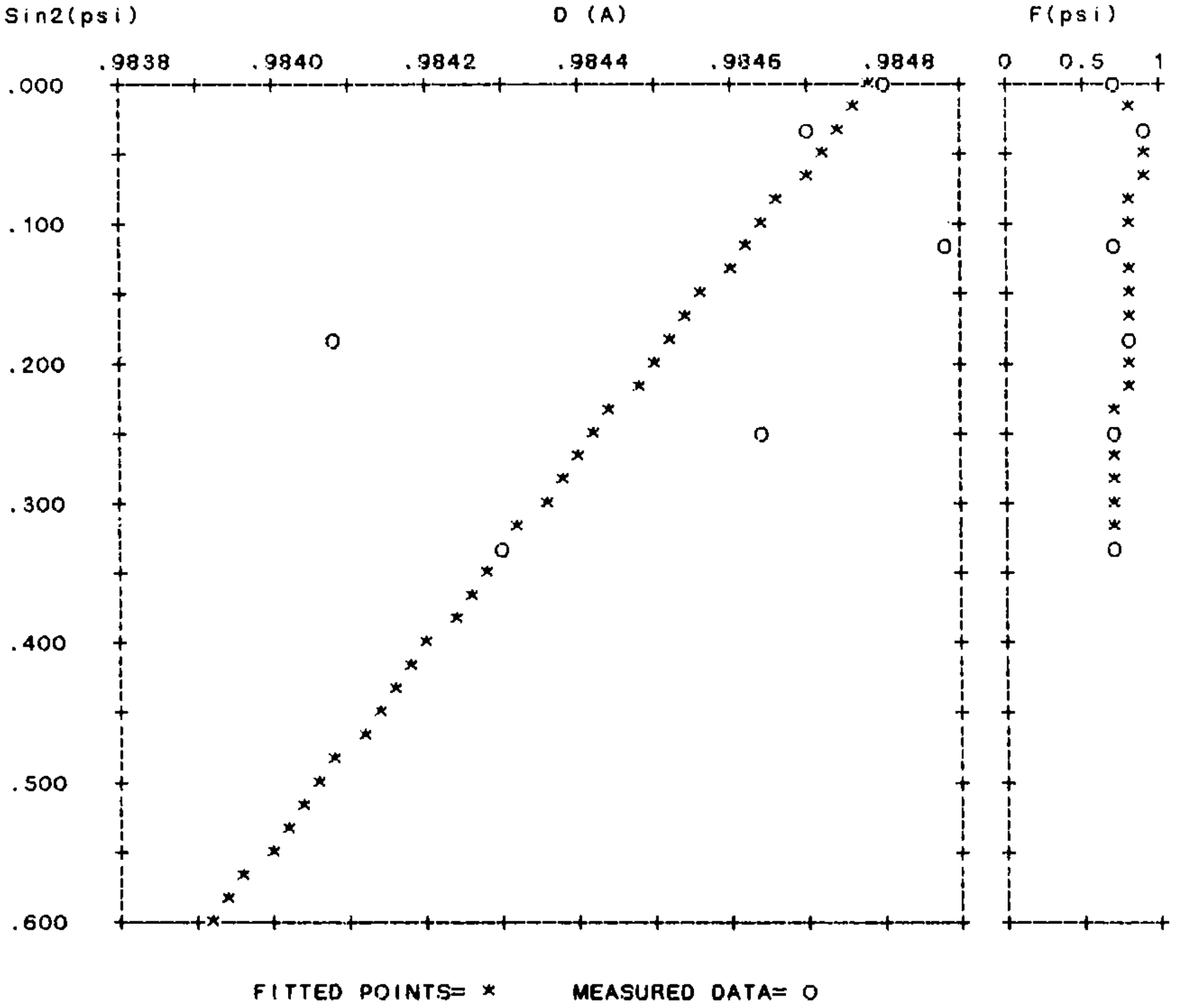

D(0) = .98480 (A) D(.3) = .98432 (A) STRESS = -49.7 +- 27.7 (ksi)

```
                          Lambda Research, Inc.
046002.i01                      SSPSI3.12                      01/18/91

           SIN(PSI)^2 X-RAY DIFFRACTION STRESS ANALYSIS                 3


046002.i01         BAIO2 Spec. O.D. Loc. Surf. Long. STATIC        9101C17GT


     PSI   2 THETA   TIME   COR. TIME     D(A)     VERTEX     F(P)  SIN(P)^2
     ---------------------------------------------------------------------

      .00   120.40   203.71   812.01
            120.65   128.77   340.45
            120.90   113.79   282.32
            121.20   133.59   363.14
            121.50   170.47   562.85      .88582  120.809     .800    .000

    18.43   120.40   236.11   740.58
            120.65   160.12   353.32
            120.90   138.16   281.39
            121.23   159.87   355.14
            121.55   211.29   593.55      .88575  120.827     .823    .100

    26.56   120.45   243.35   640.34
            120.70   177.66   354.47
            120.95   149.28   270.37
            121.30   173.29   344.80
            121.65   224.49   560.09      .88543  120.898     .875    .200

    33.21   120.40   341.33  1055.90
            120.68   247.71   501.79
            120.95   210.14   375.36
            121.23   208.30   372.40
            121.50   248.26   516.13      .88517  120.959     .744    .300

    39.23   120.35   287.62   535.82
            120.63   224.36   339.83
            120.90   183.68   249.02
            121.28   212.95   318.36
            121.65   271.36   502.08      .88564  120.851    1.000    .400

    45.00   120.40   416.61   773.82
            120.65   330.27   466.62
            120.90   266.59   321.17
            121.35   280.15   357.06
            121.80   387.24   709.65      .88518  120.955     .800    .500



    E/(1+V)=  33884.  +-    0. (ksi)          STRESS =   -41.3 +- 16.4(ksi)


    D(0) =  .88577 +-  .00013 (A)    D( .5) =  .88523 (A) SSQR = .194E-06
```

SIN(PSI)^2 X-RAY DIFFRACTION STRESS ANALYSIS 4

046002.i01 BAIO2 Spec. O.D. Loc. Surf. Long. STATIC 9101C17GT

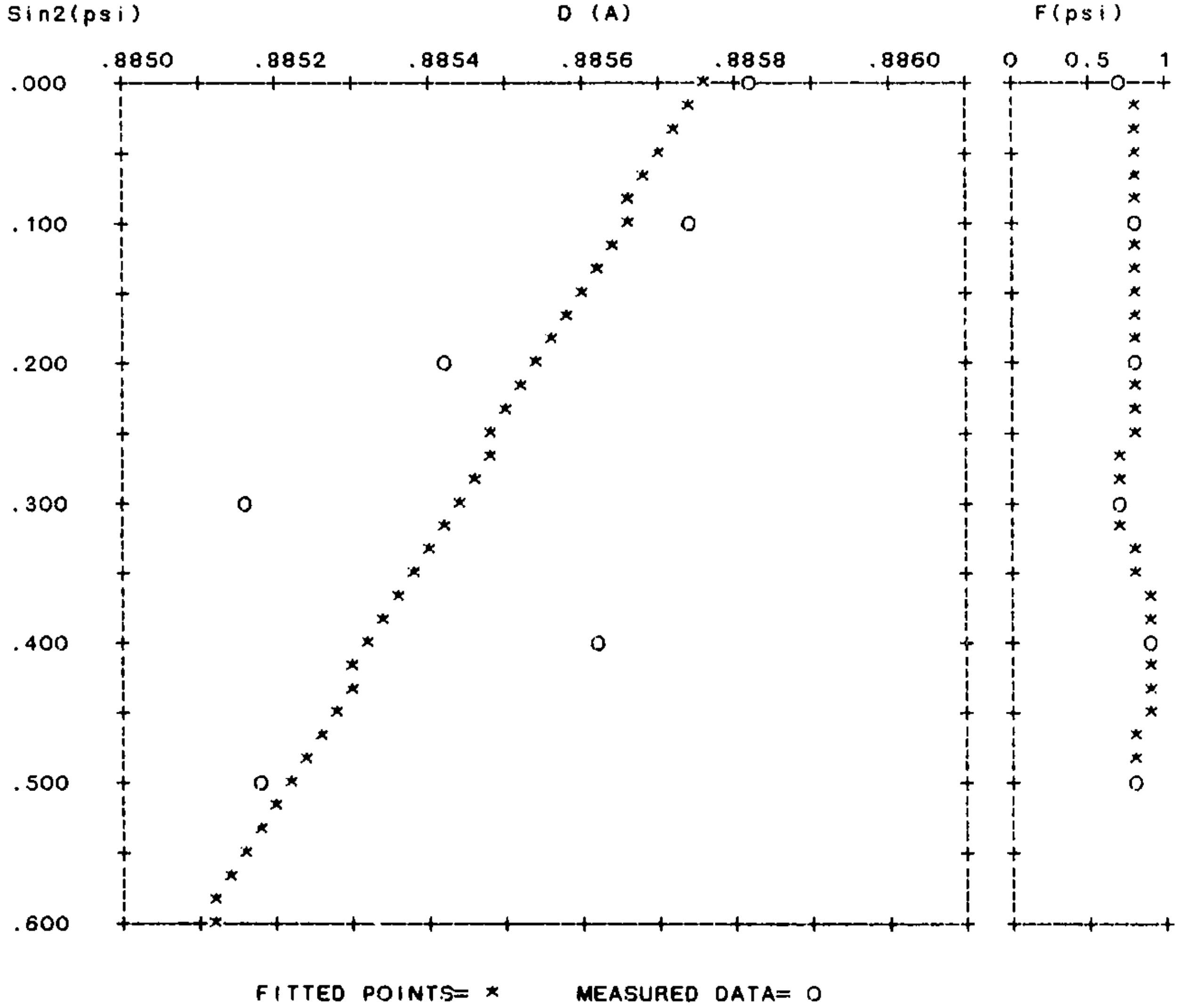

D(0) = .88577 (A) D(.5) = .88523 (A) STRESS = -41.3 +- 16.4 (ksi)

```
                         Lambda Research, Inc.
 046002.i01                   SSPSI3.12                         01/18/91

          SIN(PSI)^2 X-RAY DIFFRACTION STRESS ANALYSIS                  5


046002.i01          BAIO2 Spec. O.D. Loc. Surf. Logn. ROCK          9101C18KS


   PSI    2 THETA   TIME    COR. TIME     D(A)    VERTEX    F(P)  SIN(P)^2
   --------------------------------------------------------------------------

    .00   120.40   221.28    925.14
          120.65   141.19    382.92
          120.90   121.30    302.98
          121.23   143.83    397.00
          121.55   182.69    614.92    .88571  120.835    .968    .000

  18.43   120.40   254.34    807.46
          120.68   171.06    378.31
          120.95   149.96    308.86
          121.25   171.14    382.53
          121.55   216.40    587.70    .88563  120.853   1.000    .100

  26.56   120.30   307.24   1017.98
          120.65   202.46    420.32
          121.00   172.52    325.18
          121.25   191.82    388.57
          121.50   238.74    585.49    .88567  120.845    .914    .200

  33.21   120.40   333.46    828.55
          120.73   238.48    429.12
          121.05   209.66    350.03
          121.33   240.83    444.10
          121.60   292.58    648.66    .88544  120.896    .976    .300

  39.23   120.20   451.01   1332.85
          120.63   306.19    525.80
          121.05   247.70    366.81
          121.30   271.89    433.82
          121.55   323.73    611.63    .88547  120.891    .894    .400

  45.00   120.20   519.31   1208.37
          120.55   371.02    531.66
          120.90   284.30    334.97
          121.23   305.22    382.54
          121.55   359.93    525.77    .88547  120.890    .969    .500



  E/(1+V)=  33884.  +-     0. (ksi)        STRESS =   -21.1 +-  4.9(ksi)


  D(0) =  .88570 +-  .00004 (A)    D( .5) =  .88543 (A) SSQR = .170E-07
```

Lambda Research, Inc.
046002.i01 SSPSI3.12 01/18/91

SIN(PSI)^2 X-RAY DIFFRACTION STRESS ANALYSIS 6

046002.I01 BAIO2 Spec. O.D. Loc. Surf. Logn. ROCK 9101C18KS

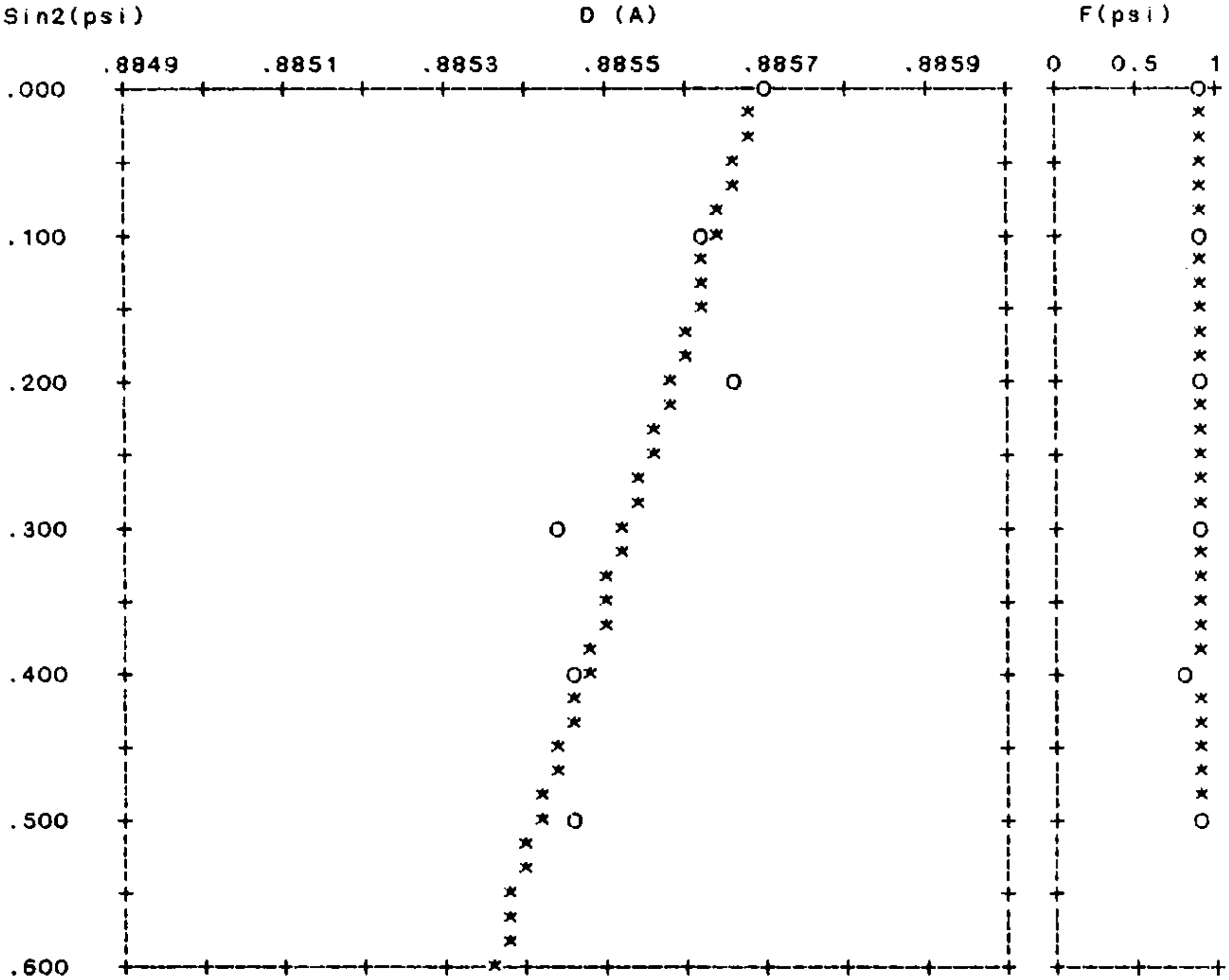

FITTED POINTS= * MEASURED DATA= O

D(0) = .88570 (A) D(.5) = .88543 (A) STRESS = -21.1 +- 4.9 (ksi)

```
                        Lambda Research, Inc.
046002.i02                     SSPSI3.12                           01/21/91

            SIN(PSI)^2 X-RAY DIFFRACTION STRESS ANALYSIS                    1


046002.I02        BA102 Spec. O.D. Lco. Surf. Long. 6ANGLE ROCK        9101C21RJ


   PSI   2 THETA   TIME   COR. TIME     D(A)     VERTEX     F(P)  SIN(P)^2
   ---------------------------------------------------------------------

    .00   120.40   199.41   770.50
          120.58   138.44   381.99
          120.75   114.93   285.79
          121.15   130.84   350.15
          121.55   181.84   639.09      .88585   120.804   1.000    .000

  18.43   120.35   278.45   910.83
          120.70   175.21   377.16
          121.05   164.91   344.92
          121.28   190.78   437.93
          121.50   224.16   588.00      .88569   120.839    .998    .100

  26.56   120.30   322.83  1079.32
          120.60   220.47   471.46
          120.90   181.73   343.15
          121.25   212.27   447.46
          121.60   280.74   791.32      .88578   120.819    .882    .200

  33.21   120.35   404.96  1068.79
          120.63   290.13   538.54
          120.90   240.66   397.55
          121.28   268.73   481.26
          121.65   361.49   865.98      .88558   120.865    .977    .300

  39.23   120.30   372.95   932.06
          120.65   255.54   410.91
          121.00   214.01   307.75
          121.30   234.03   360.01
          121.60   302.68   593.48      .88552   120.878    .938    .400

  45.00   120.35   431.40   842.32
          120.70   310.58   414.57
          121.05   281.55   353.65
          121.38   301.10   404.83
          121.70   378.70   661.33      .88539   120.909    .911    .500



  E/(1+V)=  33884.  +-    0. (ksi)         STRESS =   -33.1 +-  4.8(ksi)


  D(0) =  .88585 +-  .00004 (A)    D( .5) =  .88542 (A) SSQR = .167E-07
```

Lambda Research, Inc.

046002.i02 SSPSI3.12 01/21/91

SIN(PSI)^2 X-RAY DIFFRACTION STRESS ANALYSIS 2

046002.i02 8A102 Spec. O.D. Lco. Surf. Long. 6ANGLE ROCK 9101C21RJ

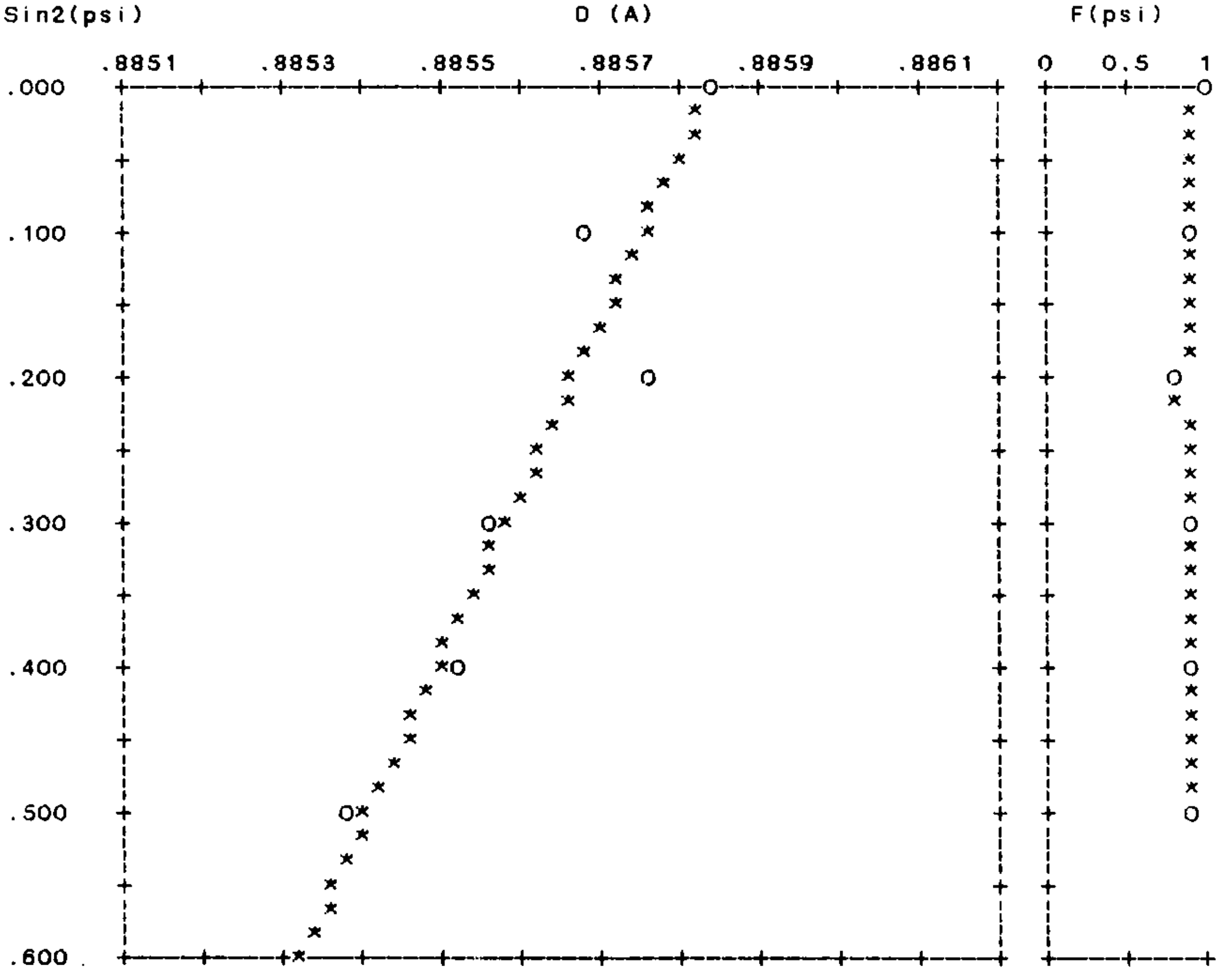

FITTED POINTS= * MEASURED DATA= O

D(0) = .88585 (A) D(.5) = .88542 (A) STRESS = -33.1 +- 4.8 (ksi)

```
                          Lambda Research, Inc.
 046002.d01                   STRESS40.15                          01/17/91

    CAUCHY SEPARATED Ka1 DIFFRACTION PEAK STRESS ANALYSIS                1


                  E/(1+v) = 33884.+-   0. Ksi    1/2 S2 =  4.28 +- .00 x 10-6 1/MPa

            046002.d01         BA102 Spec. O.D. Loc. Surf. Long. Rpt.1 ROCK        9101C15KS
Psi      2-theta    1/I     1/Icor      Psi      2-theta    1/I     1/Icor
 .00     102.48   201.94   775.04      33.21     102.24   491.48  1178.06      B 1/2 =   .56 deg.
         102.69   129.56   346.17                102.57   353.29   554.55      COLD WORK =    .0 %
         102.90    93.76   217.53                102.90   275.32   362.83      STRAIN =  .000029
         103.20   102.80   247.55                103.26   286.21   390.84      STRESS =     3.3 +- 3.6 Ksi
         103.50   170.34   564.23                103.62   411.89   804.77             =     23. +-  25. (MPa)
          99.00   414.28                          99.00   812.39
         106.00   317.51                         106.00   665.25
      d =  .98481 A                          d =  .98484 A
      2θ= 102.913 +- .002 deg.               2θ= 102.909 +- .003 deg.        DEPTH =  .0000 in. (  .000 mm)

            0046002.d01        BA102 Spec. o.D. Loc. Surf. Lpong. Rpt.2 ROCK       9101C15KS
Psi      2-theta    1/I     1/Icor      Psi      2-theta    1/I     1/Icor
 .00     102.48   186.12   733.52      33.10     102.24   416.40   983.21      B 1/2 =   .54 deg.
         102.69   111.98   292.10                102.60   288.00   436.53      COLD WORK =    .0 %
         102.90    84.84   196.79                102.96   220.24   281.75      STRAIN = -.000227
         103.17    93.64   225.76                103.32   241.49   330.52      STRESS =   -25.7 +- 3.5 Ksi
         103.44   147.76   468.32                103.68   363.53   759.51             =   -177. +-  24. (MPa)
          99.00   364.64                          99.00   710.21
         106.00   295.86                         106.00   552.24
      d =  .98499 A                          d =  .98477 A
      2θ= 102.886 +- .002 deg.               2θ= 102.919 +- .003 deg.        DEPTH =  .0000 in. (  .000 mm)

            046002.d01         BA102 Spec. O.D. Loc. Surf. Long. Rpt.3 ROCK        9101C15KS
Psi      2-theta    1/I     1/Icor      Psi      2-theta    1/I     1/Icor
 .00     102.42   218.31  1001.48      33.21     102.24   449.30  1214.47      B 1/2 =   .52 deg.
         102.69   123.79   331.17                102.60   305.95   483.82      COLD WORK =    .0 %
         102.96    90.36   210.47                102.96   243.47   327.91      STRAIN = -.000274
         103.23   107.46   269.17                103.32   256.15   362.34      STRESS =   -31.0 +- 3.5 Ksi
         103.50   166.72   564.83                103.68   372.59   802.50             =   -214. +-  24. (MPa)
          99.00   390.51                          99.00   726.37
         106.00   306.63                         106.00   546.18
      d =  .98493 A                          d =  .98466 A
      2θ= 102.895 +- .002 deg.               2θ= 102.934 +- .003 deg.        DEPTH =  .0000 in. (  .000 mm)

            046002.d01         BA102 Spec. O.D. Loc. Surf. Long. Rpt.4 ROCK        9101C15KS
Psi      2-theta    1/I     1/Icor      Psi      2-theta    1/I     1/Icor
 .00     102.53   176.29   653.01      33.21     102.33   433.50  1018.29      B 1/2 =   .48 deg.
         102.75   102.80   257.83                102.68   305.00   467.43      COLD WORK =    .0 %
         102.98    79.53   180.91                103.03   250.31   336.15      STRAIN = -.000117
         103.25    97.13   238.83                103.35   280.74   414.24      STRESS =   -13.2 +- 3.5 Ksi
         103.53   158.75   544.66                103.68   396.04   886.57             =     -91. +-  24. (MPa)
          99.00   374.57                          99.00   749.57
         106.00   284.71                         106.00   569.40
      d =  .98481 A                          d =  .98469 A
      2θ= 102.913 +- .002 deg.               2θ= 102.930 +- .003 deg.        DEPTH =  .0000 in. (  .000 mm)

            046002.d01         BA102 Spec. O.D. Loc. Surf. Long. Rpt.5 ROCK        9101C16RJ
Psi      2-theta    1/I     1/Icor      Psi      2-theta    1/I     1/Icor
 .00     102.48   164.70   578.17      33.21     102.23   398.75   990.17      B 1/2 =   .47 deg.
         102.73    95.29   233.03                102.53   286.38   456.23      COLD WORK =    .0 %
         102.98    75.85   170.90                102.83   230.61   313.08      STRAIN =  .000100
         103.20    91.22   219.80                103.25   240.67   341.22      STRESS =    11.3 +- 3.5 Ksi
         103.43   137.95   421.79                103.68   375.84   921.72             =      78. +-  24. (MPa)
          99.00   359.96                          99.00   649.66
         106.00   285.93                         106.00   527.36
      d =  .98504 A                          d =  .98514 A
      2θ= 102.879 +- .002 deg.               2θ= 102.865 +- .003 deg.        DEPTH =  .0000 in. (  .000 mm)
```

```
                              Lambda Research, Inc.
     046002.d02                    STRESS40.15                          01/17/91

          CAUCHY SEPARATED Ka1 DIFFRACTION PEAK STRESS ANALYSIS             1


                  E/(1+v) = 33884.+-   0. Ksi    1/2 S2 =  4.28 +- .00 x 10-6 1/MPa

          046002.d02          BA102 Spec. O.D. Loc. Surf. Long. RPT.1 ROCK        9101C17GT
Psi     2-theta   1/I     1/Icor      Psi     2-theta   1/I     1/Icor
------------------------------------  -------------------------------------
 .00    120.35   209.49   847.73      39.23   120.30   390.22   862.04      B 1/2 =   .64 deg.
        120.55   141.42   391.95              120.60   296.92   489.04      COLD WORK =   .0 %
        120.75   117.14   292.09              120.90   252.86   373.77      STRAIN = -.000444
        121.10   135.39   367.14              121.25   266.18   412.47      STRESS =   -37.6 +- 2.3 Ksi
        121.45   175.62   587.84              121.60   345.58   692.06             =   -259. +-  16. (MPa)
        119.00   363.07                       119.00   670.31
        127.00   323.44                       127.00   555.72
    d =  .88604 A                         d =  .88565 A
    2θ= 120.760 +- .002 deg.              2θ= 120.849 +- .003 deg.            DEPTH =  .0000 in. (  .000 mm)

          046002.d02          BA102 Spec. O.D. Loc. Surf. Long. RPT.2 ROCK        9101C17GT
Psi     2-theta   1/I     1/Icor      Psi     2-theta   1/I     1/Icor
------------------------------------  -------------------------------------
 .00    120.35   273.17  1331.66      39.23   120.25   441.03  1174.64      B 1/2 =   .59 deg.
        120.63   164.77   456.80              120.55   322.16   563.80      COLD WORK =   .0 %
        120.90   139.83   353.12              120.85   261.25   390.82      STRAIN = -.000436
        121.23   167.57   472.52              121.33   271.76   425.23      STRESS =   -36.9 +- 2.2 Ksi
        121.55   218.38   781.59              121.80   388.87   911.59             =   -255. +-  15. (MPa)
        119.00   421.17                       119.00   679.82
        127.00   385.98                       127.00   557.35
    d =  .88580 A                         d =  .88541 A
    2θ= 120.815 +- .002 deg.              2θ= 120.903 +- .003 deg.            DEPTH =  .0000 in. (  .000 mm)

          046002.d02         BAA102 Spec. O.D. Locv. Surf. Long. Rpt.3 ROCK       9101C17GT
Psi     2-theta   1/I     1/Icor      Psi     2-theta   1/I     1/Icor
------------------------------------  -------------------------------------
 .00    120.40   225.13   856.03      39.23   120.35   392.44   999.12      B 1/2 =   .61 deg.
        120.55   165.76   472.17              120.68   285.32   487.24      COLD WORK =   .0 %
        120.70   132.05   329.34              121.00   236.89   354.15      STRAIN = -.000589
        121.10   140.78   364.52              121.40   266.75   441.79      STRESS =   -49.9 +- 2.2 Ksi
        121.50   192.29   627.52              121.80   365.29   891.51             =   -344. +-  16. (MPa)
        119.00   409.59                       119.00   619.79
        127.00   360.95                       127.00   516.41
    d =  .88582 A                         d =  .88530 A
    2θ= 120.810 +- .002 deg.              2θ= 120.929 +- .003 deg.            DEPTH =  .0000 in. (  .000 mm)

          0046002.d02         BA102 Spec. O.D. Loc. Surf. Logn. Rp@t.4 ROCK       9101C17GT
Psi     2-theta   1/I     1/Icor      Psi     2-theta   1/I     1/Icor
------------------------------------  -------------------------------------
 .00    120.40   206.42   800.78      39.23   120.35   397.96   973.16      B 1/2 =   .62 deg.
        120.63   132.35   348.55              120.65   294.89   501.36      COLD WORK =   .0 %
        120.85   116.96   289.06              120.95   243.90   362.13      STRAIN = -.000637
        121.18   138.65   377.21              121.27   257.20   400.38      STRESS =   -53.9 +- 2.2 Ksi
        121.50   179.99   604.97              121.60   318.58   607.76             =   -372. +-  15. (MPa)
        119.00   367.13                       119.00   641.59
        127.00   338.61                       127.00   540.71
    d =  .88591 A                         d =  .88535 A
    2θ= 120.790 +- .002 deg.              2θ= 120.918 +- .003 deg.            DEPTH =  .0000 in. (  .000 mm)

          046002.d02          BA102 Spec. O.D. Loc. Surf. Long. Rpt.5 ROCK        9101C17GT
Psi     2-theta   1/I     1/Icor      Psi     2-theta   1/I     1/Icor
------------------------------------  -------------------------------------
 .00    120.40   224.60   922.78      39.23   120.25   429.51  1263.98      B 1/2 =   .60 deg.
        120.68   137.00   359.61              120.60   311.72   568.05      COLD WORK =   .0 %
        120.95   121.86   301.74              120.95   243.84   366.18      STRAIN = -.000480
        121.27   147.87   410.09              121.38   271.32   447.58      STRESS =   -40.6 +- 2.2 Ksi
        121.60   197.28   707.07              121.80   359.22   824.13             =   -280. +-  15. (MPa)
        119.00   387.69                       119.00   628.60
        127.00   333.01                       127.00   537.37
    d =  .88570 A                         d =  .88527 A
    2θ= 120.838 +- .002 deg.              2θ= 120.935 +- .003 deg.            DEPTH =  .0000 in. (  .000 mm)
```

Appendix B:

X-Ray Diffraction Results Supplied by P. Predecki (University of Denver)

X-RAY DIFFRACTION ANALYSIS

Paul Predecki

University of Denver
Department of Engineering
Denver, Colorado

This report provided by Dr. Paul Predecki is reproduced in its entirety.

REPORT ON β"-ALUMINA TUBE SAMPLE

March 26, 1991

To: D.S. KUPPERMAN, ARGONNE NATL LAB, MATERIALS TECHNOLOGY DIV.
From: X. ZHU AND P.K.PREDECKI. PKP

1. Objective: To try to measure residual strain in β"-Al_2O_3 tube sample from Dr. David Kupperman, Argonne National Lab.

2. Sample description: The sample is a section of tube described in Fig.1. We were told that the sample is basically β"-Al_2O_3 with small percentage of sodium. The sample was kept in the lab at room temperature and 47% relative humidity for 3 days prior to running the X-ray measurement.

3. Testing procedure:

a) Masking the sample

In order to minimize the 2θ error resulting from the curvarture of the sample surface, two strips of 0.005in thick lead tape were applied as shown in fig.2, leaving a strip 2mm wide along the axis of the sample.

b) Determination of the peaks that can be used in strain measurement:

After masking the above sample with lead tape, we found that the peaks in the range of 140 - 151 deg 2θ are well separated from other peaks, and there are no lead peaks in this range. Furthermore, lanthanium hexaboride which has two peaks (510 and 511) at 141.790 and 148.678 degree 2θ, respectively, can work as an internal standard for adjusting the sample position, as shown in Fig.3.

c) Internal standard

A very thin layer of lanthanum hexaboride powder was used as internal standard to adjust the position of the sample to eliminate the position error in 2θ resulting from different ψ-tilts (Fig.2).

d) Sample orientation:

The sample position on the diffractometer was adjusted to get the LaB_6 peaks to remain unchanged for different ψ-tilts(Fig.4).

e) Determination of d_o:

Small chips of the sample were broken off one end of the tube using a pair of pliers. These were ground dry in an α-alumina mortar and place on a quartz plate substrate coated with a thin film of vaseline. When this sample was tilted from ψ=-45° to +45°, there was < 0.02° 2θ peak shift indicating that the powder sample was on the diffractometer axis.

f) Weight gain test:

To estimate the moisture uptake of the sample, the sample was heated in an oven at 140 °C for 24 hours in air, and then weighted as a function of time after removed from the furnace. The maximum percentage of weight gain is about 0.06%, as shown in Fig. 5.

We also tried to heat the sample to 140 °C for 24 hours, and placed it in a bottle with drierite. After about 6 hours, we took it out and weigh it. The result in fig.5 shows that the sample still gained weight even when stored with drierite.

4. Results:

For 3-D strain state, we have: (Dolle, J. Appl Cryst. (1979). 12, 489-501)

$$a_1 = [\varepsilon_{\phi\psi+} + \varepsilon_{\phi\psi-}]/2 = \varepsilon_{33} + (\varepsilon_{11}\cos^2\phi + \varepsilon_{12}\sin 2\phi + \varepsilon_{22}\sin^2\phi - \varepsilon_{33})\ \sin^2\psi$$

$$a_2 = [\varepsilon_{\phi\psi+} + \varepsilon_{\phi\psi-}]/2 = (\varepsilon_{13}\cos\phi + \varepsilon_{23}\sin\phi)\ \sin|2\psi|$$

For $\phi = 0$,

$$a1 = \varepsilon_{33} + (\varepsilon_{11} - \varepsilon_{33})\ \sin^2\psi$$

$$a2 = \varepsilon_{13}\sin|2\psi|$$

Table 1. Strains (Using $2\theta_0$=143.868 deg obtained from powder sample)

ψ	2θ	$\varepsilon_{3'3'}$	a_1	a_2
0	143.874	-1.7405e-5	-1.7405e-5	0
+20	143.881	-3.7074e-5		
-20	143.852	4.5538e-5	4.232e-6	-4.131e-5
+30	143.919	-1.4514e-4		
-30	143.877	-2.5690e-5	-8.5415e-5	-5.9725e-5
+45	143.990	-3.4672e-4		
-45	143.919	-1.4514e-4	-2.4593e-4	-1.0079e-4

The plots of $\varepsilon_{3'3'}$, a_1 and a_2 are shown in Fig. 6-8. From the plots of a_1 and a_2, we can calculate that ε_{11}=-4.78e-4, ε_{33}=2.23e-5, ε_{13}= -8.90e-5. We do not have ε_{22}, ε_{23}, ε_{12} because we could not run ϕ=90 deg.

A repeat run of the X-ray measurements on the tube will be performed on a different area, to try to confirm these results. The runs take a long time (20 sec/step, 0.02° 2θ/step) even with a solid state detector.

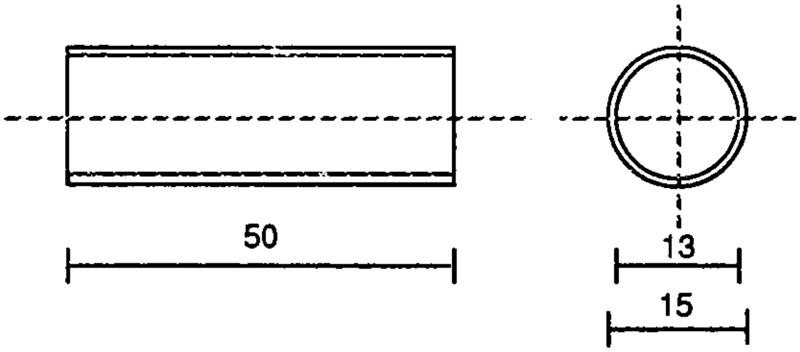

Fig.1 Sample dimensions (Unit: mm)

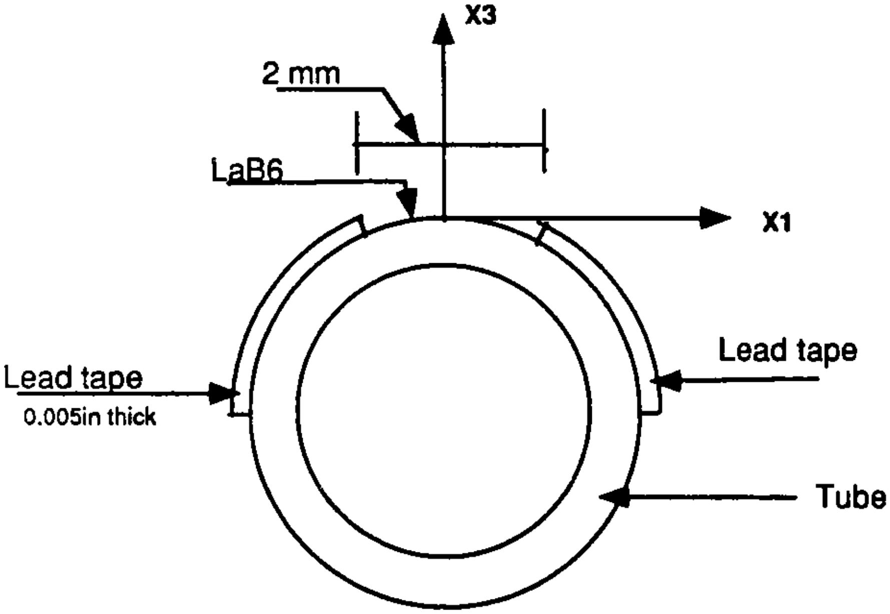

Fig.2 Sample masking

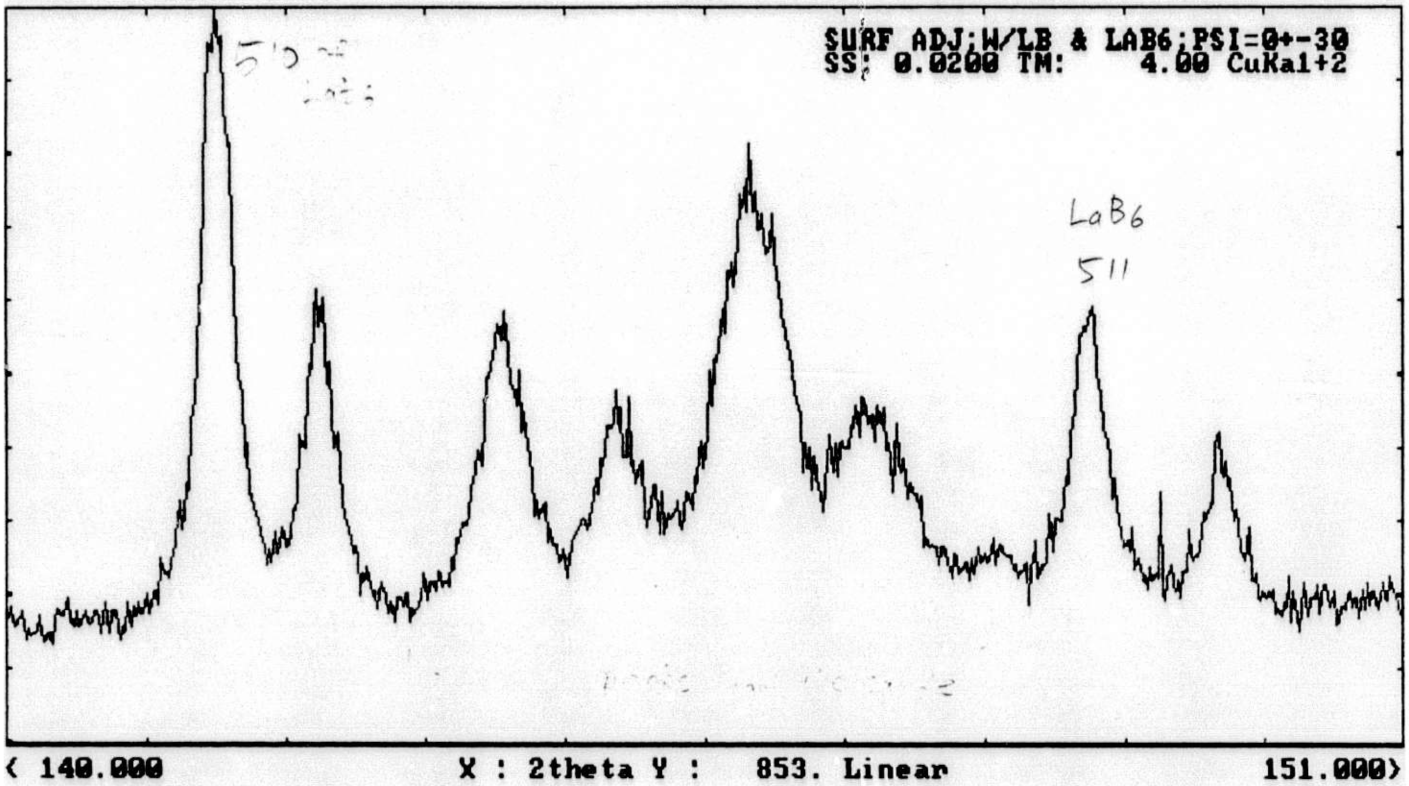
SURF ADJ;W/LB & LAB6;PSI=0+-30
SS: 0.0200 TM: 4.00 CuKa1+2
510 of LaB6
LaB6
511
< 140.000
X : 2theta Y : 853. Linear
151.000>

Fig. 3

?help Zoom Dcomp File Clear Back. K a2 Peaks Smoo. Comp. Wfile Test -> F

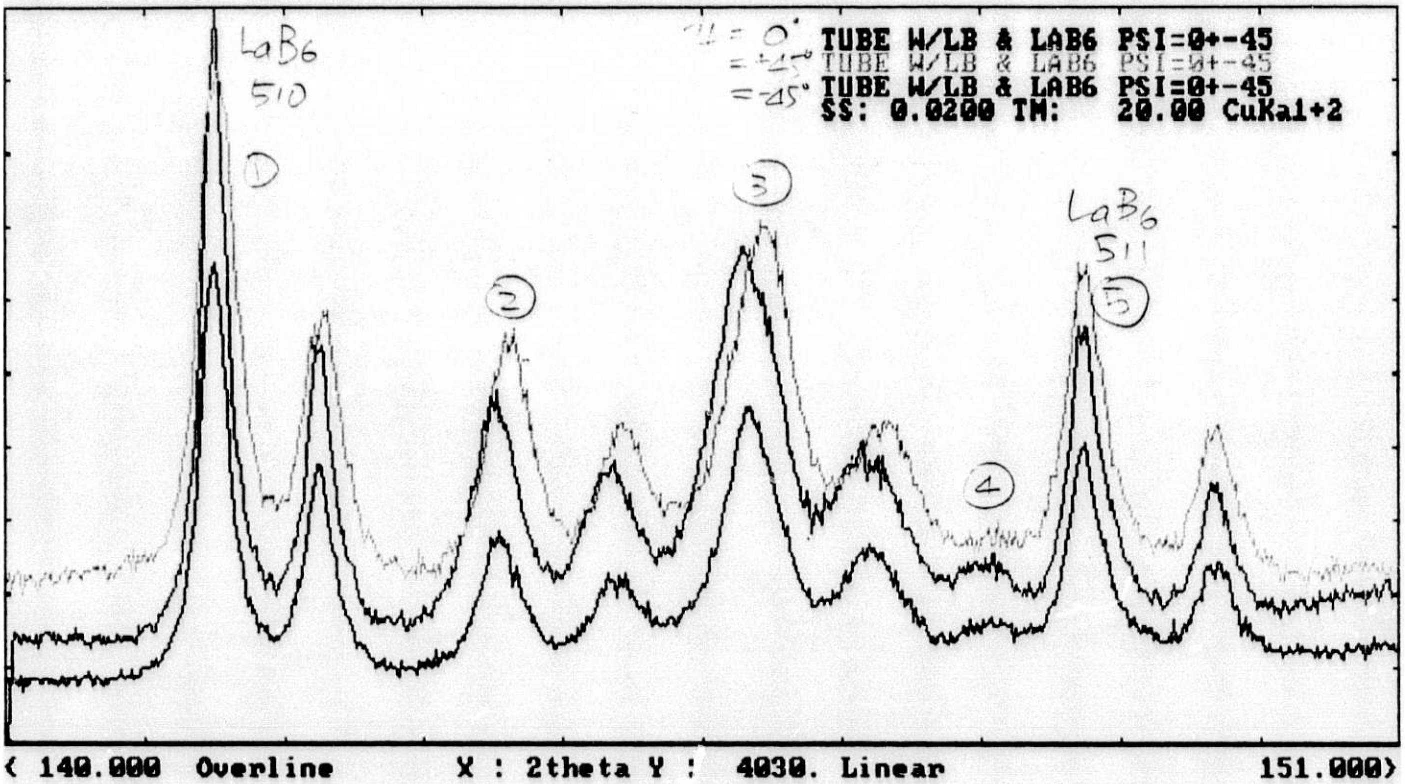
LaB6
510
①
②
③
④
LaB6
511
⑤
ψ = 0°
= +45°
= -45°
TUBE W/LB & LAB6 PSI=0+-45
TUBE W/LB & LAB6 PSI=0+-45
TUBE W/LB & LAB6 PSI=0+-45
SS: 0.0200 TM: 20.00 CuKa1+2
< 140.000 Overline X : 2theta Y : 4030. Linear 151.000>

Fig. 4

?help Zoom Dcomp File Clear Back. K a2 Peaks Smoo. Comp. Wfile Test -> D

Weight change of B"-Al2O3 Tube after been Heated at 140 deg C for 24 hrs

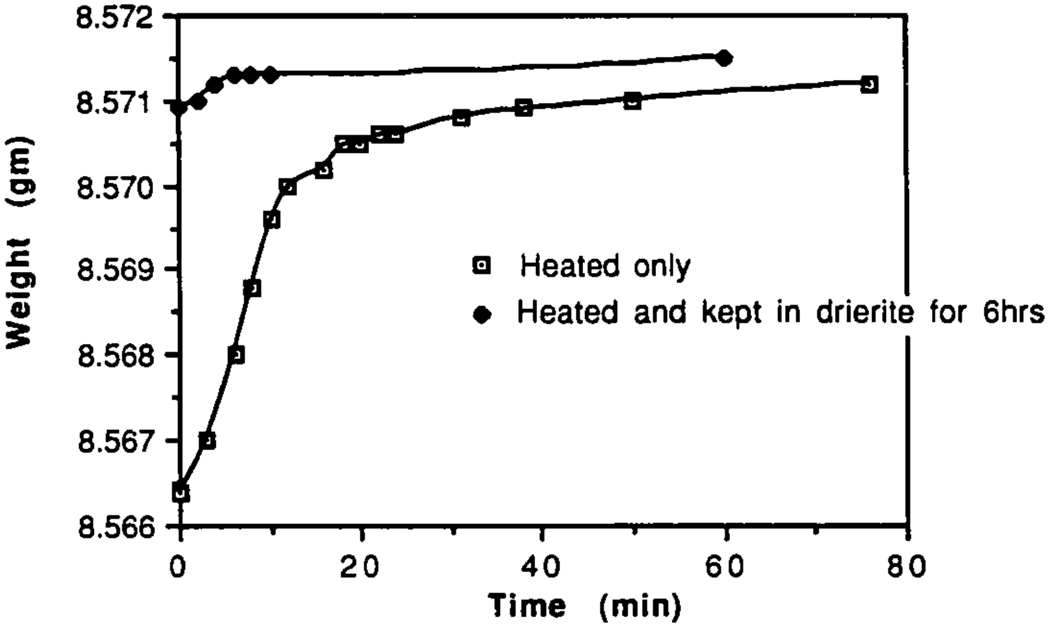

% Weight Gain of B"-Al2O3 Tube after been Heated at 140 C for 24 hrs

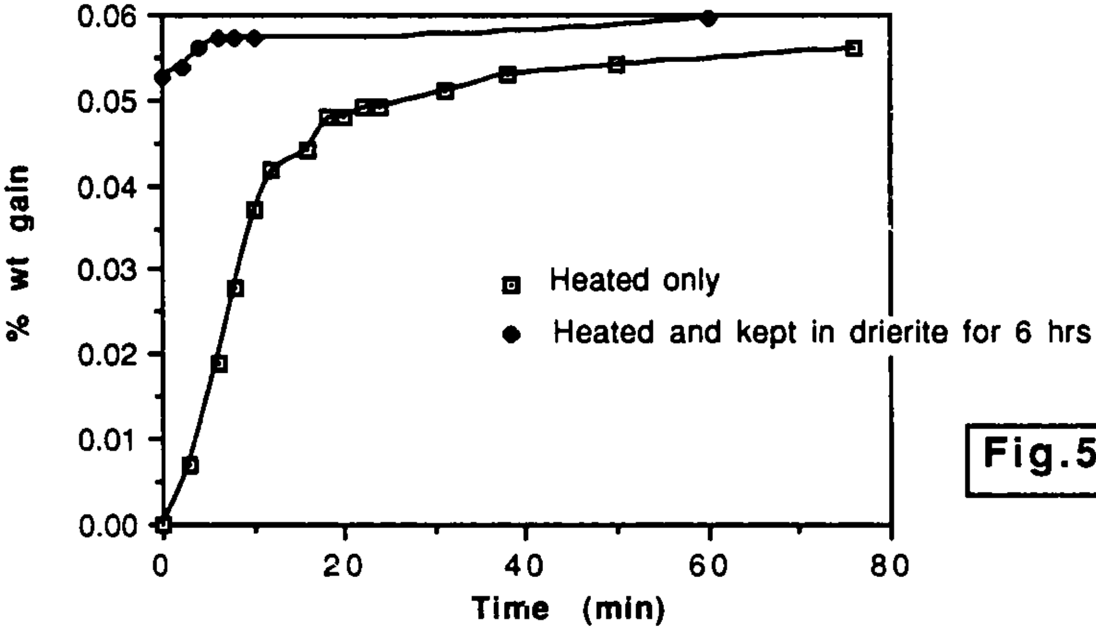

Fig.5

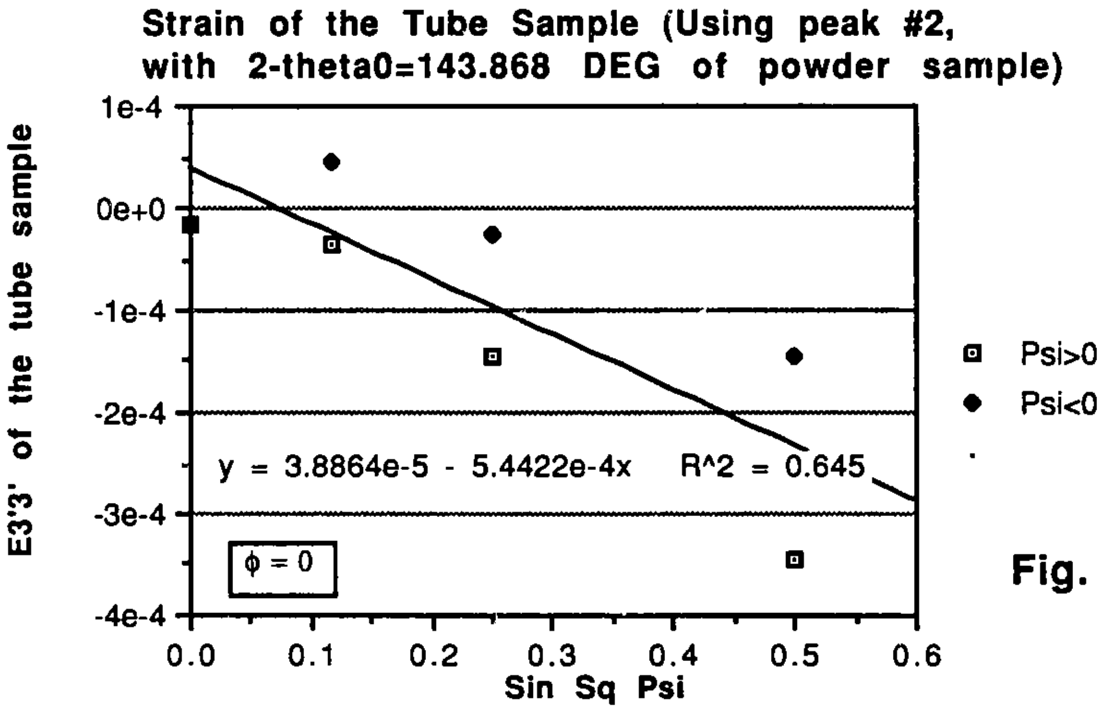
Strain of the Tube Sample (Using peak #2, with 2-theta0=143.868 DEG of powder sample)
E3'3' of the tube sample
1e-4
0e+0
-1e-4
-2e-4
-3e-4
-4e-4
0.0
0.1
0.2
0.3
0.4
0.5
0.6
Sin Sq Psi
y = 3.8864e-5 - 5.4422e-4x R^2 = 0.645
ϕ = 0
Psi>0
Psi<0

Fig. 6

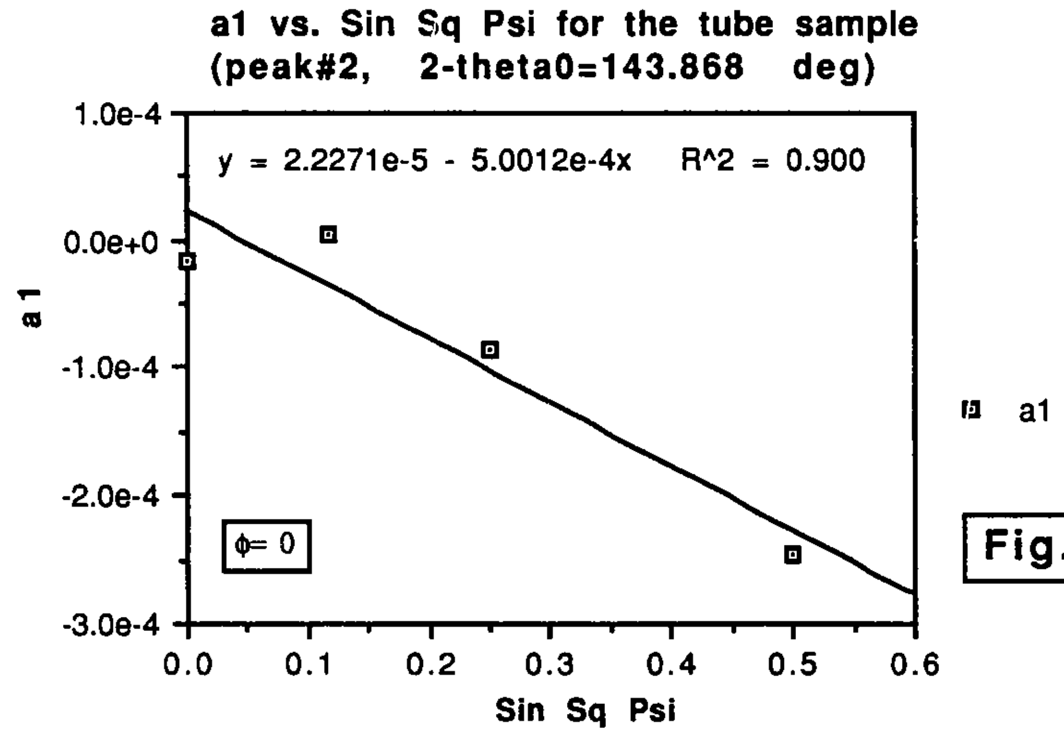
a1 vs. Sin Sq Psi for the tube sample
(peak#2, 2-theta0=143.868 deg)
y = 2.2271e-5 - 5.0012e-4x R^2 = 0.900
1.0e-4
0.0e+0
-1.0e-4
-2.0e-4
-3.0e-4
a 1
φ= 0
0.0
0.1
0.2
0.3
0.4
0.5
0.6
Sin Sq Psi
a1

Fig.7

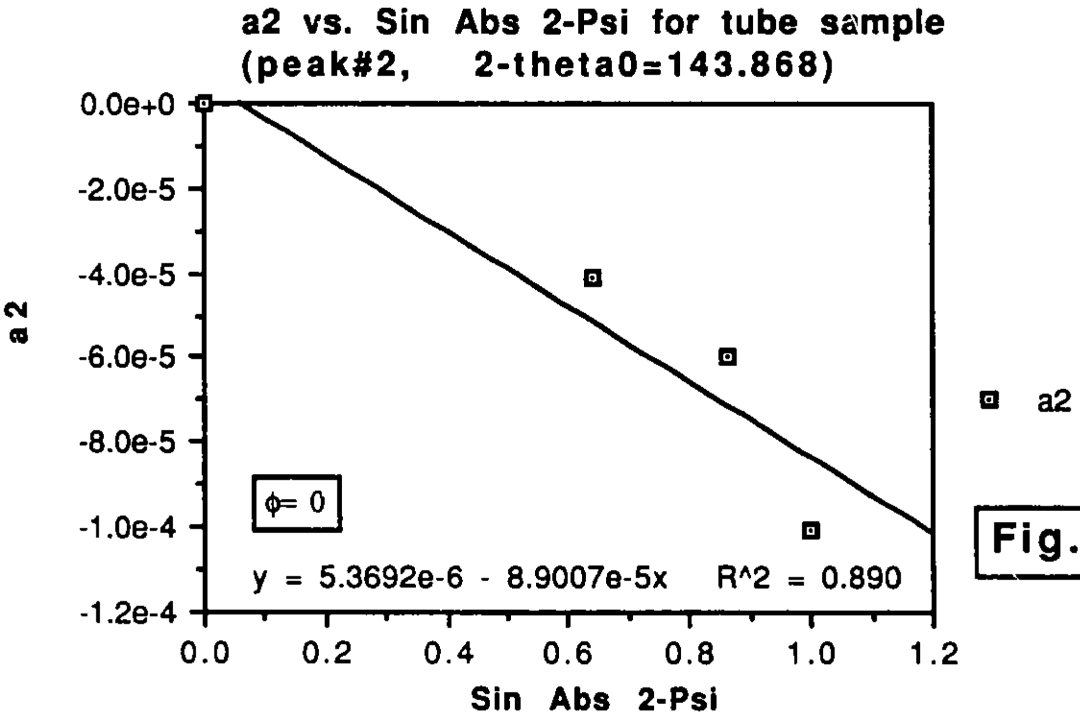
a2 vs. Sin Abs 2-Psi for tube sample
(peak#2, 2-theta0=143.868)
0.0e+0
-2.0e-5
-4.0e-5
-6.0e-5
-8.0e-5
-1.0e-4
-1.2e-4
a 2
φ= 0
y = 5.3692e-6 - 8.9007e-5x R^2 = 0.890
0.0
0.2
0.4
0.6
0.8
1.0
1.2
Sin Abs 2-Psi
a2

Fig.8

Appendix C:

X-Ray Diffraction Analysis Supplied by Technology for Energy Corporation

A-RAY DIFFRACTION ANALYSIS

Technology for Energy Corporation
One Energy Center, Lexington Dr.
P. O. Box 22996
Knoxville, Tennessee

Only parts of the reports provided by TEC are reproduced here.

ARGONNE NATIONAL LABORATORY
RESIDUAL STRESS SUMMARY
AL_20_3 TUBES

CONDITION and LOCATION	RESIDUAL STRESS, ksi CIRCUMFERENTIAL	LONGITUDINAL
	A. Tube CTI-2592-07	
1. As Received		
1G	-8.9 ± 2.8	-1.3 ± 3.9
2. After 30 minutes exposure to room humidity		
1G	+9.0 ± 5.9	+15.3 ± 6.4
3. After 5 days' exposure to room humidity*		
1G	+26.0 ± 17.1	+39.5 ± 25.1
1	+12.3 ± 21.1	-38.9 ± 28.5
	B. Tube CXI-2606-06 Bent EXP 90-2	
1. As received		
1	-1.5 ± 3.8	-1.6 ± 4.7
	C. Tube CXI-2598-16 Bent EXP 90-1	
1. As received		
1	+73.2 ± 18.5	+36.9 ± 24.6

* The large error bars for this condition were attributed to low signal-to-noise ratio of the diffraction peaks.

Sample Description :
ARGONNE NATIONAL LABORATORY AL2O3 TUBE CTI-2592-07
LOCATION 1G/LONGITUDINAL

Stress Spectra File Specifications 146300.SPC

Residual Stress	(ksi)	-1.32	(mpa)	-9.10
Statistical Error (+/-)	(ksi)	3.91	(mpa)	26.99

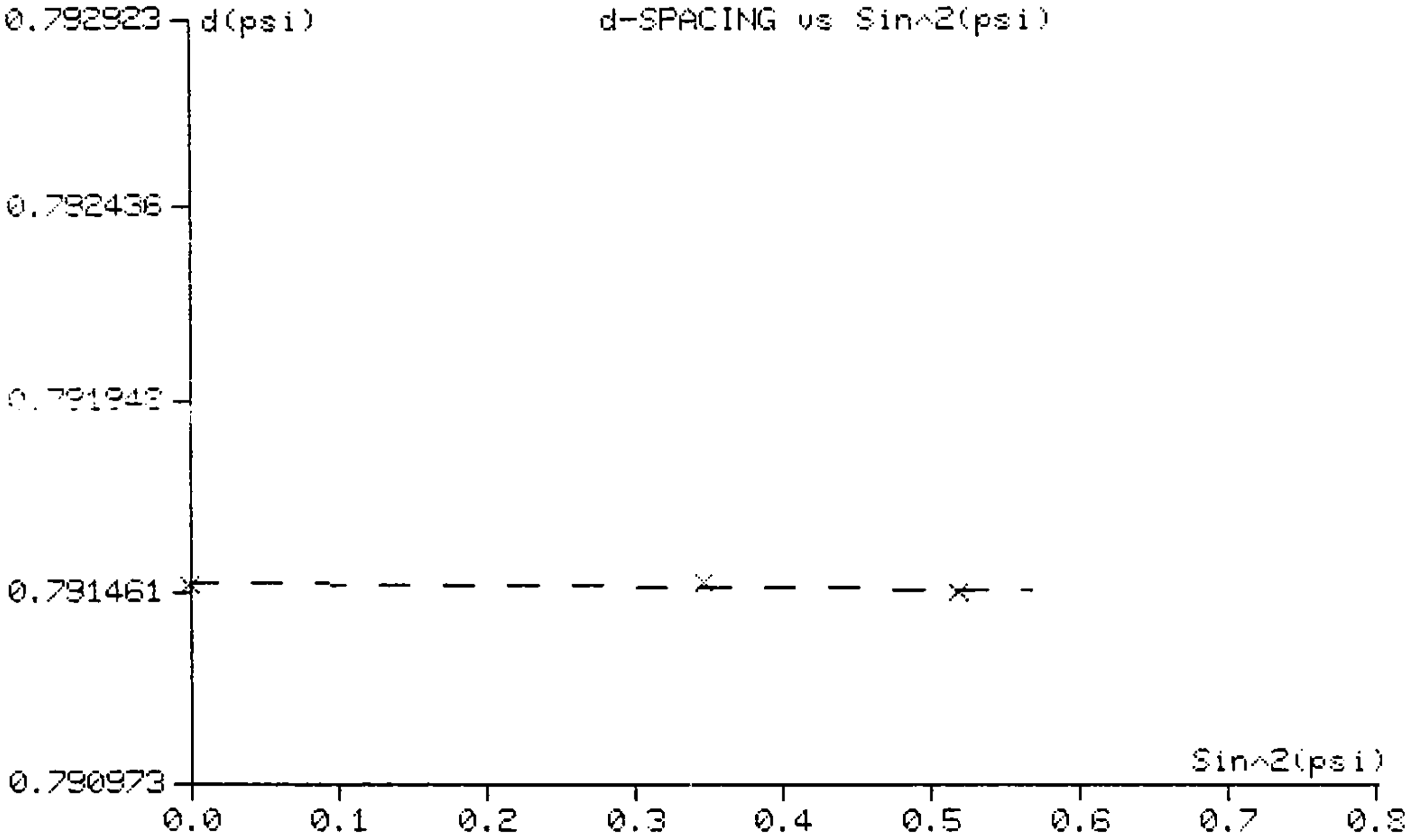

Sample Description :
ARGONNE NATIONAL LABORATORY ALLOY TUBE [illegible]
LOCATION 18, CIRCUMFERENTIAL

Stress Spectra File Specifications 001462.SPC

Residual Stress	(ksi)	-8.91	(mpa)	-61.40
Statistical Error (+/-)	(ksi)	2.78	(mpa)	19.14

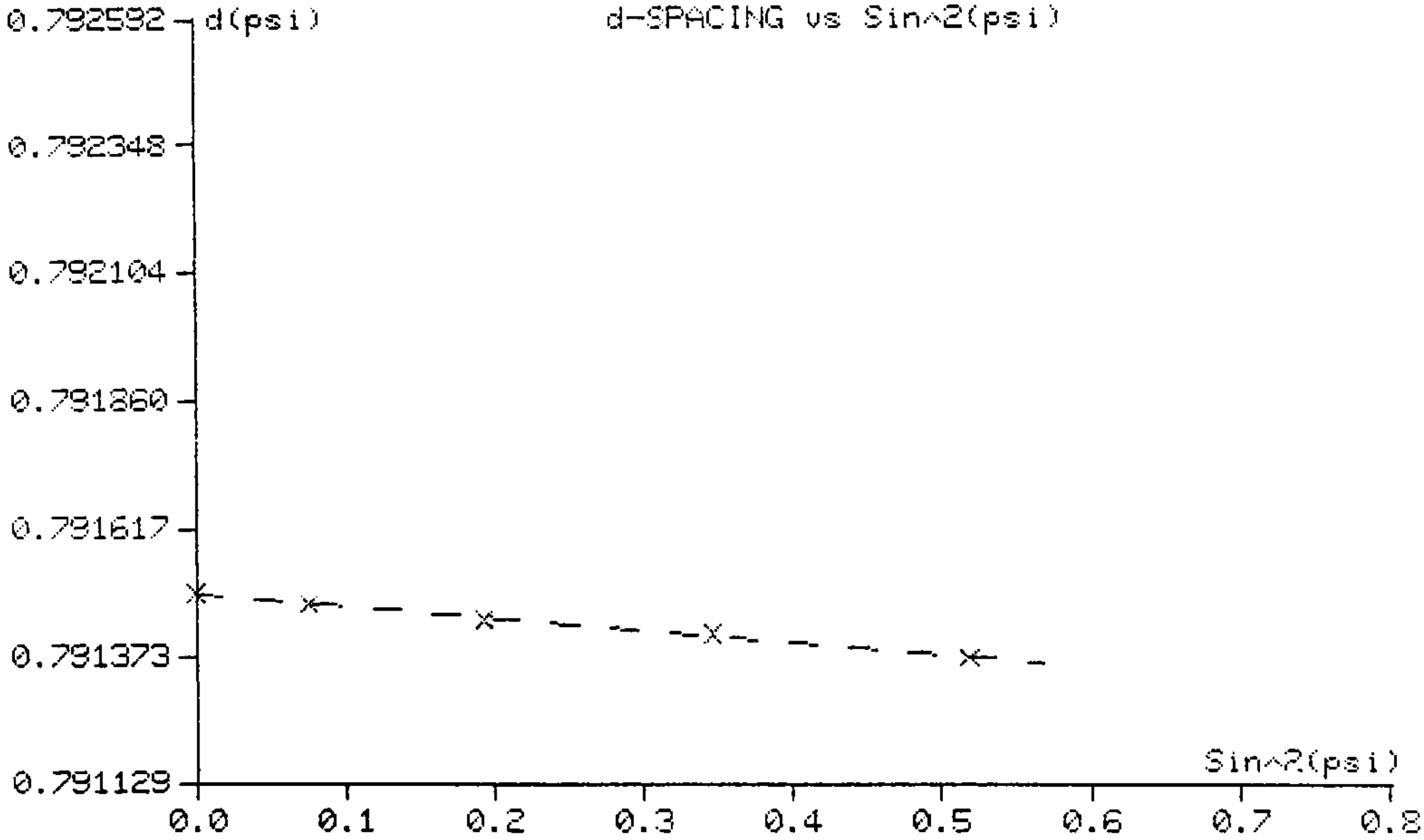

ARGONNE NATIONAL LABORATORY
RESIDUAL STRESS SUMMARY
AL_20_3 TUBE T867 V2 8P

LOCATION	RESIDUAL STRESS, ksi CIRCUMFERENTIAL	 LONGITUDINAL
1	+2.4 ± 4.3	+16.4 ± 3.7
2	+9.9 ± 7.3	+10.2 ± 5.7
2 (After 3 Days Exposure to Room Humidity)	+1.9 ± 5.1	+6.0 ± 4.7
3	+3.5 ± 4.8	+4.0 ± 2.9

Sample Description :
ARGONNE NATIONAL LABORATORY/AL2O3 TUBE
LOCATION 2/CIRCUMFERENTIAL

Stress Spectra File Specifications 001377.SFC

Residual Stress	(ksi)	1.86	(mpa)	12.79
Statistical Error (+/-)	(ksi)	5.07	(mpa)	34.96

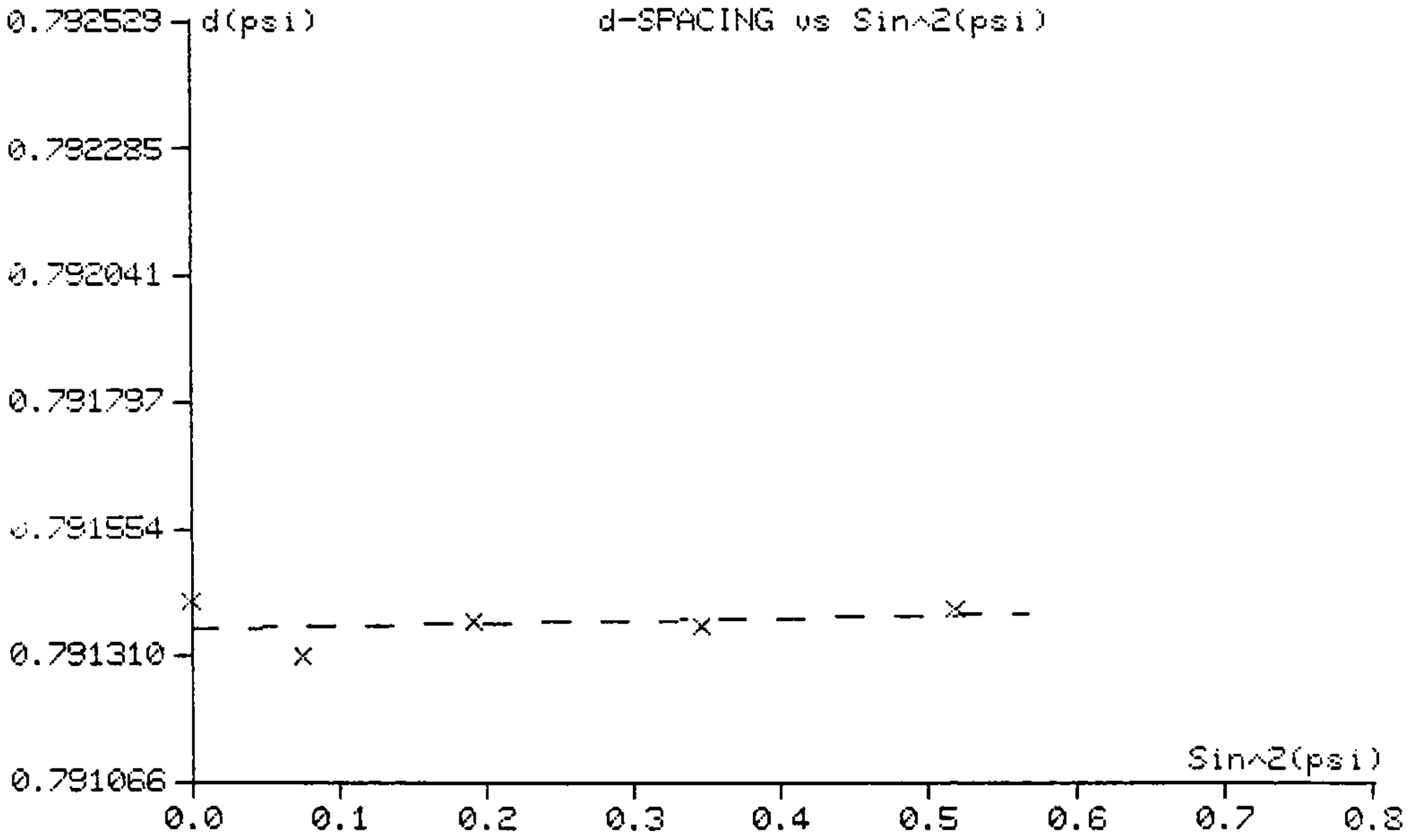

```
Sample Description :
ARGONNE NATIONAL LABORATORY/AL2O3 TUBE
LOCATION 2/LONGITUDINAL

Stress Spectra File Specifications                                    001353.SFC

Residual Stress                          (ksi)     10.24            (mpa)     70.61
Statistical Error (+/-)                  (ksi)      5.72            (mpa)     39.45
```

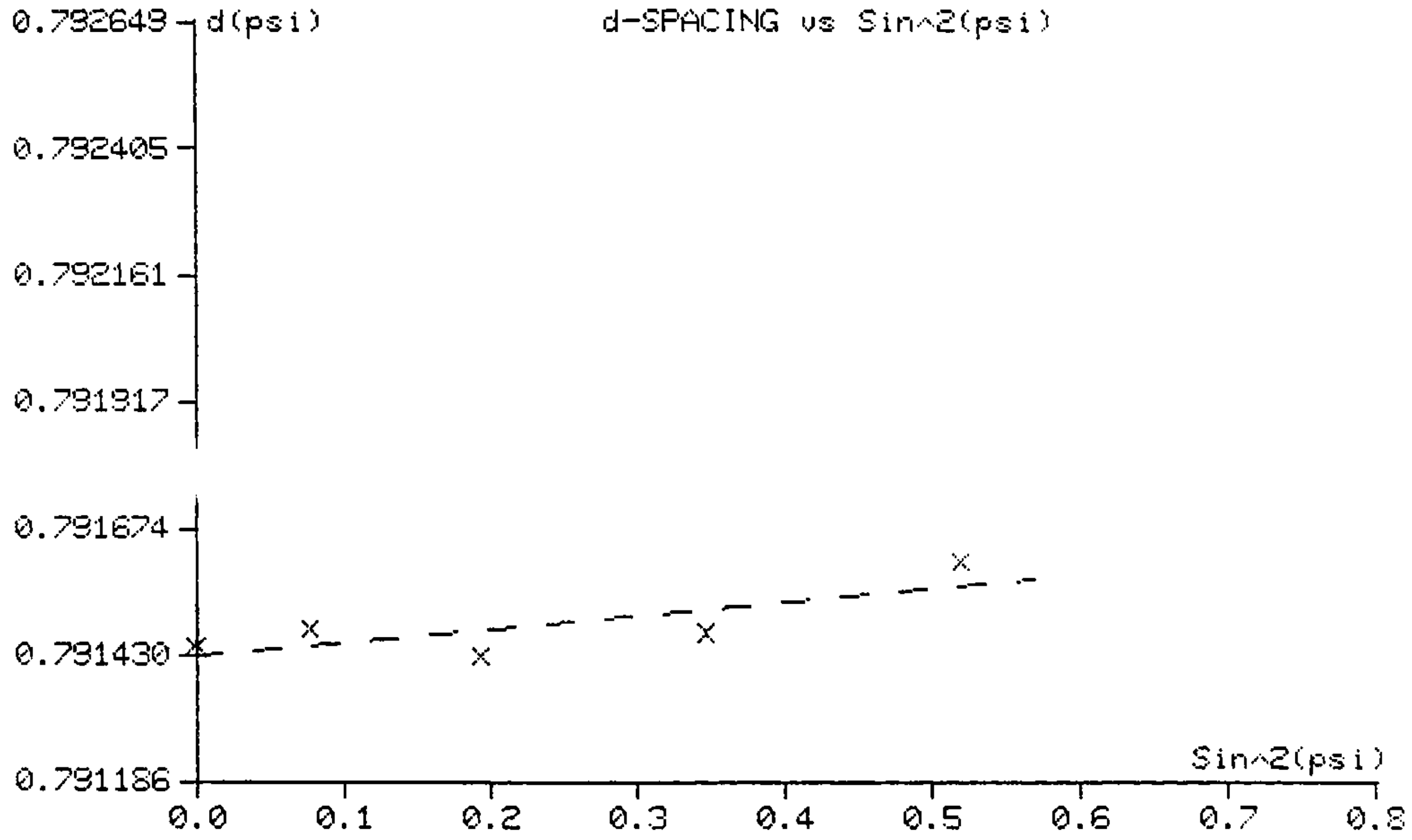

```
Sample Description :
ARGONNE NATIONAL LABORATORY AL2O3 TUBE
LOCATION 2/CIRCUMFERENTIAL

Stress Spectra File Specifications                                    001356.SPC

Residual Stress                             (ksi)     9.89            (mpa)     68.18
Statistical Error (+/-)                     (ksi)     7.32            (mpa)     50.50
```

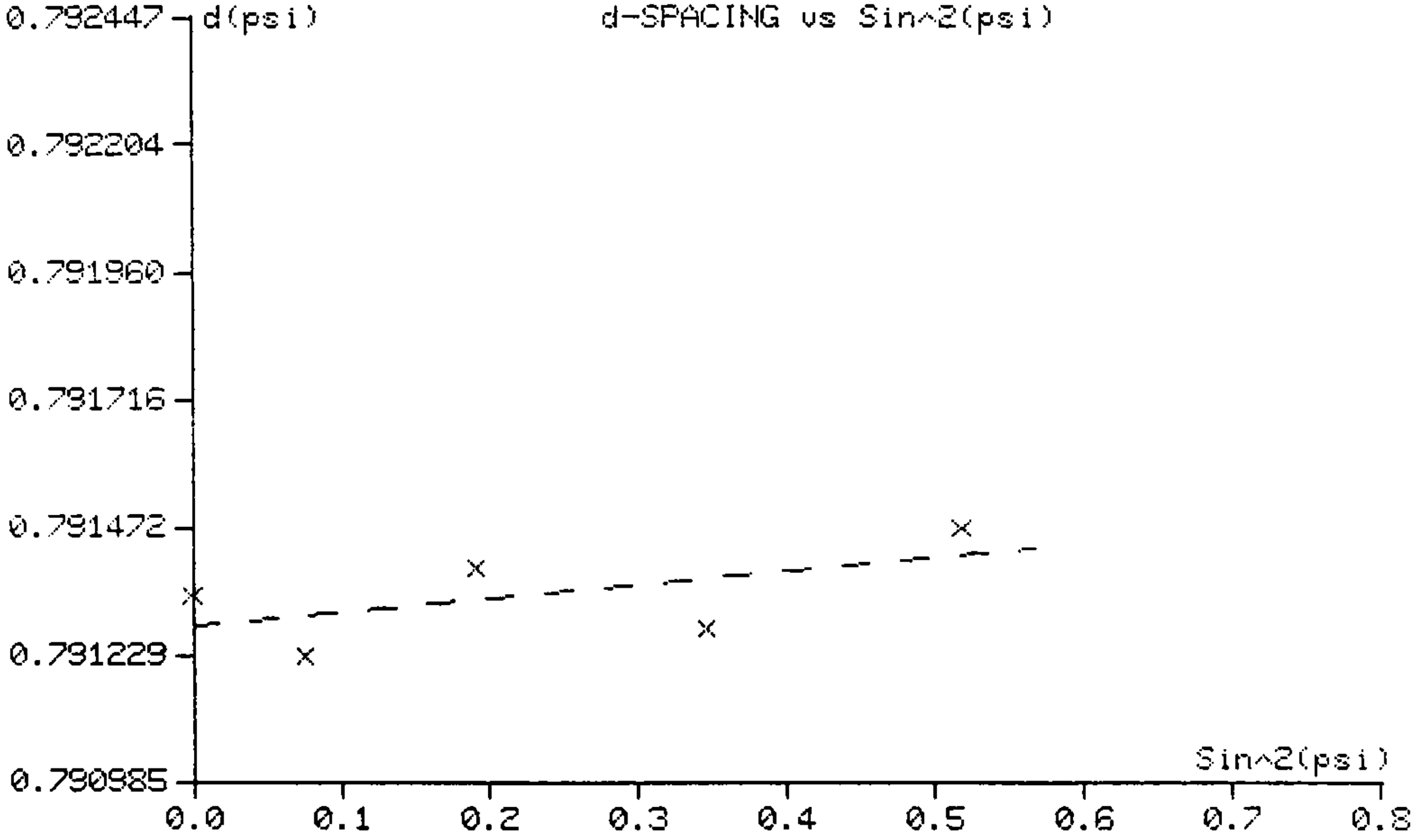

Sample Description :
ARGONNE NATIONAL LABORATORY/AL2O3 TUBE
LOCATION 1/CIRCUMFERENTIAL

Stress Spectra File Specifications 001357.SPC

Residual Stress	(ksi)	2.41	(mpa)	16.63
Statistical Error (+/-)	(ksi)	4.32	(mpa)	29.78

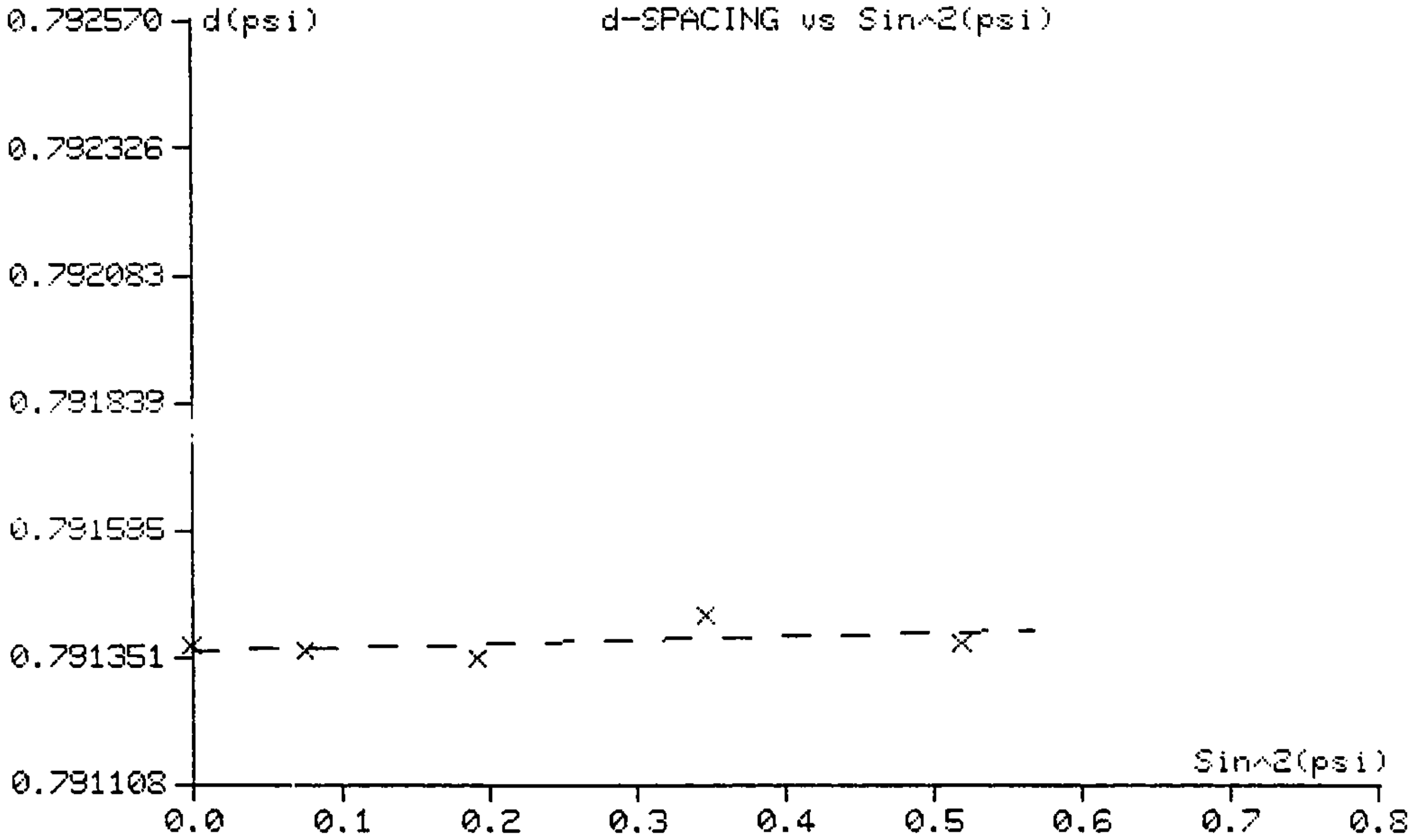

Sample Description :
ARGONNE NATIONAL LABORATORY/AL2O3 TUBE
LOCATION 1/LONGITUDINAL

Stress Spectra File Specifications 001352.SPC

Residual Stress	(ksi)	16.39	(mpa)	113.01
Statistical Error (+/-)	(ksi)	3.68	(mpa)	25.40

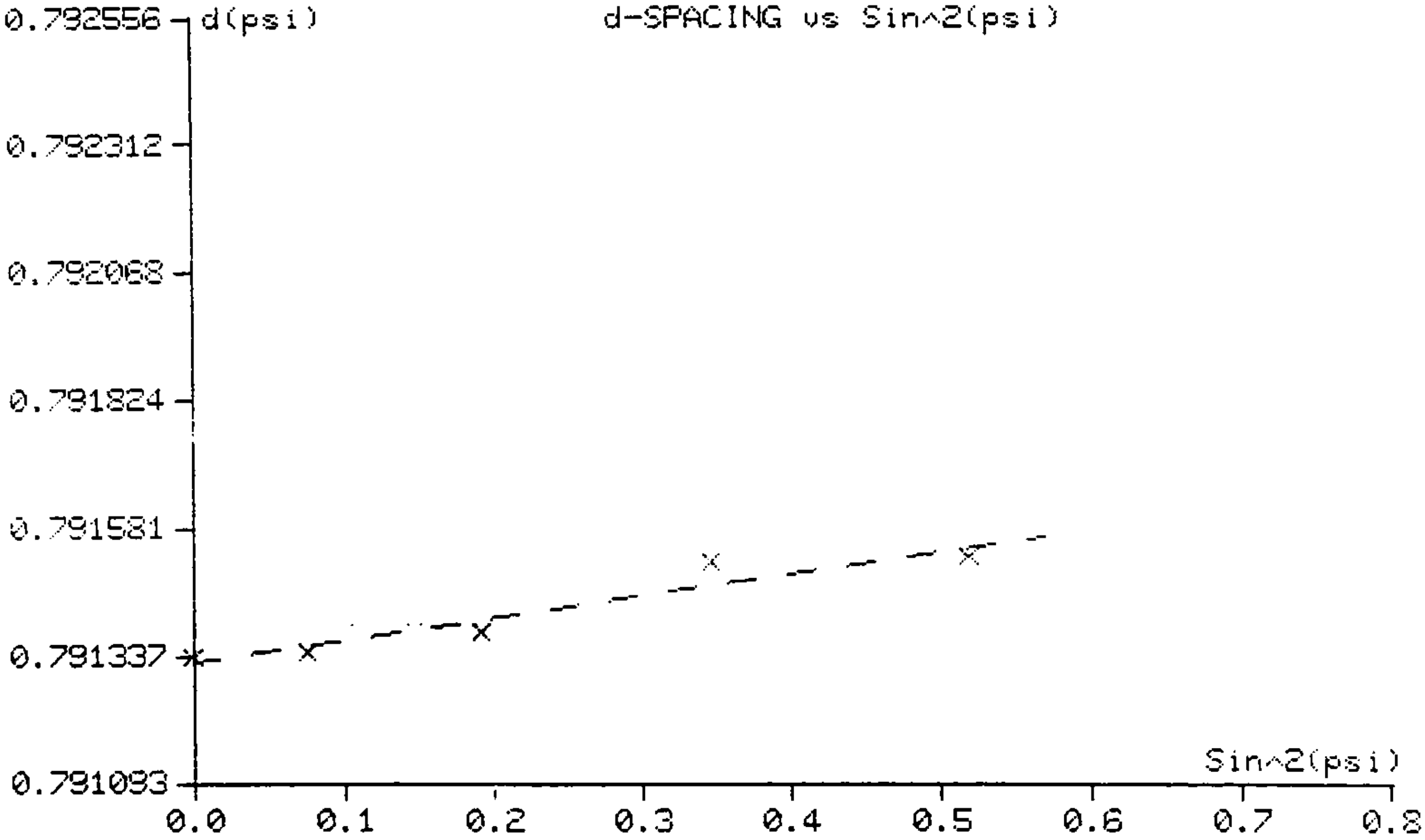

Sample Description :
ARGONNE NATIONAL LABORATORY/AL2O3 TUBE
LOCATION 3/LONGITUDINAL

Stress Spectra File Specifications 001354.SPC

Residual Stress	(ksi)	3.95	(mpa)	27.25
Statistical Error (+/-)	(ksi)	2.85	(mpa)	19.65

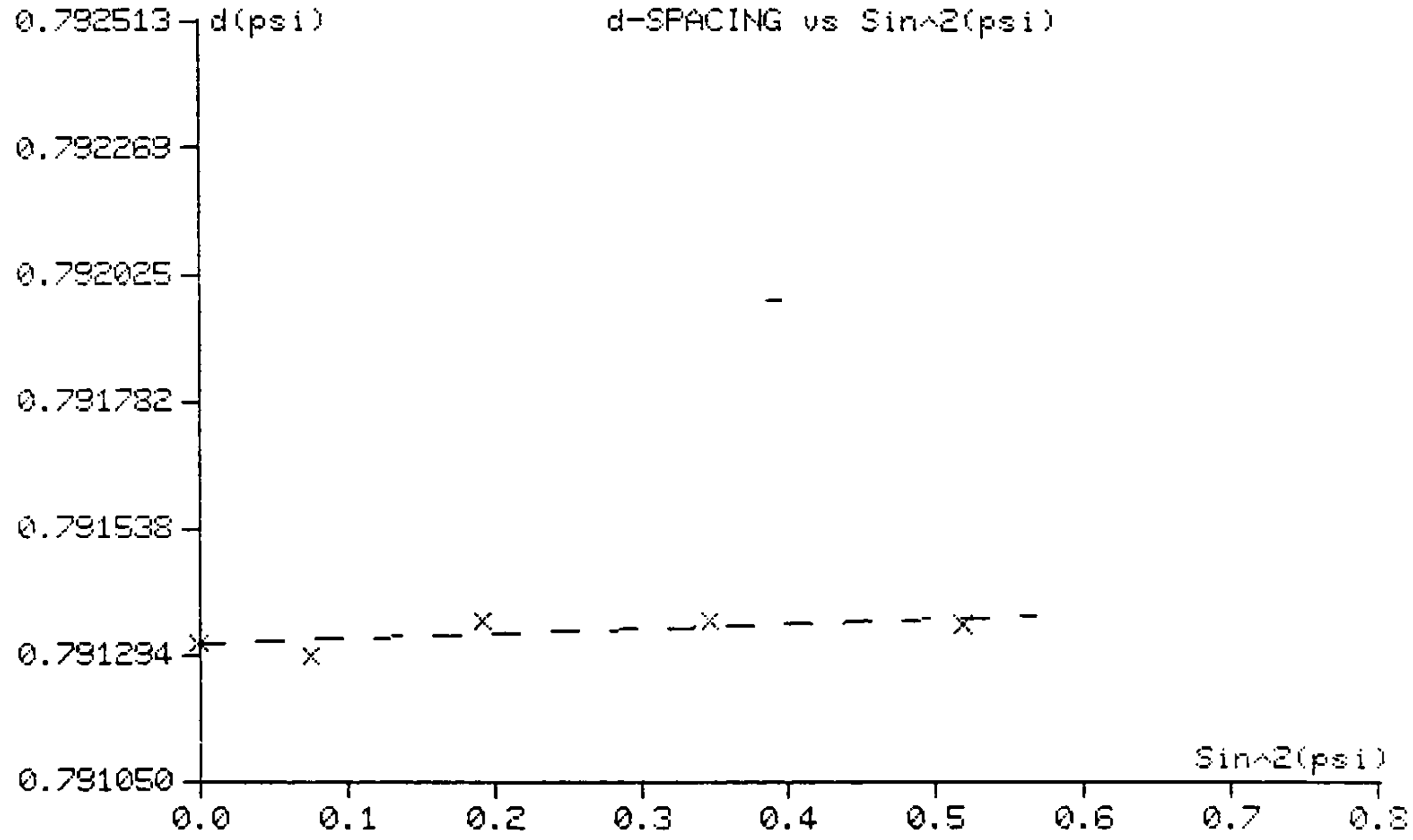

```
Sample Description :
ARGONNE NATIONAL LABORATORY/AL2O3 TUBE
LOCATION 3/CIRCUMFERENTIAL

Stress Spectra File Specifications                                  001355.SPC

Residual Stress                    (ksi)     3.45              (mpa)     23.82
Statistical Error (+/-)            (ksi)     4.82              (mpa)     33.24
```

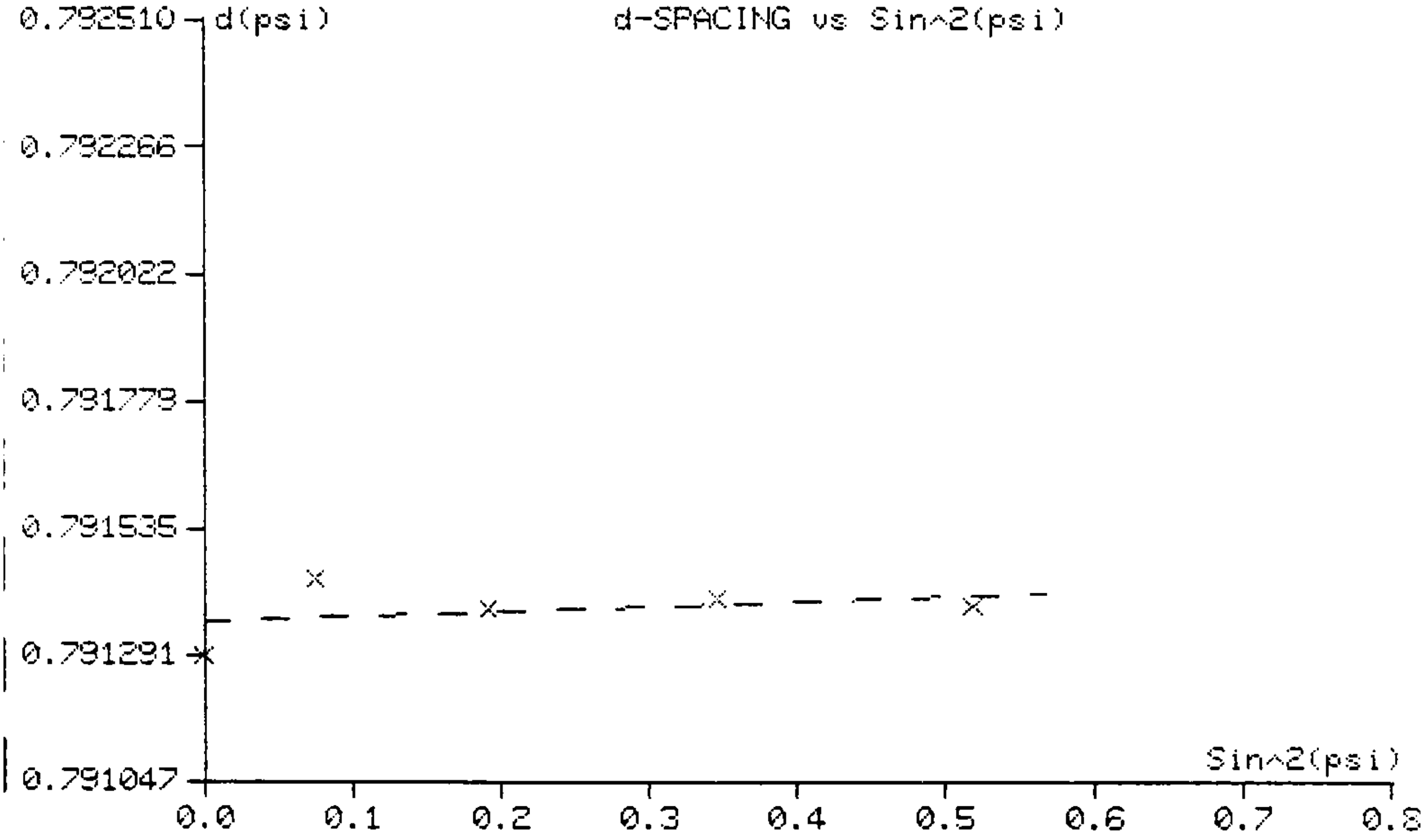

Sample Description :
ARGONNE NATIONAL LABORATORY ALLOY TUBE
LOCATION 2/LONGITUDINAL

Stress Spectra File Specifications A01778.SPC

Residual Stress	(ksi)	5.98	(mpa)	41.25
Statistical Error (+/-)	(ksi)	4.73	(mpa)	32.62

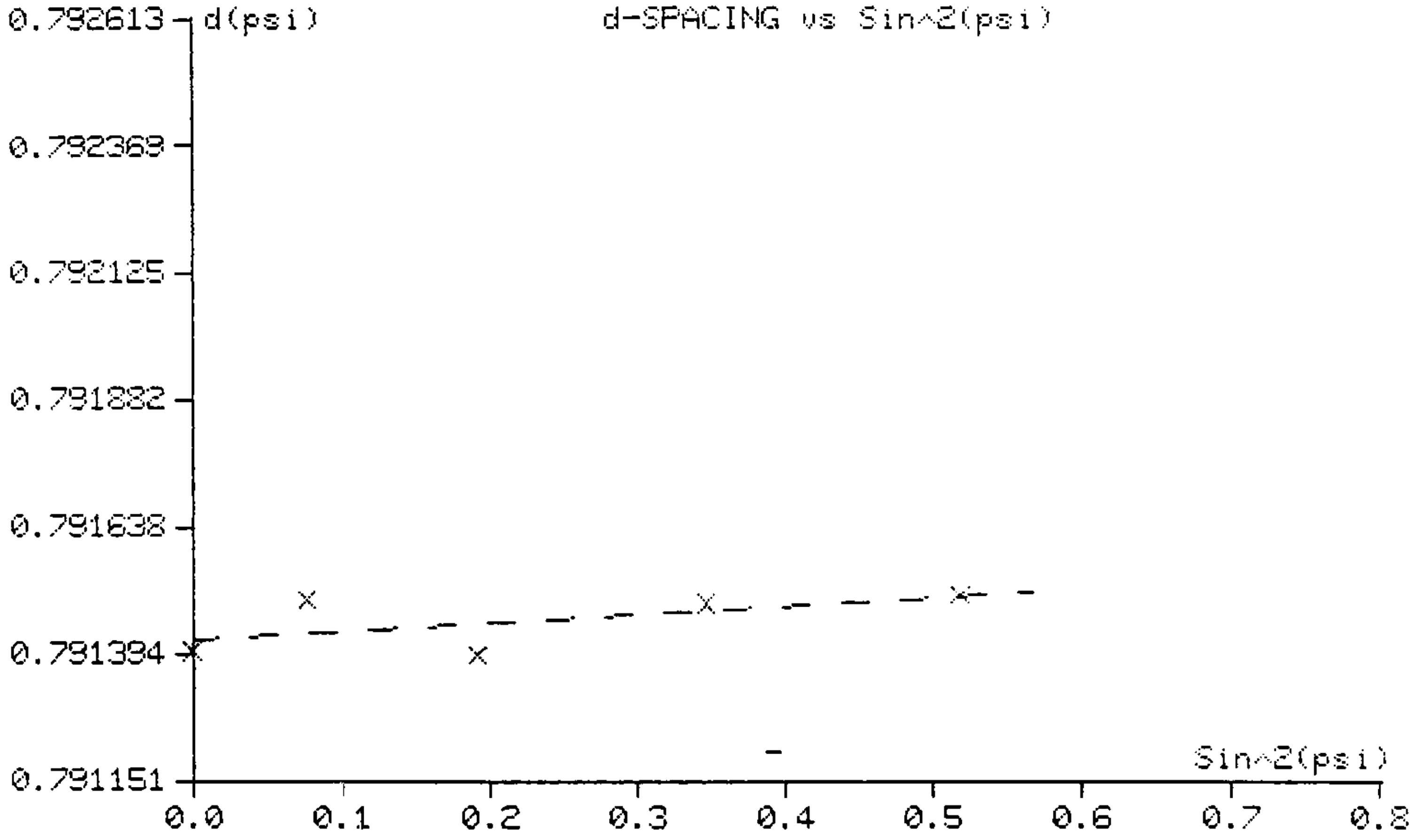

ARGONNE NATIONAL LABORATORY
RESIDUAL STRESS SUMMARY
AL_20_3 ROD

LOCATION	RESIDUAL STRESS, ksi	
	CIRCUMFERENTIAL	LONGITUDINAL
1	+32.7 ± 8.6	+15.8 ± 3.5
3	+15.6 ± 4.6	+15.0 ± 6.6
6	+8.2 ± 6.0	+19.6 ± 10.1

Sample Description :
ARGONNE NATIONAL LABORATORY, AL2O3
LOCATION 1/LONGITUDINAL

Stress Spectra File Specifications 001109.SPC

Residual Stress	(ksi)	15.79	(mpa)	108.90
Statistical Error (+/-)	(ksi)	3.49	(mpa)	24.05

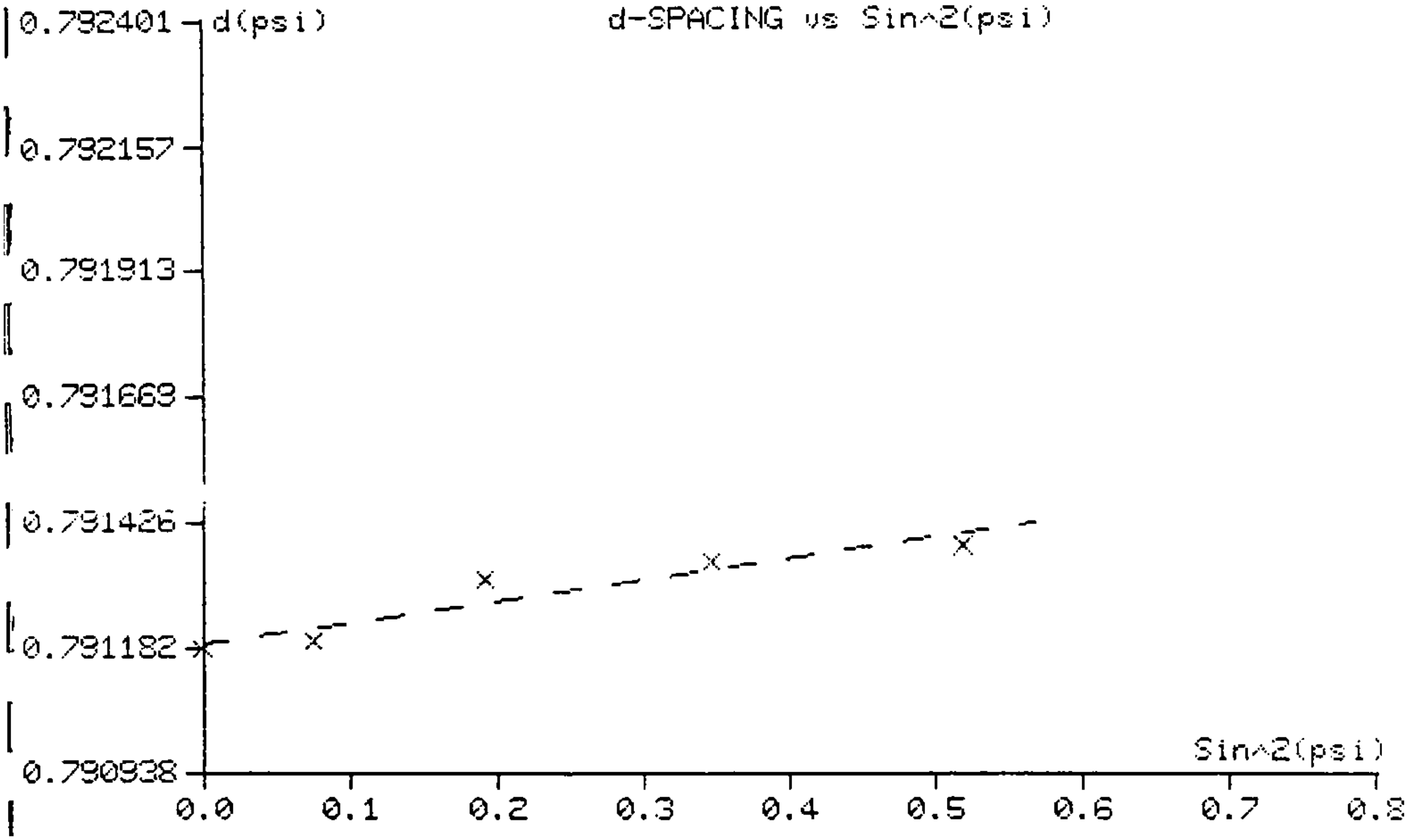

Sample Description :
ARGONNE NATIONAL LABORATORY/AL2O3
LOCATION 1/CIRCUMFERENTIAL

Stress Spectra File Specifications 001112.SPC

Residual Stress	(ksi)	32.72	(mpa)	225.57
Statistical Error (+/-)	(ksi)	8.63	(mpa)	59.51

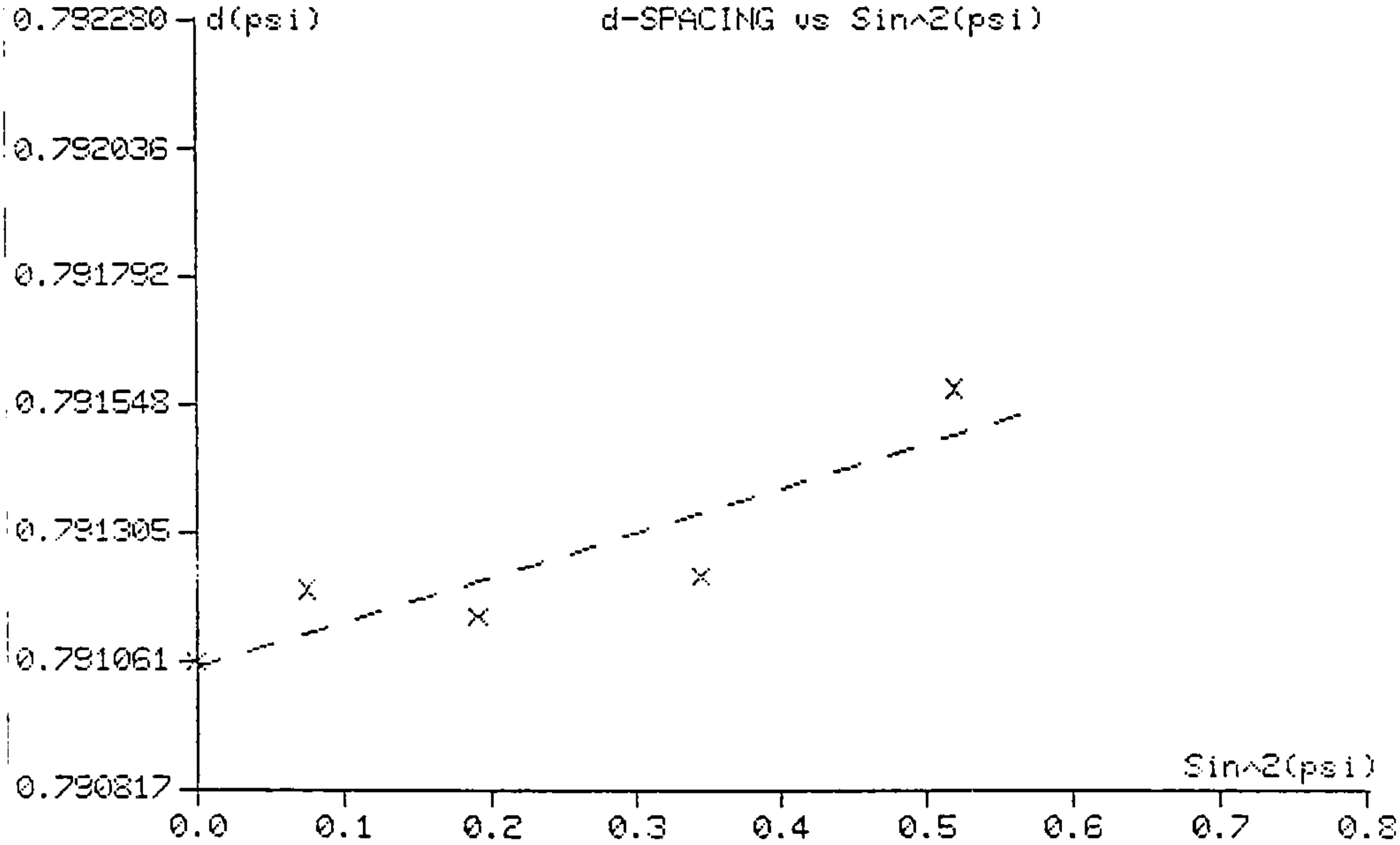

Sample Description :
ARGONNE NATIONAL LABORATORY/AL2O3
LOCATION 6/LONGITUDINAL

Stress Spectra File Specifications 111600.SPC

Residual Stress	(ksi)	19.57	(mpa)	134.92
Statistical Error (+/-)	(ksi)	10.06	(mpa)	69.39

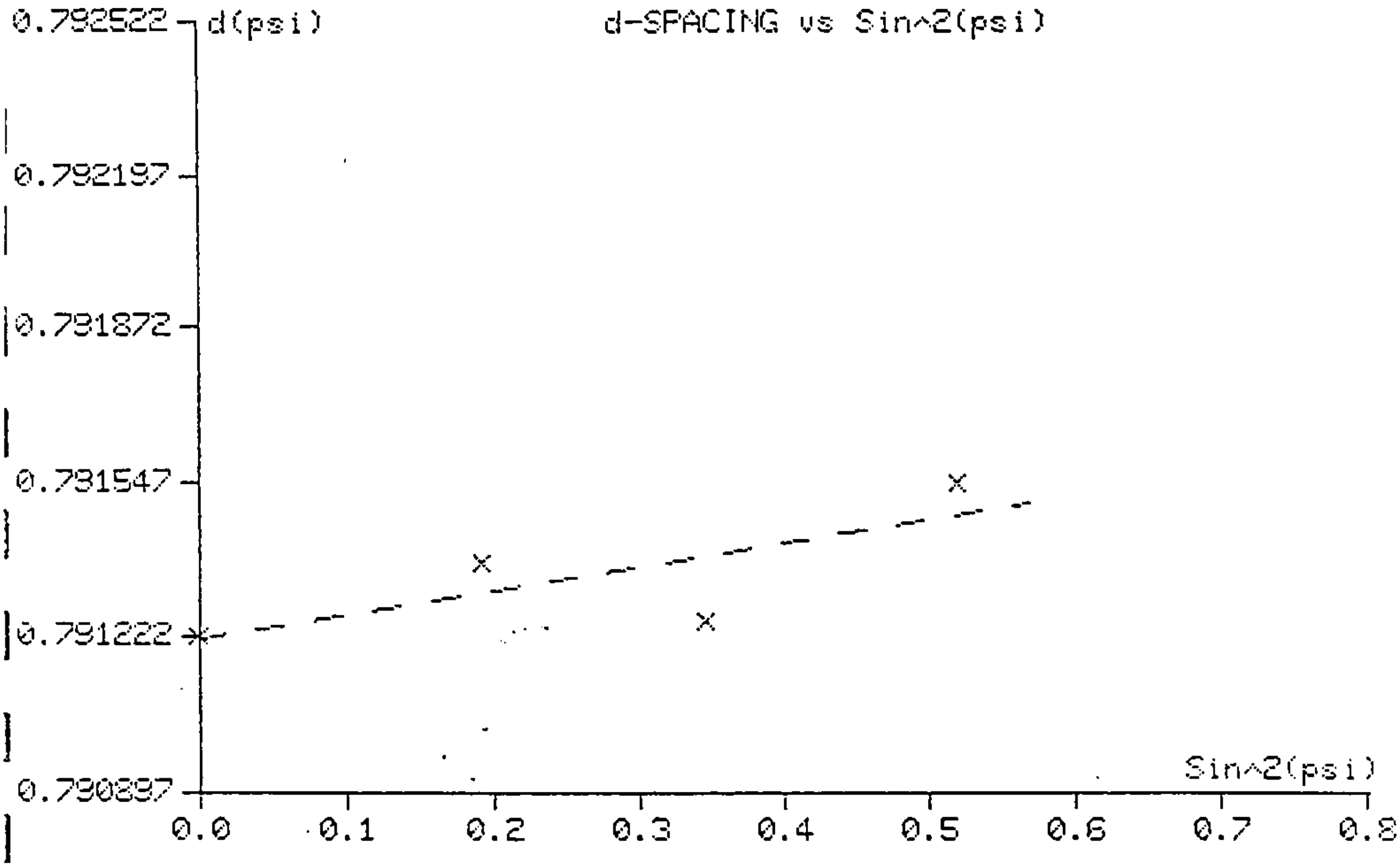

Sample Description :
ARGONNE NATIONAL LABORATORY/AL2O3
LOCATION 6/CIRCUMFERENTIAL

Stress Spectra File Specifications 001114.SFC

Residual Stress	(ksi)	8.16	(mpa)	56.23
Statistical Error (+/-)	(ksi)	6.00	(mpa)	41.39

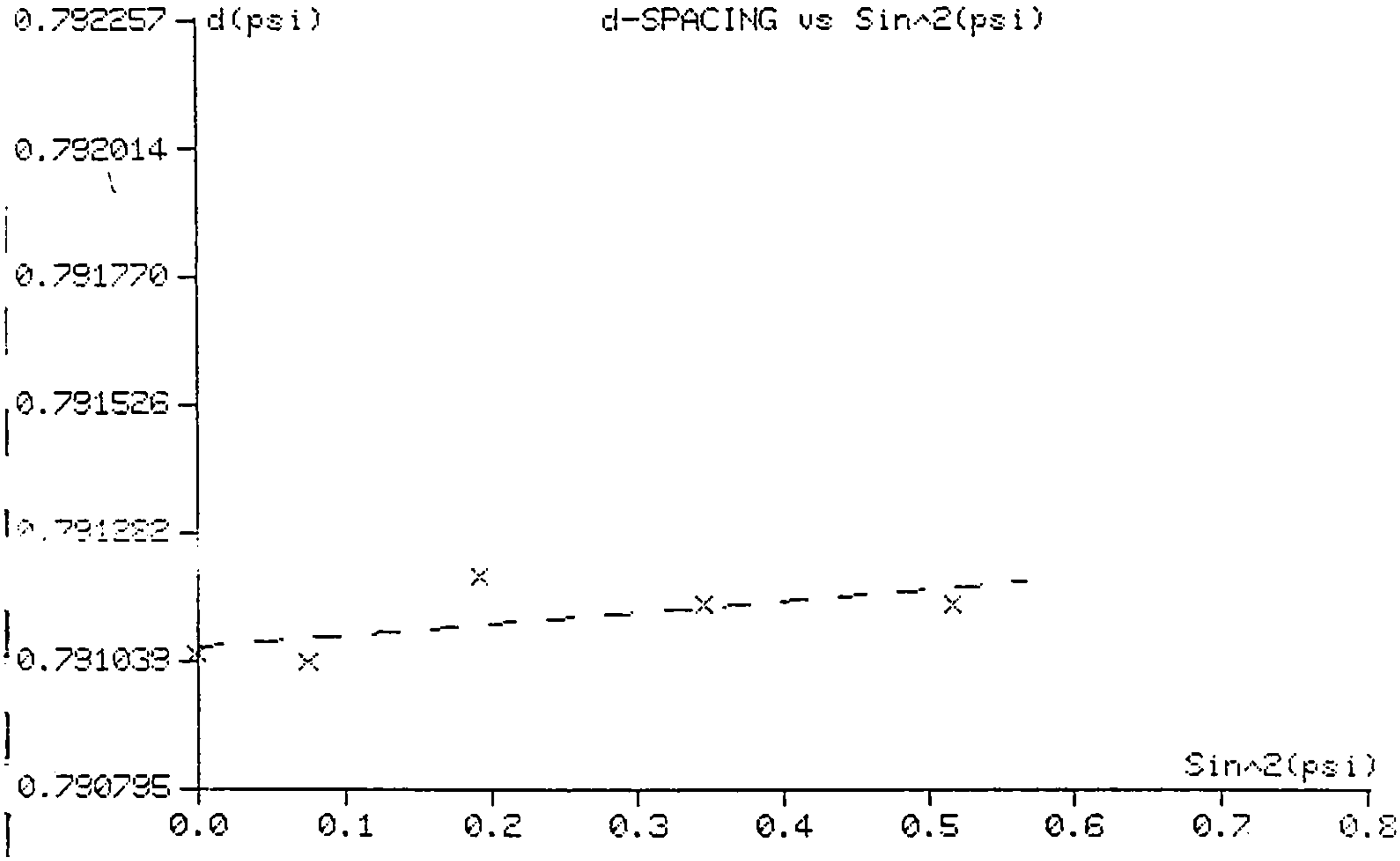

ample Description :
RGONNE NATIONAL LABORATORY/AL2O3
OCATION 3/LONGITUDINAL

tress Spectra File Specifications 001115.SPC

esidual Stress	(ksi)	15.04	(mpa)	103.70
tatistical Error (+/-)	(ksi)	6.60	(mpa)	45.50

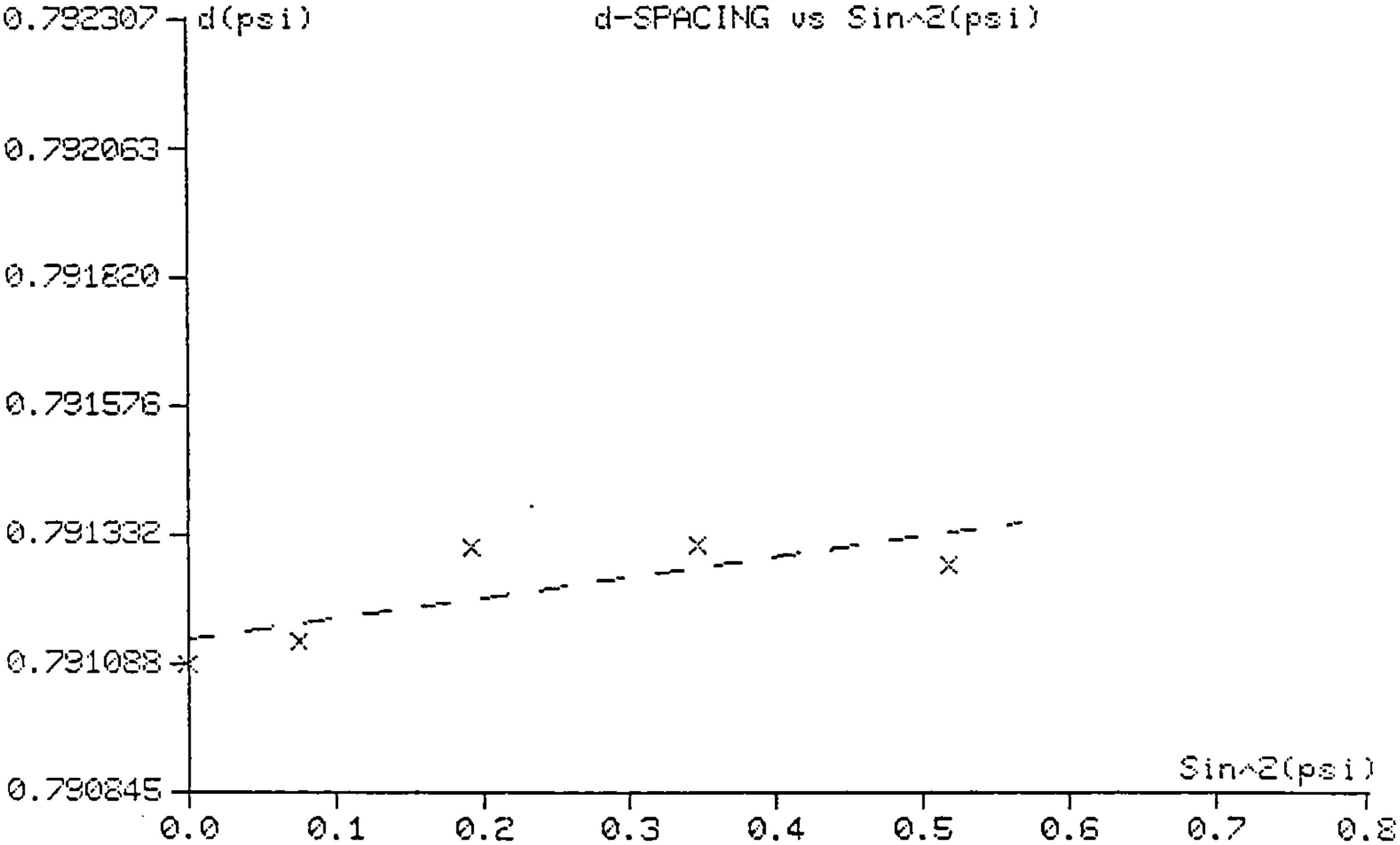

Sample Description :
ARGONNE NATIONAL LABORATORY/AL2O3
LOCATION 3/CIRCUMFERENTIAL

Stress Spectra File Specifications 001113.SPC

Residual Stress	(ksi)	15.63	(mpa)	107.75
Statistical Error (+/-)	(ksi)	4.60	(mpa)	31.70

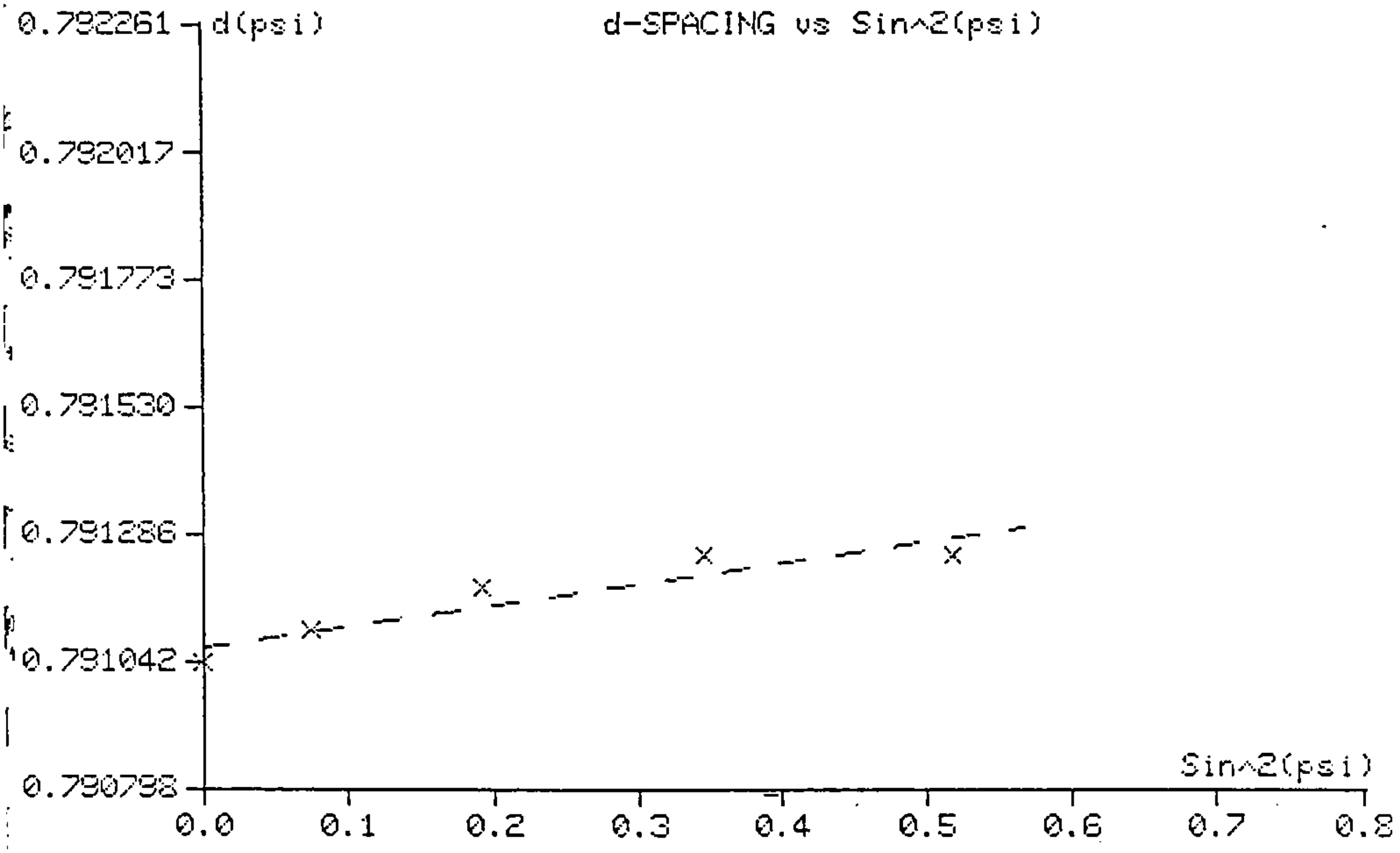

Distribution List for ANL-91/45

Internal:

S. L. Dieckman
S. Dorris
N. Gopalsami
J. S. Gregar
K. Hurley
R. A. Jaross
D. L. Johnson
D. S. Kupperman
C. A. Malefyt (2)
S. Majumdar
R. B. Poeppel
A. C. Raptis
M. Rixner
W. W. Schertz
W. J. Shack
J. P. Singh (2)
R. A. Valentin (2)
R. W. Weeks
ANL Patent Dept.
ANL Contract File
TIS Files (3)

External:

DOE-OSTI (12)
ANL Libraries
Chicago Operations Office, DOE
  Manager
  F. Herbaty
  J. Jonkouski
  J. A. Mavec
  S. Waslo
William P. Parks, Jr., Office of Industrial Technologies, DOE
Materials and Components Technology Division Review Committee:
  H. Berger, Industrial Quality, Inc., Gaithersburg, MD
  M. S. Dresselhaus, Massachusetts Institute of Technology, Cambridge, MA
  S. J. Green, Electric Power Research Institute, Palo Alto, CA
  R. A. Greenkorn, Purdue University, West Lafayette, IN
  C.-Y. Li, Cornell University, Ithaca, NY
  P. G. Shewmon, The Ohio State University, Columbus
  R. E. Smith, Electric Power Research Institute, Charlotte, NC
G. Miller, Carborundum Company, Phoenix, AZ
ERIM, Ann Arbor, MI
  T. K. Hunt
  J. T. Kummer
Oak Ridge National Laboratory
  P. Becher
  R. A. Bradley
  N. C. Cole
  R. Judkins

R. A. Lowden
V. J. Tennery
University of Utah, Salt Lake City
D. K. Shetty
A. V. Virkar
R. C. Bradt, University of Nevada–Reno
Virginia Polytechnic Institute and State University, Blacksburg
J. Brown, Jr.
R. S. Gordon
D. P. H. Hasselman